DYNAMICS OF UNBALANCED DRILL COLLARS IN A SLANTED HOLE

by

Olivier F. Rey

Maîtrise de Mécanique
University of Nantes, France, 1981

Degree of Ingénieur en Constructions Mécaniques et Navales
Ecole Nationale Supérieure de Mécanique
Nantes, France, 1982

Submitted to the Department of
Ocean Engineering
in Partial Fulfillment of the
Requirements of the
Degree of

Master of Science

at the

MASSACHUSETTS INSTITUTE OF TECHNOLOGY

May, 1983

Signature of Author _____
Department of Ocean Engineering
May, 1983

Certified by _____
Prof. J. Kim Vandiver
Thesis Supervisor

Accepted by _____
Prof. A.D. Carmichael
Departmental Graduate Committee

DYNAMICS OF UNBALANCED DRILL COLLARS IN A SLANTED HOLE

Olivier F. Rey

ABSTRACT

This study examines the side-cutting forces exerted by an oil-drilling bit boring in a slanted hole and mounted on an unbalanced shaft.

Appendix A shows how the partial differential equation for the movement of the lower part of the drill string is obtained and can be solved under certain assumptions. Appendix B deals with the implementation of a computer program to get the displacements of the drill collars and the side-forces that stem therefrom.

The discussion of results investigates how sensitive the rotating forces are to various parameters. The forces at the bit and at the stabilizer are plotted out, and the curves show the effects of driving torque, weight on bit, end conditions at stabilizer, bit embedding, and eventually investigate several mass eccentricity distributions.

In conclusion, a proposition is made for increasing drilling efficiency and for a more thorough study that would account for static forces more systematically.

Thesis Supervisor: Prof. J. Kim Vandiver

Title: Associate Professor of Ocean Engineering

ACKNOWLEDGEMENTS

I would like to express my thanks to Professor J. Kim Vandiver for his advice, enthusiasm and stimulating discussions during the development of this work.

I am also grateful to Anna Markowitz for helping me type this thesis.

And I would like to express my deepest gratitude to Maurice, Paul and Antoinette for their love and support throughout my studies. This work is dedicated to them.

TABLE OF CONTENTS

	Page
Abstract	1
Aknowledgements	2
Table of Contents	3
Nomenclature	6
INTRODUCTION.	10
DISCUSSION OF RESULTS.	14
1. Presentation.	14
2. Testing of the Validity of COLLAR.	18
3. Effect of Torque.	20
4. Effect of Weight on Bit and Boundary Condition at Stabilizer.	21
5. Effect of Mud Damping.	22
6. Effect of Bit Embedding.	22
7. Effect of Mass Eccentricity Distribution.	24
8. Figures 1 to 20.	27
9. Typical Printout from COLLAR.	70
CONCLUSION	71
BIBLIOGRAPHY.	72

APPENDIX A : DERIVATION OF GOVERNING PARTIAL DIFFERENTIAL EQUATION. 73

A.1 Methodology. 73

A.2 Effect of Flexural Stiffness. 76

A.3 Effect of Coupling Torque-Bending. 79

A.4 Effect of External and Internal Damping. 82

A.5 Effect of Transverse Mud Thrust. 83

A.6 Effect of Gravity. 85

A.7 Effect of Coupling Compression-Bending. 87

A.8 Dimensional Partial Differential Equation:

a. In the Static Frame. 91

b. In the Rotating Frame. 94

A.9 Boundary Conditions and External Torques:

a. At Bit. 95

b. At Stabilizers. 99

A.10 Non-Dimensionalization of the Problem. 101

A.11 Ultimate Dimensionless Formulation in Terms of Ordinary Differential Equations. 103

APPENDIX B : IMPLEMENTATION OF COMPUTER PROGRAM COLLAR. 105

B.1 Calculation of solution s_ϕ. 105

1.1 Finite-Difference Formulation. 105

1.2 Boundary Conditions:

a. At Bit. 108

b. At Stabilizers. 109

1.3 Construction of the Finite-Difference Matrix. 111

1.4 Dimensional Forces at Bit and Stabilizers. 114

B.2 Calculation of Solution r_e. 117

2.1 Modification of the Finite-Difference Matrix. 117

2.2 Dimensional Forces at Bit and Stabilizer. 117

B.3 Total Forces at Bit and Stabilizers. 119

NOMENCLATURE

A	Cross-section area of the drill-collars.
$a_1,...a_9$	Dimensionless coefficients for the dimensionless ordinary differential equations.
a(z)	Component along $\vec{U}$ of $\vec{CG}$.
b(z)	Component along $\vec{V}$ of $\vec{CG}$.
C	Centroid of the cross-section area, or mid-point of inner diameter.
c	Continuous choice coefficient for the boundary condition at the stabilizers: c = 0: pinned ; c = 1: clamped. An "in between" value is defined as c = 1 - (QL/EI)/2N
C_e	Coefficient of mud external damping. Ce = lbs/(ft/s)/foot of pipe
C_i	Coefficient of internal (structural) damping. Same units as Ce.
C_M	Mass coefficient = 1 + Mm/Ms with Mm = mass of trapped mud + mass of volume of mud diplaced by a solid cylinder of same outer diameter (per foot). Ms = mass of steel per foot.
$c_1,...c_5$	Dimensionless constants corresponding to the pentadiagonal complex conjugate finite-difference matrix.
D	Depth of the bit.

$e'(z)$ Complex eccentricity of the center of gravity.

$$e'(z) = a(z) + i\, b(z)$$

$e(w)$ Dimensionless eccentricity: $e(z) = e'(z)/L$.

EI Flexural stiffness. For steel, $E = 4.28 * 10^9$ lbs/ft^2 .

$\overrightarrow{F_{b1}}$ (F_{b1}) Vector (complex) side-force exerted by the bit onto the wall; corresponds to s_ϕ.

$\overrightarrow{F_{b2}}$ (F_{b2}) Same as above, but corresponds to r_e.

$\overrightarrow{F_{s1}}$ (F_{s1}) Vector (complex) side-force exerted by the stabilizer onto the wall; corresponds to s_ϕ.

$\overrightarrow{F_{s2}}$ (F_{s2}) Same as above, but corresponds to r_e.

G Center of gravity of the slice.

g Acceleration of gravity.

h $1 - \rho_m/\rho$

i $i^2 = -1$.

k' Dimensional characteristic radius of the bit for computing embedding restoring moment.

k Dimensionless characteristic radius: $k = k'/L$

L Length of concern, between the bit and the first set of stabilizers.

l'_o Dimensional actual length of compression:

$$T_o = A \rho g\, l'_o \cos\phi$$

l_o $= l'_o/L$

l'_1 Dimensional effective length of compression:

$$T_1 = A \rho g\, h\, l'_1 \cos\phi$$

l_1 $= l'_1/L$

N Number of segments for discretization of the collars.

$\vec{n}$ Vector orthogonal to the slice, tangent to central line.

O Origin of the trihedrals OXYZ and OUVZ, located at bit.

$\vec{Q}$ Driving torque.

$\vec{Q}_n$ Component of $\vec{Q}$ along $\vec{n}$.

$\vec{Q}_p$ Component of $\vec{Q}$ in the plane of the slice.

$r'(z,t)$ Complex dimensional displacement in rotating frame OUVZ:

$$r' = u + i\,v.$$

$r(w,\tau)$ $= r'(z,t)/L$.

$r_e(w,\tau)$ In rotating frame, dimensionless complex solution with the time-independent mass-eccentricity excitation only.

$s'(z,t)$ Complex dimensional displacement in fixed frame OXYZ:

$$s' = x + i\,y.$$

$s(w,\tau)$ $= s'(z,t)/L$.

$s_\phi(w,\tau)$ In the fixed frame, dimensionless complex solution with the time-independent $g.\sin\phi$ excitation only.

$T(z)$ Dimensional tensile force (compression) at cut z.

T_o Dimensional actual compression at the bit.

$$T_o = \left\{W(1-\rho_m/\rho) - T_{rig}\right\}\cos\phi + \rho_m gDA$$

T_1 Dimensional effective compression (weight on bit) due to the soil only

$$T_1 = \left\{W(1-\rho_m/\rho) - T_{rig}\right\}\cos \equiv W_b \cos\phi$$

Although T_o is the true compression at the bit, it is

	T_1 that appears in the ultimate equations.
T_{rig}	Weight (tension) supported by the drilling rig.
t	Dimensional time.
U,V	Axes rotating about Z.
u,v,z	Dimensional coordinates of C(z) in OUVZ.
W	Total weight of the string in the hole, from the bottom to the very top (steel only).
w	Dimensionless cut along Z.
W_b	Apparent weight of drill string minus tension from rig. See T_1
X,Y,Z	Fixed trihedral. Z intersects the centerline of the pipe at the bit and at the stabilizers. OYZ is a vertical plane.
x,y,z	Dimensional coordinates of C(z) in OXYZ.

Greek Symbols

ρ	Density of steel.
ρ_m	Density of surrounding mud.
τ	Dimensionless time: $\tau = \omega_o t$.
ϕ	Mean slope of the hole between bit and stabilizers.
Ω	Rotation speed of the shaft.
ω_o	Time-change factor: $\omega_o = (EI/A\rho C_M L^4)^{1/2}$

INTRODUCTION

The goal of this thesis is to address the side-cutting forces exerted by an oil-drilling bit boring in a slanted hole and mounted on unbalanced collars.

Usually, when a bit undergoes too large a compression, the behavior of the soil being bored makes it deviate from the vertical, for some stability reason. Thus, the driller in charge of the well is faced with two problems:

- On the one hand, if the bit is only lightly loaded, the penetration rate is too slow. Consequently, overall drilling time and equipment wear are substantially increased.
- On the other hand, if the bit is overloaded, the hole tends to climb and to build up an angle with the vertical. A potentially troublesome point is that the contract issued by the oil company and signed by the driller may stipulate that the hole be not off the vertical by an angle more than four or five degrees. If the slope of the hole is ten degrees, even locally, the conditions of the contract may not be satisfied.

Coming back to the subject of this study, oil drillers have now discovered that when the last part of the drilling string, just above the bit, is made up with an unbalanced pipe, they can afford to increase the weight on bit without jeopardizing the verticality of the hole, or even while dropping angle if the hole has some slant already (World Oil, 1971 and 1978).

This study doesn't address the entire problem: in particular, the very fact that unbalanced collars in a slanted hole tend to recover the vertical is not explained. Answering this question would require a deterministic solution of the

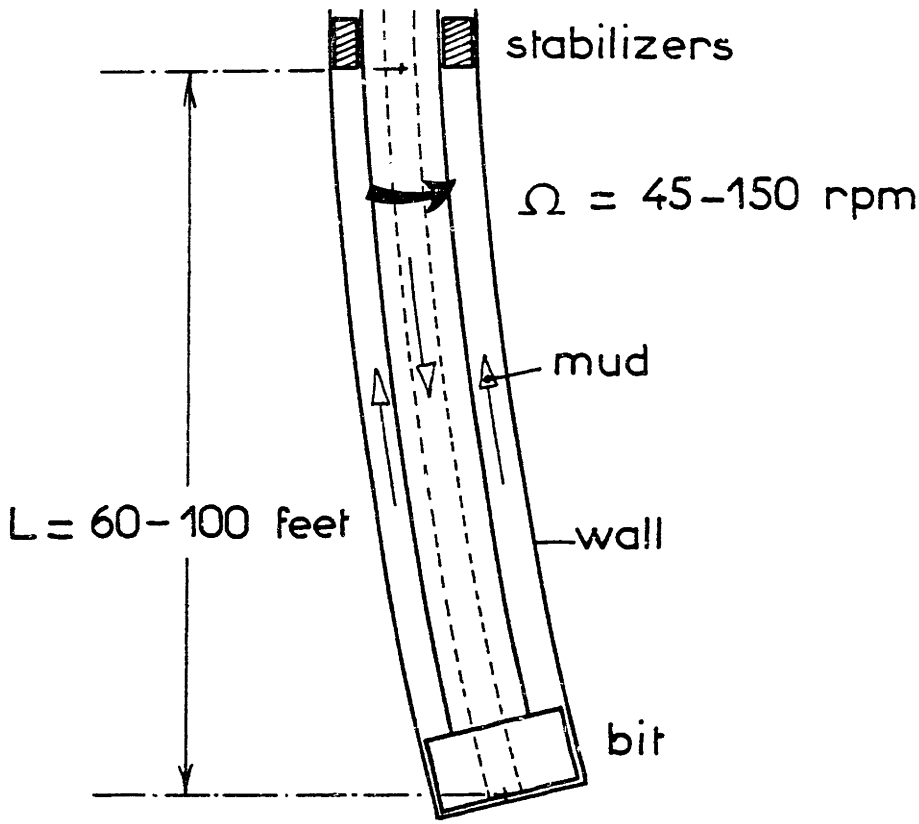

Fig. 0 - Idealization of the Bottom-Hole Assembly.

highly non-linear behavior of the soil being drilled through. Furthermore, the model deliberately assumes that the local slope of the hole as well as the transverse displacements are small, and that the borehole walls are rigid and never hit by the pipe. The effect of the drill string beyond the stabilizer is assumed to be contained in the boundary conditions.

We shall concentrate on the part of the drill collars between the bit and the first set of stabilizers. In order to get the constraining forces at these two locations, the displacement of the portion of the pipe between the stabilizer and the bit is needed: the length of these drill collars is typically 60-100 feet, and most of the time the collars remain entirely in compression. This is why the collars are thick-walled pipes, which are resistant to buckling. Mud is pumped inside the drill string and drags away the debris (Figure 0).

Appendix A is devoted to deriving the partial differential equation governing the motion with respect to time of an infinitesimal slice of the shaft at cut z. Special care is given to the thrust of the mud. The shaft is supposed stable, so the transient response is ignored. Here may lie the most questionable part of the model. However, assuming the shaft stable permits steady-state solution to be obtained by separation of the temporal and spatial variables.

As the separation of variables proves successful, appendix B is devoted to the implementation of a computer program that gives the forces exerted by the bit and the stabilizers onto

the sides of the wall. Program COLLAR is based on the finite-difference method, which readily allows for the non-trivial boundary condition considered. On the other hand, as stated above, no allowance whatsoever has been made for the pipe to undergo any type of vibration mode beside the overall rotating motion.

After checking the validity of COLLAR with two intuitive runs, the discussion of the results concentrates on the rotating side-forces only. It shows how buckling torque and buckling load can be found, investigates the effects of boundary conditions at bit and stabilizers, and eventually tests different mass eccentricity distributions. In conclusion, orientation is given for further research.

DISCUSSION OF RESULTS

1. Presentation.

Emphasis has been given to the variation w.r.t. rotation speed of the side-forces at bit and stabilizers, to the prejudice of the fixed components. Because of the non-linear behavior of the soil, the reason that unbalanced drill collars tend to recover the vertical seems to be buried in these rotating forces.

The underlying partial differential equation is the dimensionless equation (A.27) derived in appendix A.10:

$$\ddot{s} + \frac{c_e + c_i}{A\rho C_M \omega_o}\dot{s} + \frac{\partial^4 s}{\partial w^4} + i\frac{QL}{EI}\frac{\partial^3 s}{\partial w^3} + \frac{h}{C_M}\frac{g\cos\phi}{L\omega_o^2}\left\{(\ell_1 - w)\frac{\partial^2 s}{\partial w^2} - \frac{\partial s}{\partial w}\right\} - i\frac{C_i\Omega}{A\rho C_M \omega_o^2}s$$

$$= \frac{\Omega^2}{\omega_o^2}e(w)\,e^{i\frac{\Omega}{\omega_o}\tau} - i\frac{h}{C_M}\frac{g\sin\phi}{L\omega_o^2} \qquad (1.1)$$

The different parameters are explained in the nomenclature.

$s = (x+iy)/L$ is the complex dimensionless displacement of the shaft in the static frame OXYZ (figure A.1), and $e(w) = e'/L$ is the complex dimensionless eccentricity (Figure A.2). Appendix A.11 shows that s can be cast into the form $s = s_h + s_e + s_\phi$; s_e is the solution corresponding to the eccentricity forcing term $\frac{\Omega^2}{\omega_o^2}e(w)\,e^{i\frac{\Omega}{\omega_o}\tau}$,

and is the only contribution of interest for obtaining the rotating side-forces. Setting $s_e = r_e . e^{i \frac{\Omega}{\omega_o} \tau}$, appendix A.11 also shows that r_e is the particular solution of the ordinary differential equation (A.34):

$$\frac{d^4 r_e}{dw^4} + i \frac{QL}{EI} \frac{d^3 r_e}{dw^3} + \frac{h}{c_M} \frac{g \cos\phi}{L \omega_o^2} \left\{ (\ell_1 - w) \frac{d^2 r_e}{dw^2} - \frac{dr_e}{dw} \right\}$$

$$- \left[\frac{\Omega^2}{\omega_o^2} - i \frac{c_e \Omega}{A \rho c_M \omega_o^2} \right] r_e = \frac{\Omega^2}{\omega_o^2} e(w) \qquad (1.2)$$

After obtaining the dimensionless solution r_e, appendix B.2 demonstrates that the dimensional complex forces exerted onto the borehole walls are :

$$\cdot F_{\substack{rot. \\ stab.}} = A \rho c_M \Omega^2 L^2 \int_0^1 \left[r_{(w)} + e_{(w)} \right] w \, dw$$

$$- k T_1 \left(\frac{dr}{dw} \right)_{w=0} + c \frac{EI}{L^2} \left(\frac{d^2 r}{dw^2} \right)_{w=1} \qquad (1.3)$$

$$\cdot F_{\substack{rot. \\ bit}} = A \rho c_M \Omega^2 L^2 \int_0^1 \left[r_{(w)} + e_{(w)} \right] dw - F_{\substack{rot. \\ stab.}} \qquad (1.4)$$

The parameter $k = k'/L$ is a dimensionless coefficient that

allows for an embedding of the bit. The physical significance of k' and the corresponding moment are explained in appendix A.9.a and figures A.16 to A.19. The parameter c describes the boundary condition at the set of stabilizers: its value is 0 if pinned, 1 if clamped, and intermediate values may be considered as exemplified in appendix B.1.2.b. Although only $c = 0$ and $c = 1$ are presented here, the particular value $c = 1 - (QL/EI)/2N$ was tried (Figures B.2 and B.3) with no damping, $C_e = 0$. The corresponding force curves exhibited a somewhat intermediate situation between pinned and clamped, but the interesting result was that these curves were astonishingly comparable to those with $c = 1$ and $C_e = 0$, as if some damping had been introduced.

All the cases presented here give the variation w.r.t. rotation speed of the magnitude of $\overrightarrow{F_{bit}}$ and $\overrightarrow{F_{sta}}$, along with the variation of the phase angles. The examination of the phase curves not only allows one to spot the resonances more accurately, but also gives the relative phase shift between the two forces.

The most favorable situation seems to be reached when rotating forces are large at bit to increase efficiency, while small enough at stabilizers not to damage the borehole wall. It must be kept in mind that the bit advances into the ground; consequently, the side-forces are exerted onto the formation for only a few moments. A large rotating force at bit does not necessarily imply a larger borehole.

Case & Figures	Q lbs*ft	Φ deg	ρ_m lbs/gal	C_e lb*s/ft^2	k' in	W_b lbs	c
Testing of the Program COLLAR							
1							0
2							1
Effect of Torque							
3	10000						0
4	10000						1
5	10^6						1
6	2.10^6						1
Effect of Weight on Bit and Bound. Cond. at Stabilizer							
7	10000	10	12			10000	1
8	10000	10	12			30000	1
9	10000	10	12			60000	1
10	10000	10	12			10000	0
11	10000	10	12			30000	0
Effect of Mud Damping							
12	10000	10	12	0.8		30000	1
Effect of Bit Embedding							
13		10	12		15	30000	1
14		10	12		1000	30000	1

Effect of Mass-Eccentricity Distribution (inches)

Same Parameters as in Case 8, Except e'(z):

	$0 \leq z < L/4 < z < L/2 < z < 3L/4 < z \leq L$			
15	e'(z) = 0.1	0.1	-0.1	-0.1
16	e'(z) = 0.1	0.1	0.1	0
17	e'(z) = 0.1	0	0	0
18	e'(z) = -0.1	0.1	0.1	0.1
19	e'(z) = 0	0.1	-0.1	0
20	e'(z) = 0.1	-0.1	0.1	-0.1

Table 1 - Input Parameters for Example Calculations.

The characteristics of the shaft considered are:

OD = 7.50 inches

ID = 2.81 inches (= $2\,^{13}/_{16}$ in)

L = 100 feet

ρ = 15.2 slugs/ft^3

Unless specified, mass eccentricity is constant over the length:

e' = 0.1 inches.

The parameters for each case are in Table 1.

2. Testing of the Validity of Program COLLAR.

The validity of COLLAR is tested in two cases where results are almost known in advance: bit pinned - stab. pinned (case 1, Figures 1) and bit pinned - stab. clamped (case 2, Figures 2). As expected, in each case the curves undergo a dramatic increase about two rotation speeds over the range of rotation rates considered in the analysis, which correspond to the first two critical speeds of the shaft in bending. To get an idea of the accuracy of the numerical results, these critical speeds are compared to those from theory. The theoretical formula given below assumes zero tension throughout the length of the shaft, whereas the tension considered by COLLAR is equal to the weight of the collars at z = L and linearly goes to zero at the bit. Thus we know in advance that the critical speeds from COLLAR should be slightly higher.

Let $\nu = \frac{30}{\pi L^2}\sqrt{\frac{EI}{A\rho}}$ (rpm)

Theory gives:

	Ω_1 (rpm)	Ω_2 (rpm)
case 1, pin-pin	$\pi^2 \nu$	$(2\pi)^2 \nu$
case 2, pin-cla	$(3.927)^2 \nu$	$(7.069)^2 \nu$

With ν being here 2.6737 rpm and the shaft being discretized into N = 31 segments, one finds:

	Ω_1 (rpm)		Ω_2 (rpm)	
	Theory	COLLAR	Theory	COLLAR
case 1, pin-pin	26.39	28.95	105.55	107.89
case 2, pin-cla	41.23	42.63	133.59	134.78

As expected, theoretical values are a little lower. In each case, the two mode shapes given by COLLAR are drawn (Figures 1.c and 2.c). For case 1, they can be fitted exactly by sinusoids. All these results confirm the conclusions of previous studies showing that linearly varying tension hardly affects resonance frequencies and mode shapes. However, the effect of tension does appear in figure 1.a. In this case, both bit and stabilizer are pinned. If the tension were constant, the forces would be always rigorously equal in magnitude, as was verified in a case, not shown here, where $\phi = 90°$ suppressed the contribution of the gravity forces. For $\phi \neq 90°$, the varying tension makes the two forces different about the second critical speed.

3. Effect of Torque.

Although the exact value of Q is not known, the order of magnitude can be obtained by referring to tables giving the initial make-up torque at joints (Drilco, 1982).

Cases 3 and 4 are identical to 1 and 2, except that Q = 10000 lbs.ft is now introduced: the out-of-plane contribution of Q creates some phase modifications, but Q is not large enough to cause a visible change in the magnitude of the forces or in the natural frequencies. This result is consistent with those of Eshleman and Eubanks (1969). These authors show that things are not significantly modified until QL/EI = 2. Using their notations, the parameter H = QL/EI as it appears in equation (1.2) is, for case 4:

$$H = \frac{QL}{EI} = \frac{(10\,000).(100)}{3.1426\ 10^{7}} = 0.032$$

Cases 5 and 6 test $Q = 10^{6}$ and 2.10^{6} lbs.ft respectively, although such high values are never actually used (figures 5 and 6).

Case	Q (lbs.ft)	H = QL/EI	Ω_1 (rpm)	Ω_2
4	10^4	0.032	42.6	134.8
5	10^6	3.2	41	130
6	2.10^6	6.4	?	118

For case 6, H is greater than the threshold 2π mentioned by Golomb and Rosemberg (1961), and indeed buckling has most likely occurred.

4. Effect of Weight on Bit and Boundary Condition at Stabilizer.

As seen in appendix A.7, a parameter the driller can play with, beside the rotation speed, is W_b = apparent weight of drill string minus tension from rig. The actual weight on bit is $T_1 = W_b \cos\phi$. Cases 7, 8 and 9 were done with W_b = 10000, 30000 and 60000 lbs, assuming a built-in condition at the stabilizers.

From corresponding Figures 7, 8 and 9, we can notice a left-bound shift of the natural frequencies: the first mode is obtained successively at 35, 27 and 13 rpm, the second at 118, 112 and 101 rpm. Likewise, for W_b = 30000 lbs, compare case 8 (c = 1) to case 11 (c = 0). An idea of how critical the situation is stems from the first natural frequency: the lower it is, the closer the buckling. Theoretically, the shaft buckles when the first natural frequency hits zero; practically, the various vibrations undergone trigger buckling well before the theoretical value is attained.

Case	W_b (lbs)	c	Ω_1 (rpm)	Ω_2
7	10000	1	35	118
8	30000	1	27	112
9	60000	1	13	101
10	10000	0	21	92
11	30000	0	11	84

As expected, the shaft supports compression much better when

its upper end is clamped.

5. Effect of Mud Damping.

When the shaft is surrounded by mud, every slice is submitted to a drag force that COLLAR sets equal to:

$$\vec{F}_{mud} = - C_e \cdot \vec{V}_{(c)} \cdot dz$$

Actually, $\vec{F}_{mud}$ is better modeled by the non-linear expression:

$$\vec{F}_{mud} = - \frac{1}{2} C_e \rho_m S V_{(c)} \cdot \vec{V}_{(c)}$$

For every rotation speed, every slice should be assigned a different C_e which depends on the unknown V, and consequently several iterations should be performed to obtain a result for a single case. However, in order to get a general feeling of the effect of C_e, the value $C_e = 0.8$ has been considered in case 12. As a matter of fact, this value represents:

$$C_e = 0.8 \sim \frac{1}{L} \int_0^L C_e(z)\, dz$$

When compared to $C_e = 0$, $C_e \neq 0$ limits the peaks and heightens the minima, but the value $C_e = 0.8$ is too small to affect the critical speeds significantly.

6. Effect of Bit Embedding.

A potential embedding of the bit is taken care of by introducing a length k', which is the lever at which the weight on bit is applied, thus creating a restoring moment (appendix A.9.a). Since Q = 10000 lbs.ft is too small to have any effect

on the graph of the forces, Q is equated to zero so that the mode shapes at resonance are contained in a plane and can be plotted out.

It appears that physically acceptable values for k', i.e. on the order of the radius of the bit, have little influence, if any, on the mode shapes, which look very much like those on Figures 1.c or 2.c. However, it can be verified that k' has a stiffening effect by pushing up critical speeds, which allows for more weight on bit before buckling. This is exemplified dramatically in case 14, using the non-realistic value k' = 1000 inches. In this case, the mode shapes indeed reflect the effect of restoring moment (Figure 14.c).

Case	W_b (lbs)	k' (in)	c	Ω_1 (rpm)	Ω_2
11	30000	0	0	11	84
13	30000	15	0	12	94
8	30000	0	1	27	112
14	30000	1000	0	27	109

It is worth noting that figure 14.a is almost the negative of Figure 8.a: the force at stabilizer of case 14 looks like the bit force of case 8, and vice-versa. In case 8 one has stab. clamped - bit pinned, in case 14 the stabilizer is pinned and k' is so large that the bit is practically clamped. The critical speeds are surprisingly close.

7. Effect of Mass Eccentricity Distribution.

So far, a uniform mass eccentricity distribution has been used, namely one tenth of an inch over the entire length. Assuming clamped stabilizer, various configurations have been tested with the underlying intention to maximize F_{bit} in order to increase drilling efficiency, while minimizing F_{sta} to prevent the stabilizers from abrading the borehole wall. This friction would increase the torque requirements and the equipment wear, and diminish the actual weight on bit.

As will be seen in the following, one sometimes comes up with a rotation speed that fulfills such requirements, except that it may be as large as 200 rpm. In order to reduce this "optimum" speed to a more practical value, one can increase L or the weight on bit W_b, or decrease EI. However, this also reduces the first natural frequency, which makes the shaft more sensitive to buckling.

Case 15 excites the second mode:

$$e'(z) = \begin{cases} 0.1 \text{ inches} & 0 \leqslant z < L/2 \\ -0.1 \text{ inches} & L/2 < z \leqslant L \end{cases}$$

Figure 15.a shows how the second resonance is amplified, with a peak width at 200 lbs larger than in any other case. After this resonance, the force at stabilizer vanishes around 170 rpm whereas the force at bit never goes below 140 lbs. However, compared to case 8 that has a uniform distribution, Case 15 doesn't appear worth it.

Case 16 is run with

$$e'(z) = \begin{cases} 0.1 \text{ inches} & 0 \leqslant z < 3L/4 \\ 0 & \text{elsewhere} \end{cases}$$

Unlike other cases, F_{stab} remains small for a wide range of rpm's, but F_{bit} is not much larger either.

Case 17 considers $e(z) = \begin{cases} 0.1 \text{ inches} & 0 \leqslant Z < L/4 \\ 0 & \text{elsewhere} \end{cases}$

It reveals a striking result: since the eccentricity of the shaft is located near the bit, rotating forces were expected to be greater at the bit than at the stabilizer. Going against intuition, Figure 17.a shows that F_{sta} is a lot greater than F_{bit} after the second resonance. The case, not shown here, where the lower half of the drill collars had a uniform eccentricity of 0.1 inches looked very much alike. It is worth noting that the shapes of the curves are very different from Case 16, where the lower three quarters of the shaft are eccentric.

For case 18, $e'(z) = \begin{cases} -0.1 \text{ inches} & 0 \leqslant z < L/4. \\ 0.1 \text{ inches} & \text{elsewhere} \end{cases}$

The "optimum" speed seems to be around 190 rpm, with F_{sta} = 20 lbs and F_{bit}= 200 lbs.

Another interesting configuration is tested in Case 19, with

$$e'(z) = \begin{cases} 0 & 0 \leqslant z < L/4 \\ 0.1 \text{ in} & L/4 < z < L/2 \\ -0.1 \text{ in} & L/2 < z < 3L/4 \\ 0 & 3L/4 < z \leqslant L \end{cases}$$

At 195 rpm, F_{sta} vanishes and F_{bit} attains 320 lbs.

But from all the eccentricity distributions tried here, the most spectacular is Case 20 with

$$e'(z) = \begin{cases} 0.1 \text{ inches} & 0 \leqslant z < L/4 \\ -0.1 \text{ inches} & L/4 < z < L/2 \\ 0.1 \text{ inches} & L/2 < z < 3L/4 \\ -0.1 \text{ inches} & 3L/4 < z \leqslant L \end{cases}$$

At 208 rpm, F_{sta} vanishes while F_{bit} = 750 lbs. As suggested above, an attempt has been made to reach the same situation at a lower frequency by taking L = 120 feet instead of 100 feet. The corresponding figures are not shown here, but F_{stab} vanished at 142 rpm while F_{bit} was 300 lbs. This case, however, was not conceivable either, for the first critical speed had disappeared, indicating that buckling had occurred.

8. Figures 1 to 20.

Figure 1.a - Testing of the Program COLLAR, c = 0

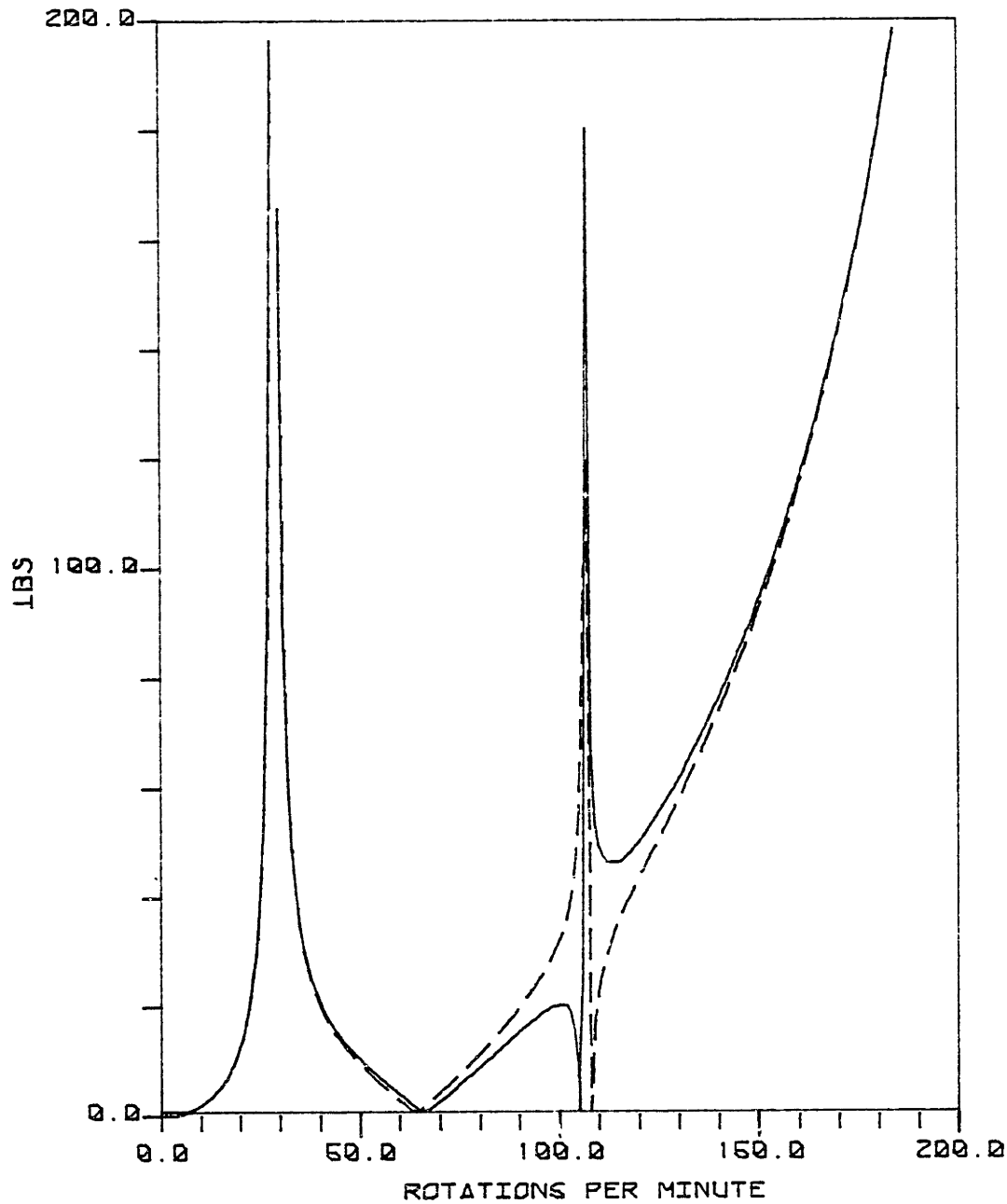

Figure 1.b

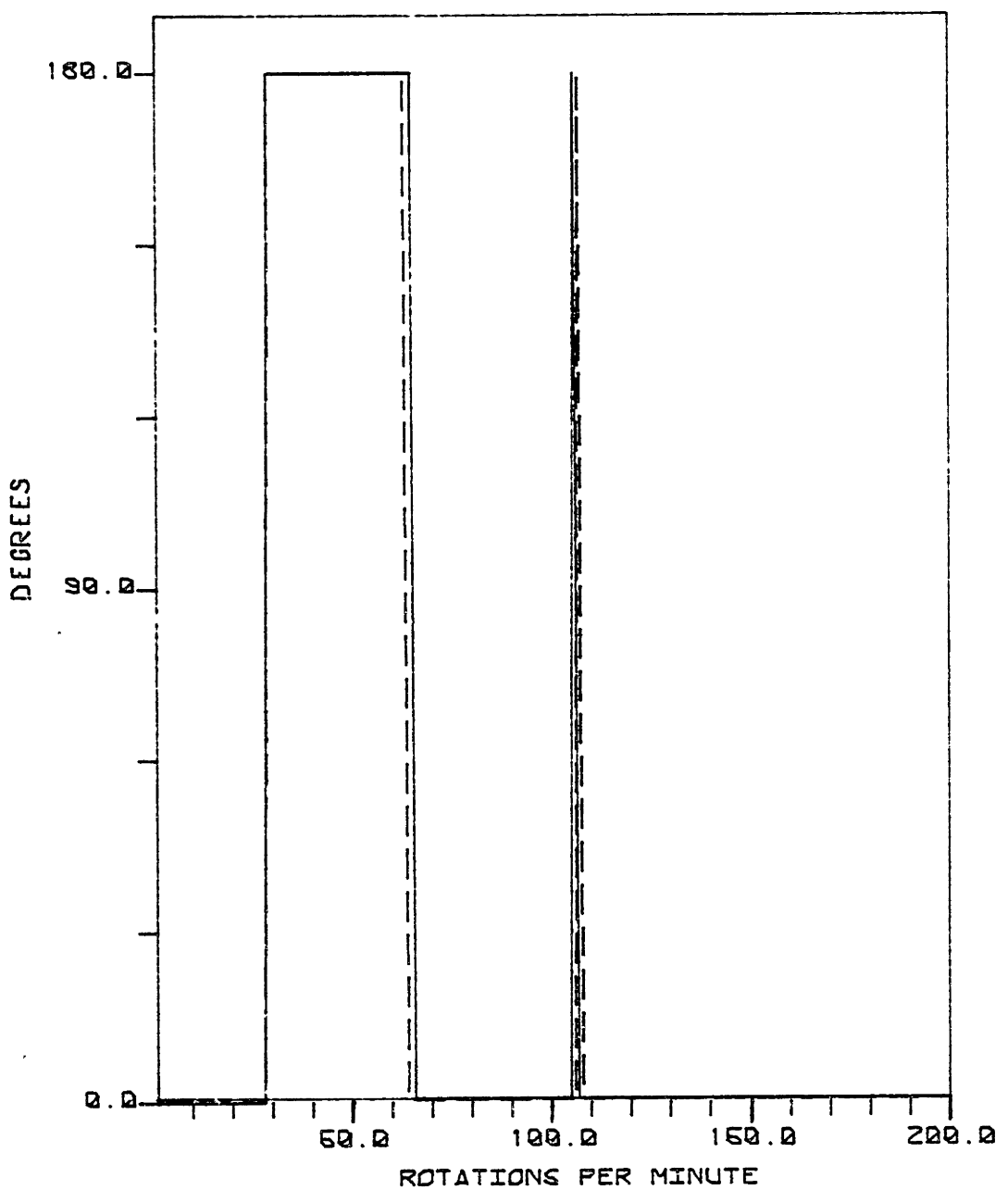

PHASE ANGLE OF FORCE: AT BIT ——
AT STABILIZER — —

Figure 1.c - Mode Shapes at Resonance

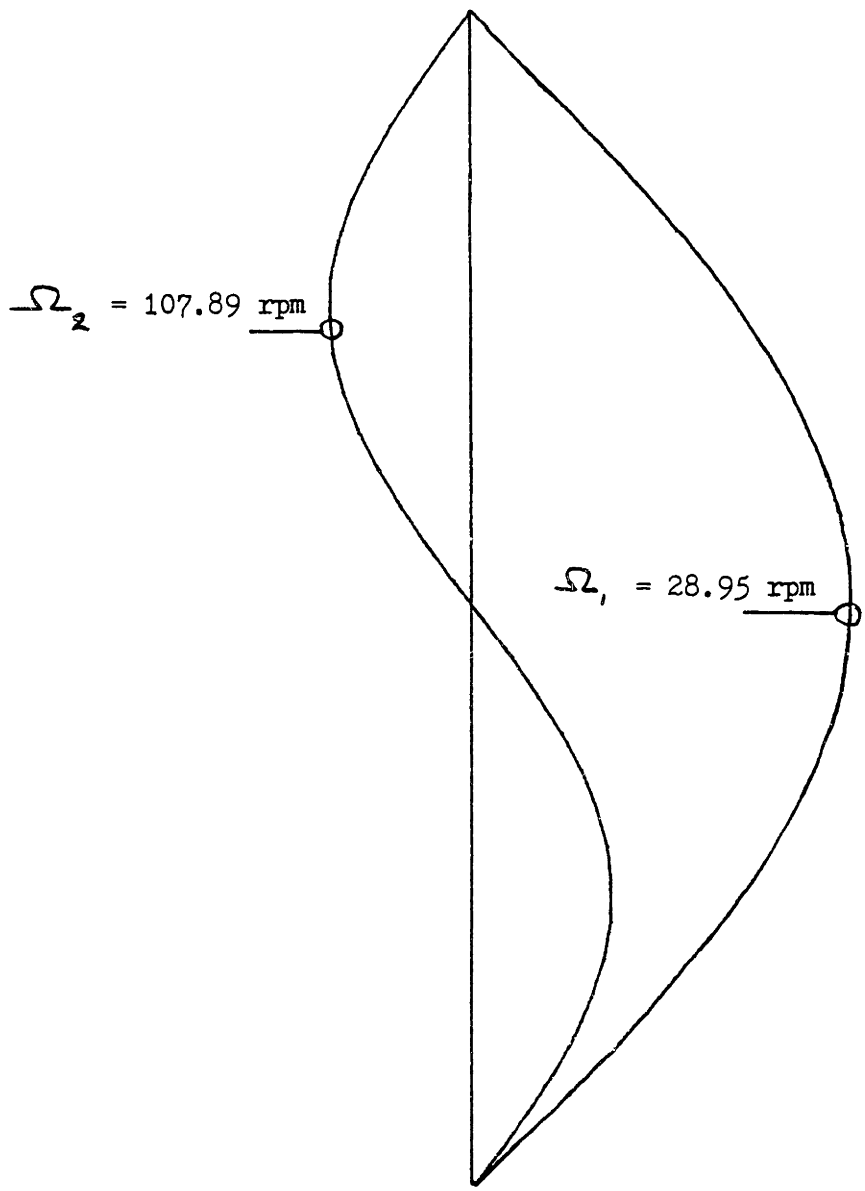

Figure 2.a - Testing of the Program COLLAR, c = 1

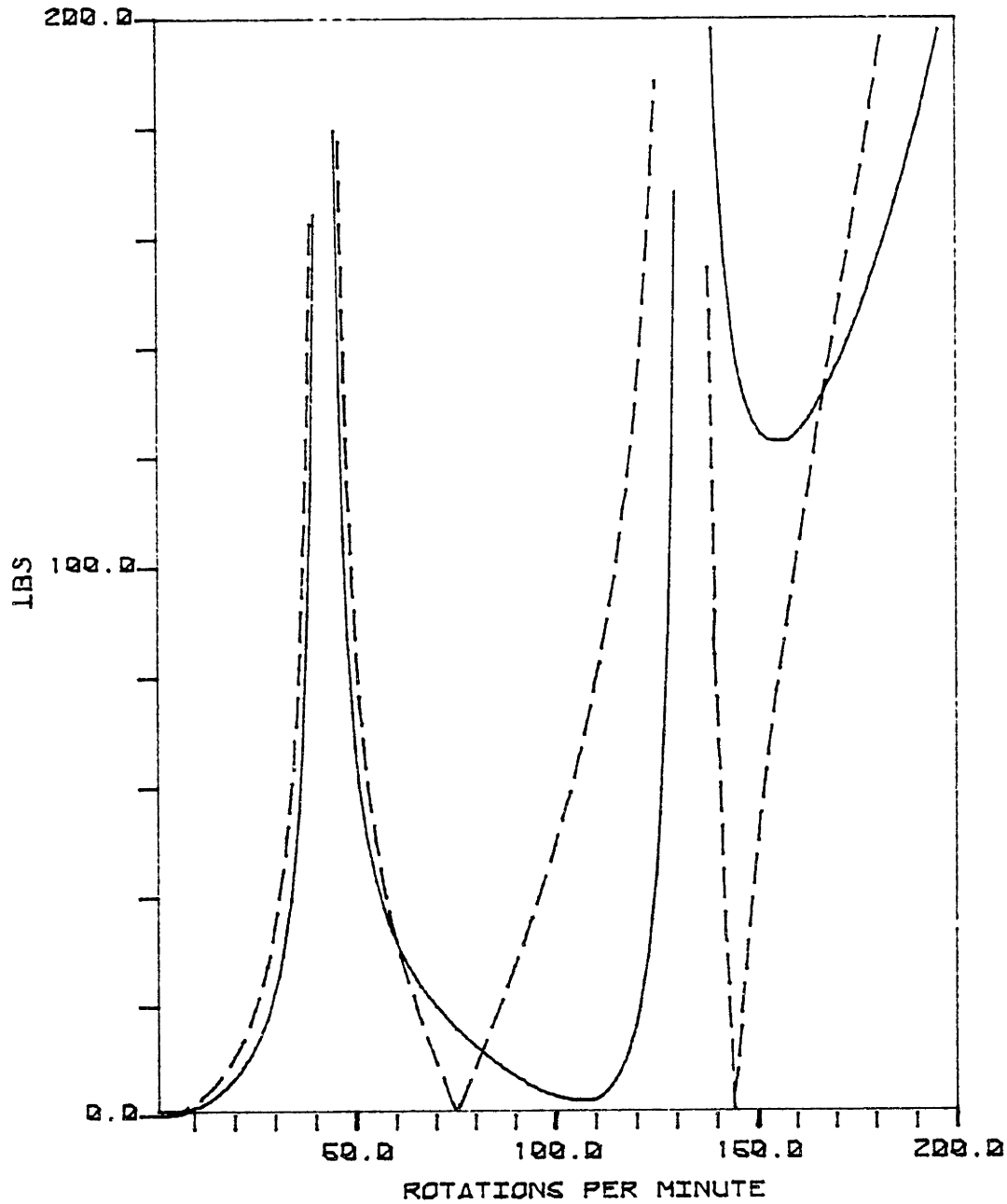

Figure 2.b

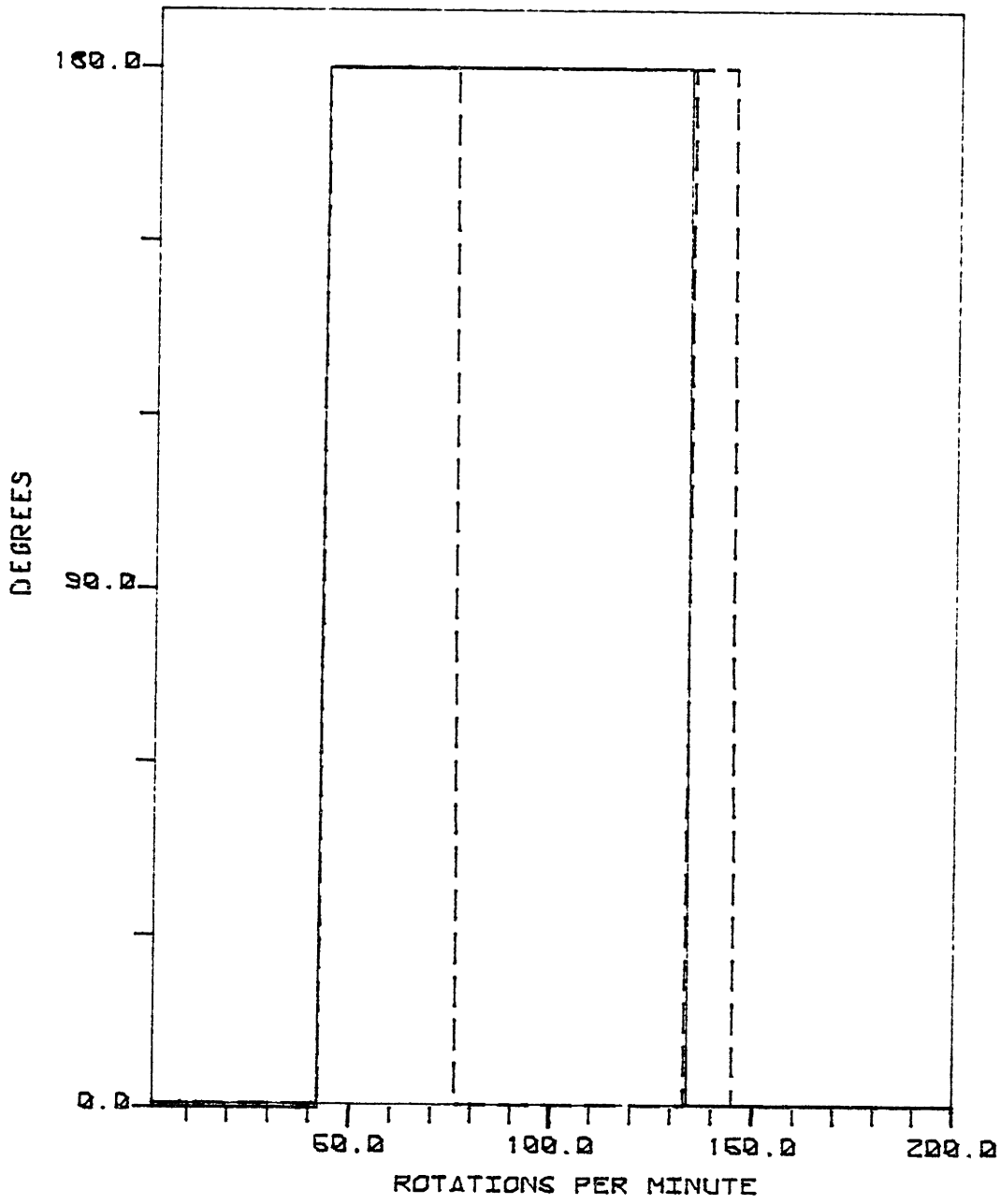

PHASE ANGLE OF FORCE: AT BIT ———
AT STABILIZER — —

Figure 2.c - Mode Shapes at Resonance.

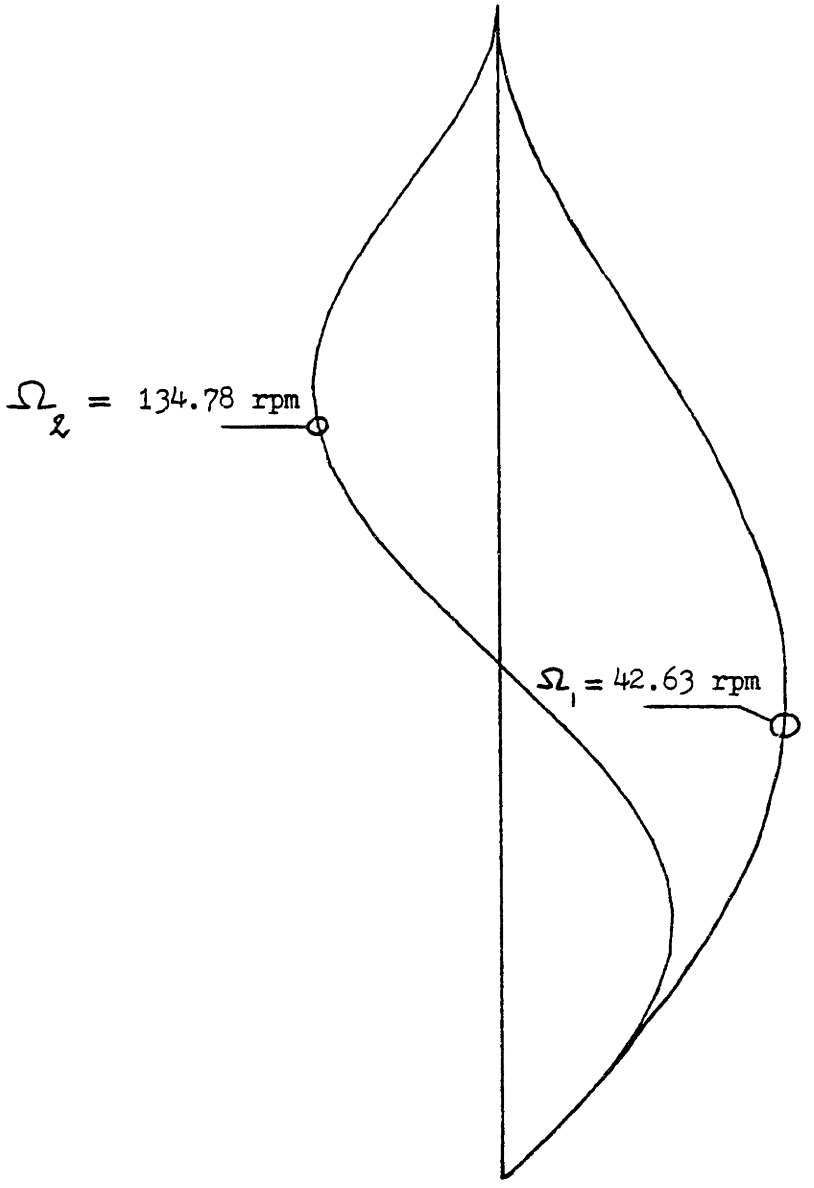

Fig. 3.a - Effect of Torque, Q = 10000 lbs.ft
c = 0

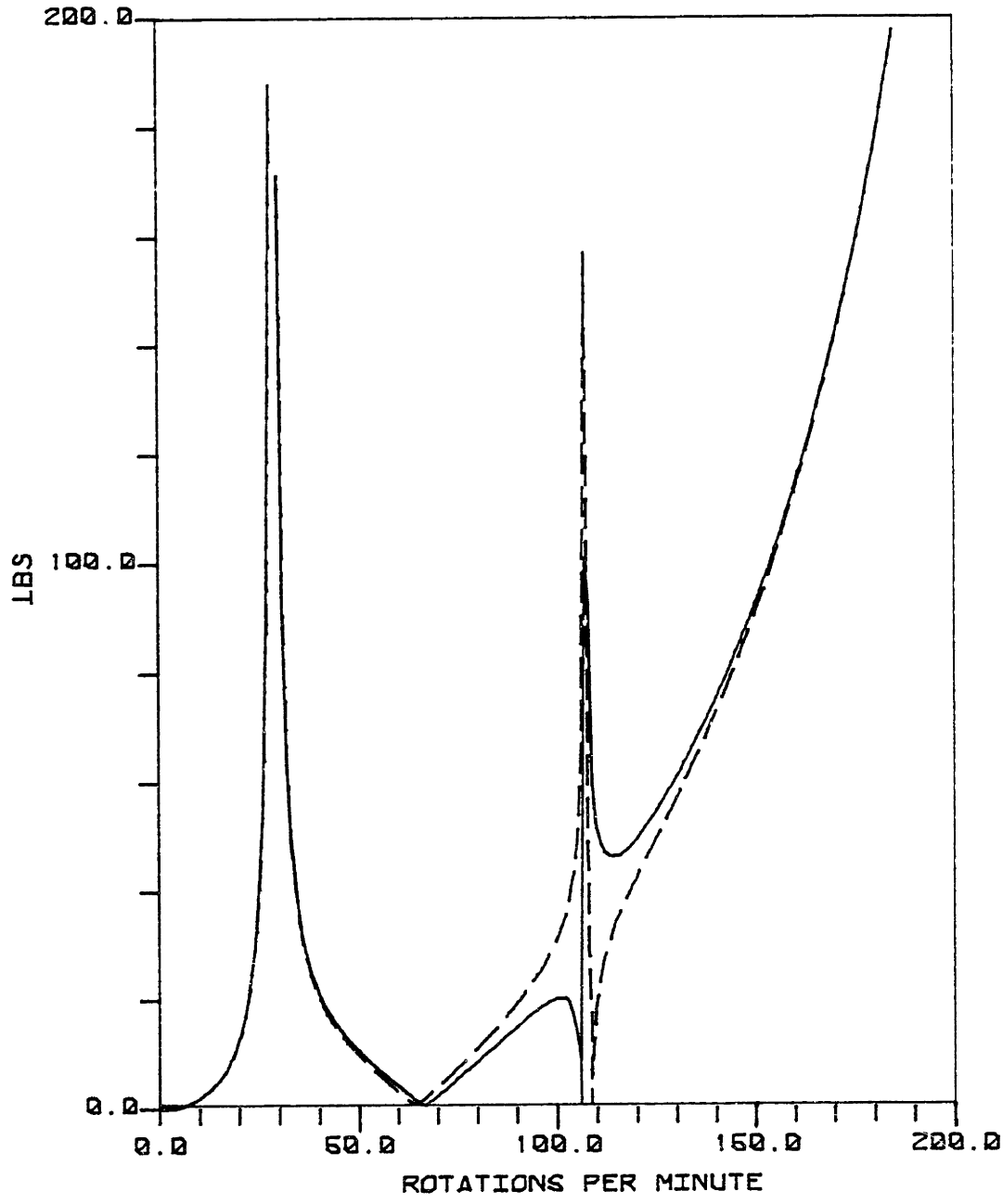

ROTATING SIDE-FORCE: AT BIT ———
AT STABILIZER – – –

Figure 3.b

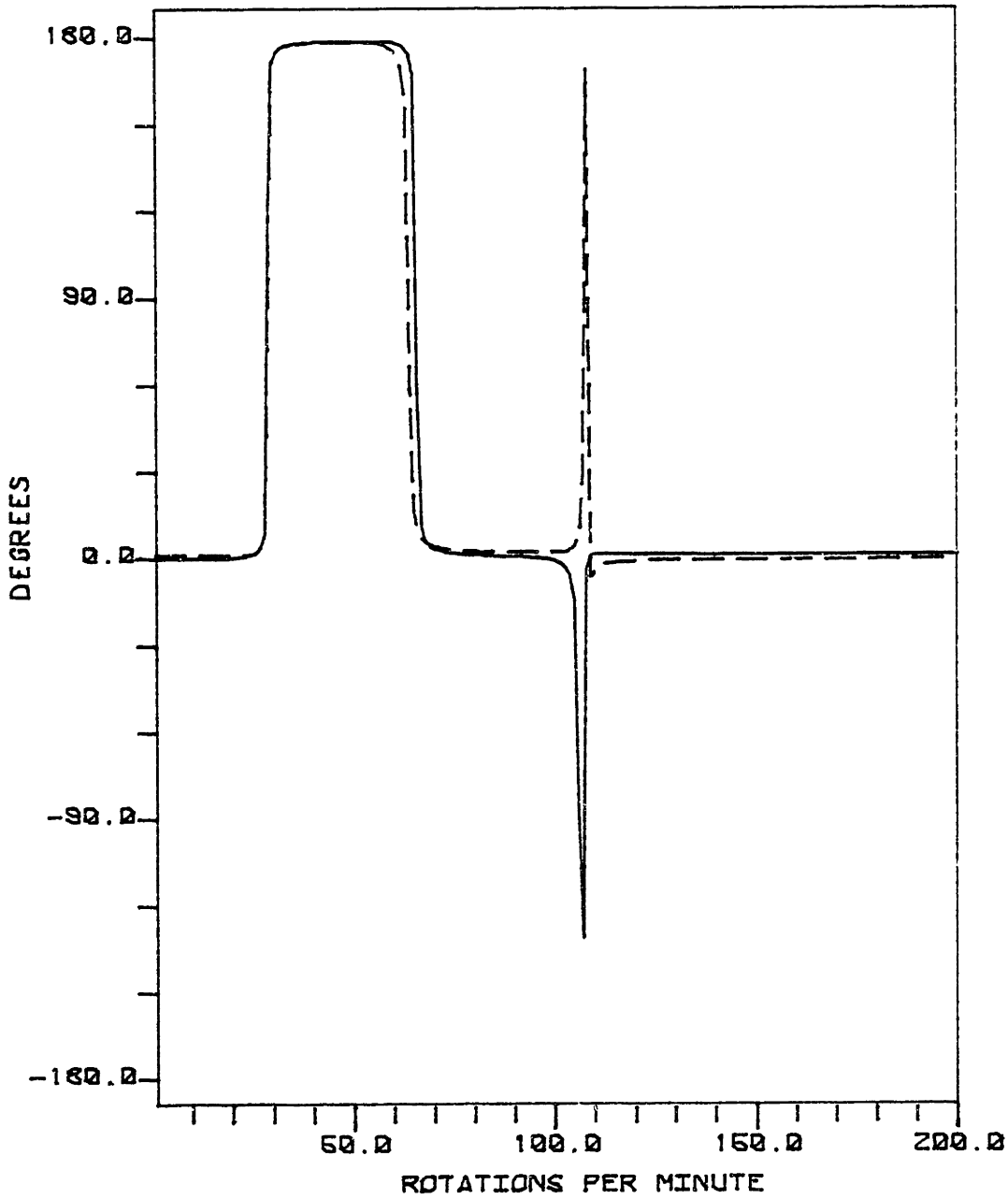

PHASE ANGLE OF FORCE: AT BIT ———
AT STABILIZER – – –

Figure 4.a - Effect of Torque, Q = 10000 lbs.ft
c = 1

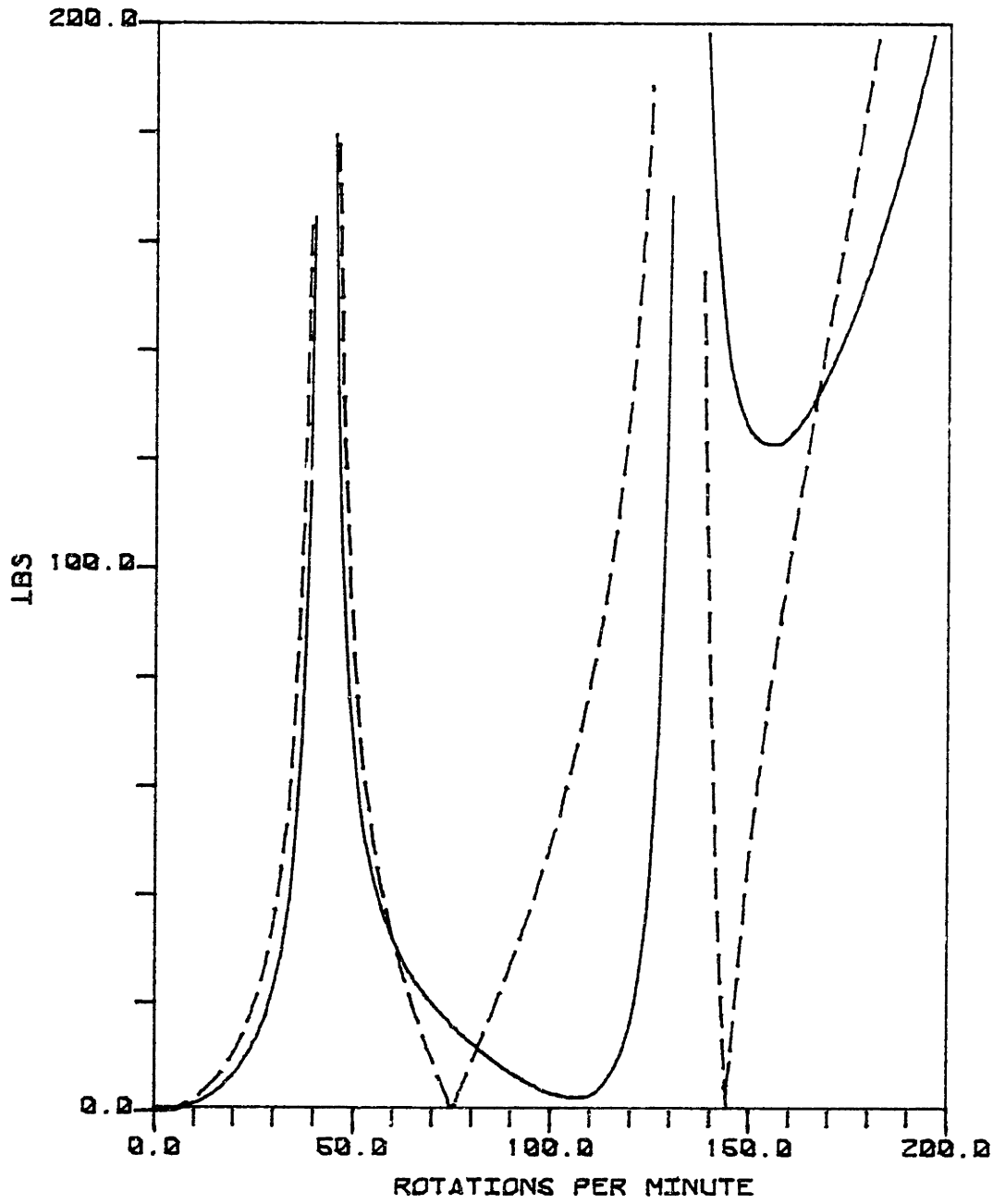

ROTATING SIDE-FORCE: AT BIT ———
AT STABILIZER — — —

Figure 4.b

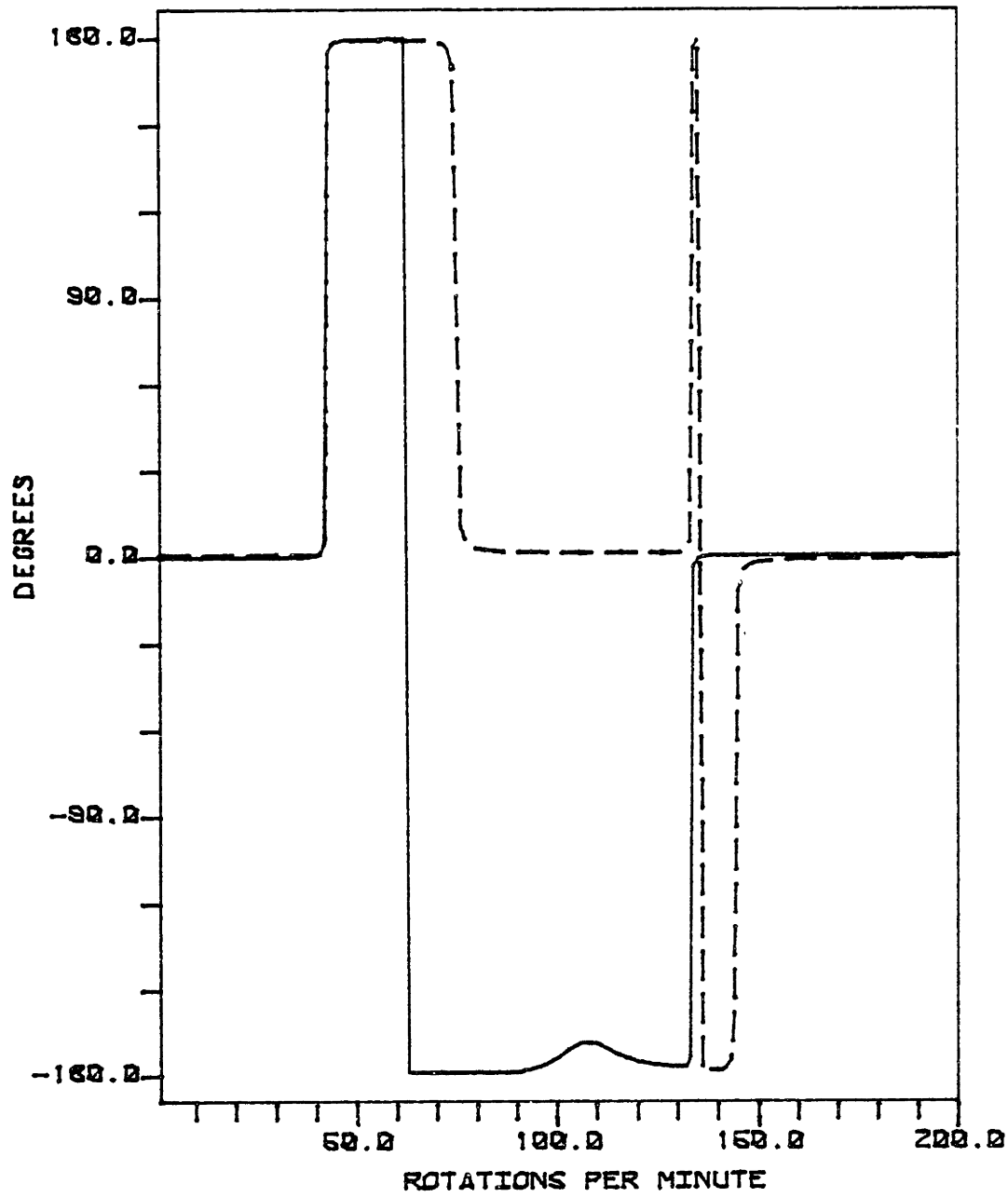

PHASE ANGLE OF FORCE: AT BIT ———
AT STABILIZER – – –

Figure 5.a - Effect of Torque, Q = 10^6 lbs.ft

c = 1

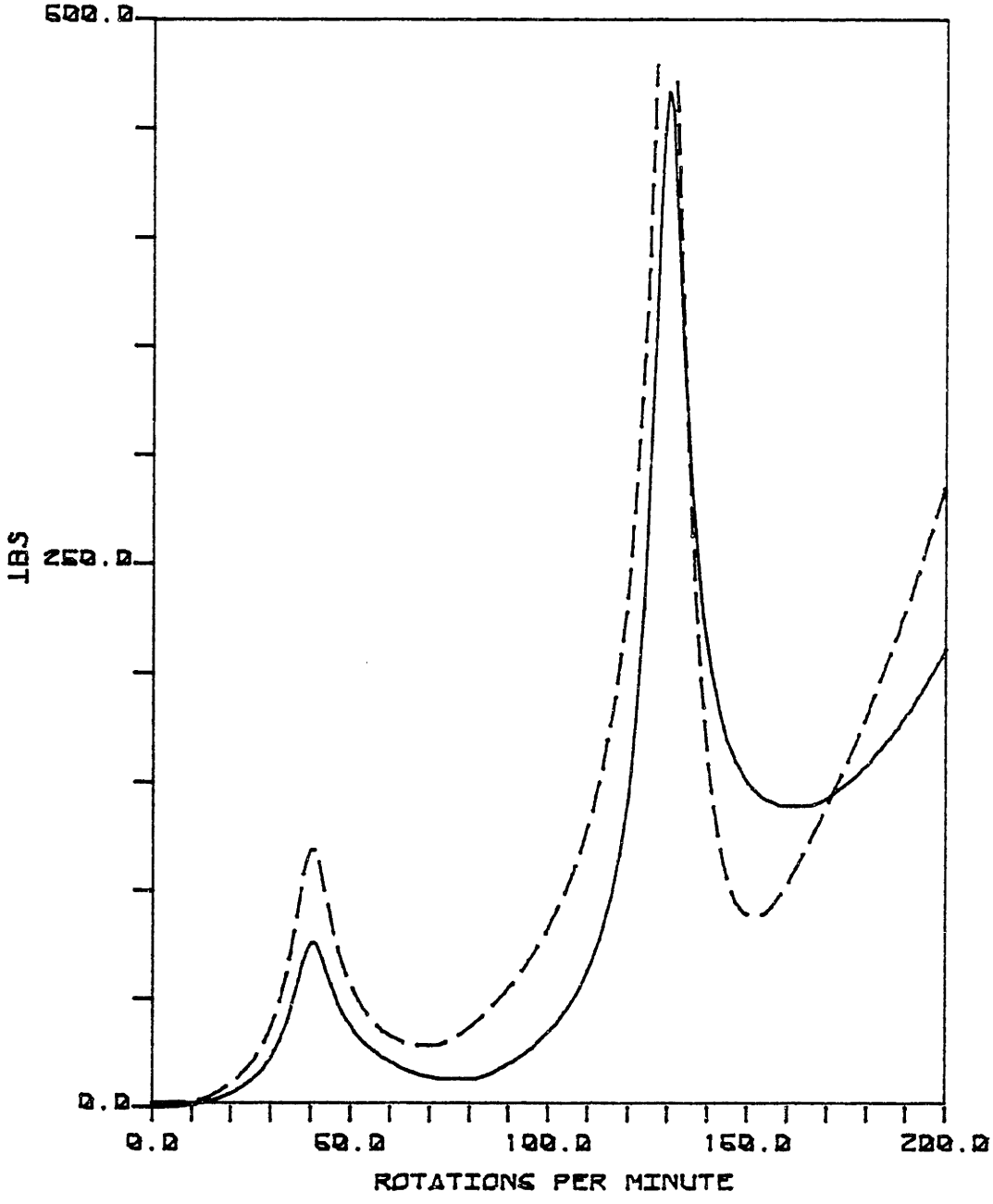

ROTATING SIDE-FORCE: AT BIT ———

AT STABILIZER — —

Figure 5.b

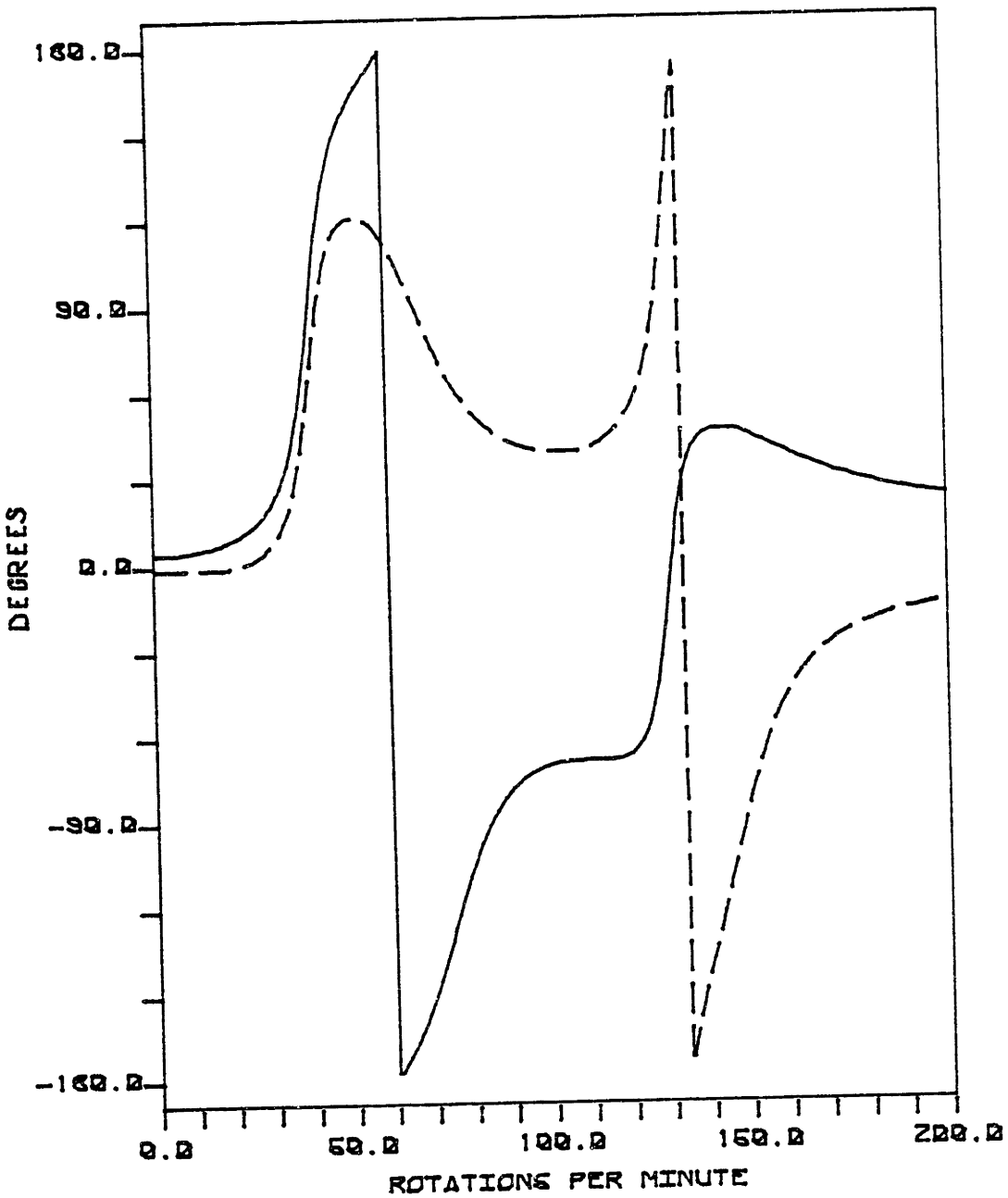

PHASE ANGLE OF FORCE: AT BIT ———
AT STABILIZER — —

Figure 6.a - Effect of Torque, Q = $2*10^6$ lbs.ft
c = 1

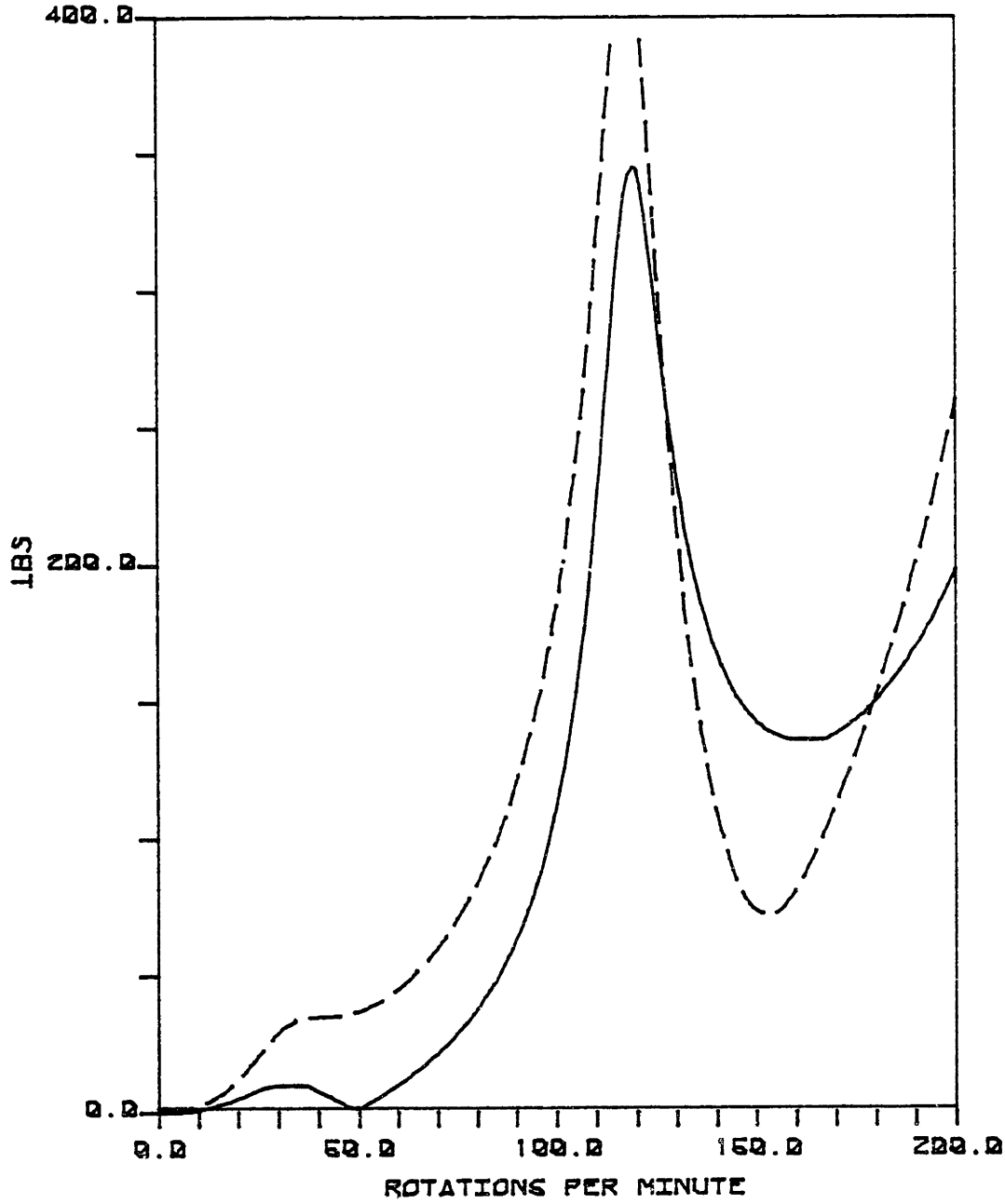

Figure 6.b

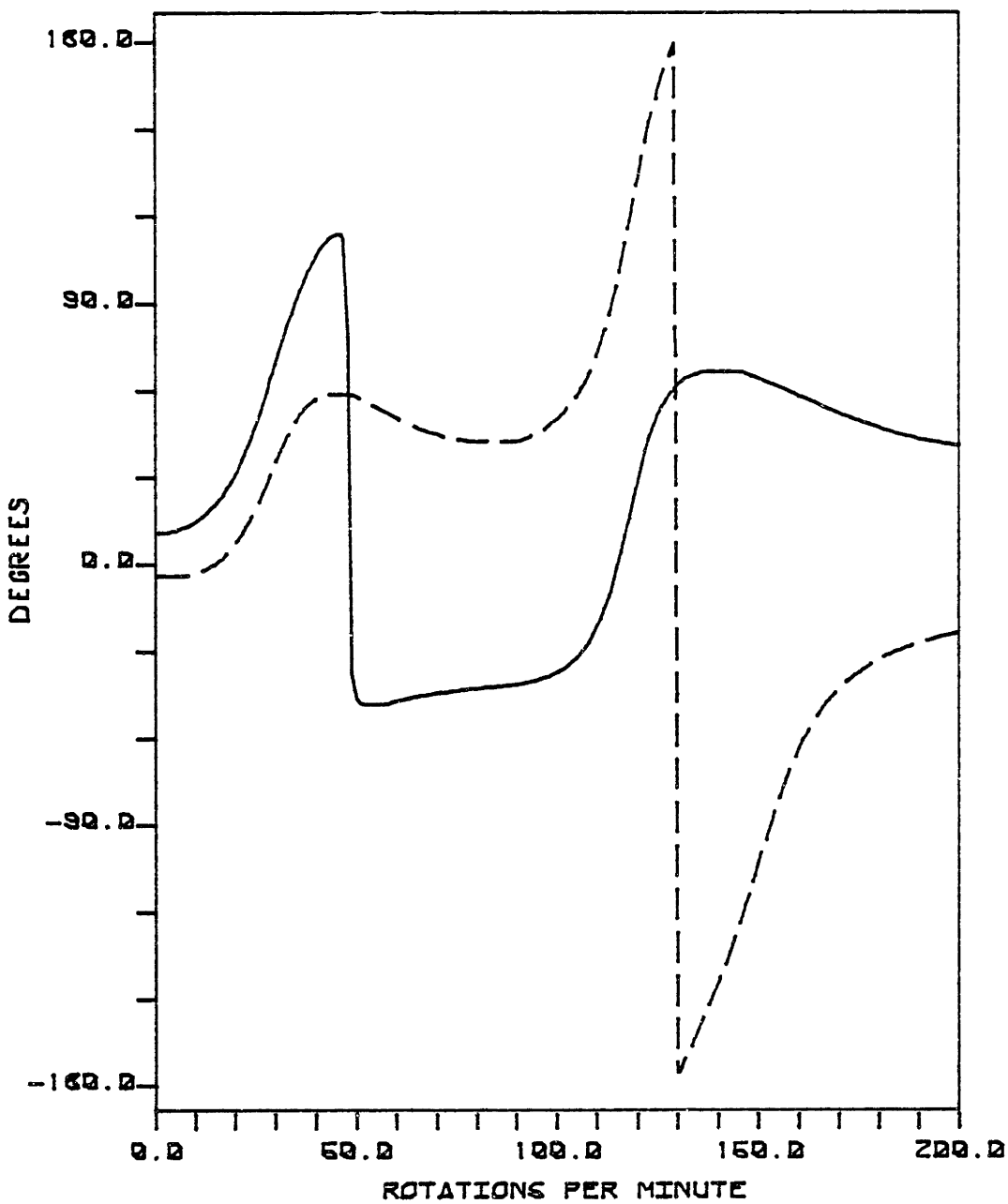
160.0
90.0
0.0
-90.0
-160.0
DEGREES
0.0
50.0
100.0
150.0
200.0
ROTATIONS PER MINUTE
PHASE ANGLE OF FORCE: AT BIT
AT STABILIZER

Figure 7.a - Effect of Weight on Bit
and Boundary Conditions at Stabilizer.

W_b = 10000 lbs
c = 1

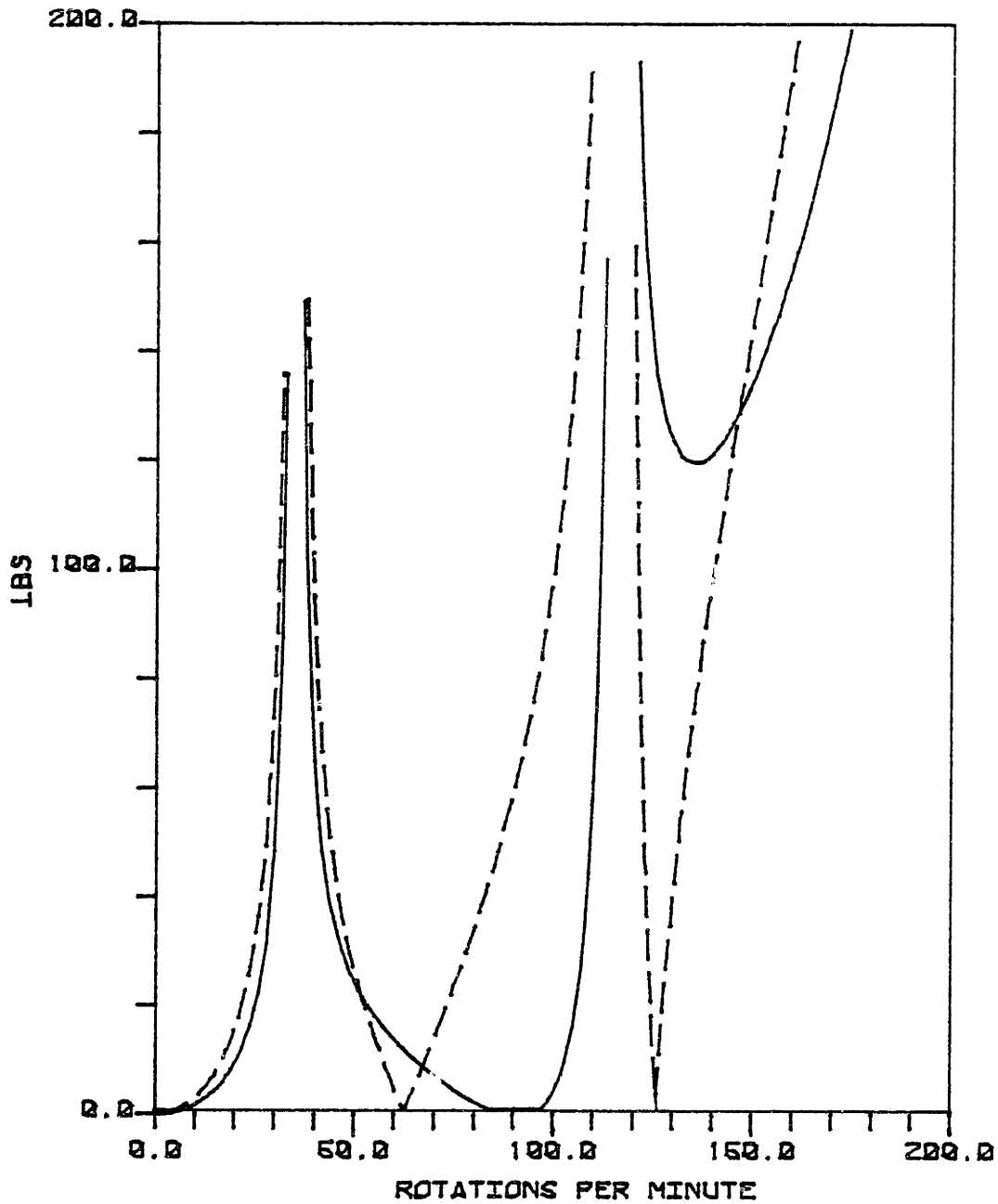

Figure 7.b

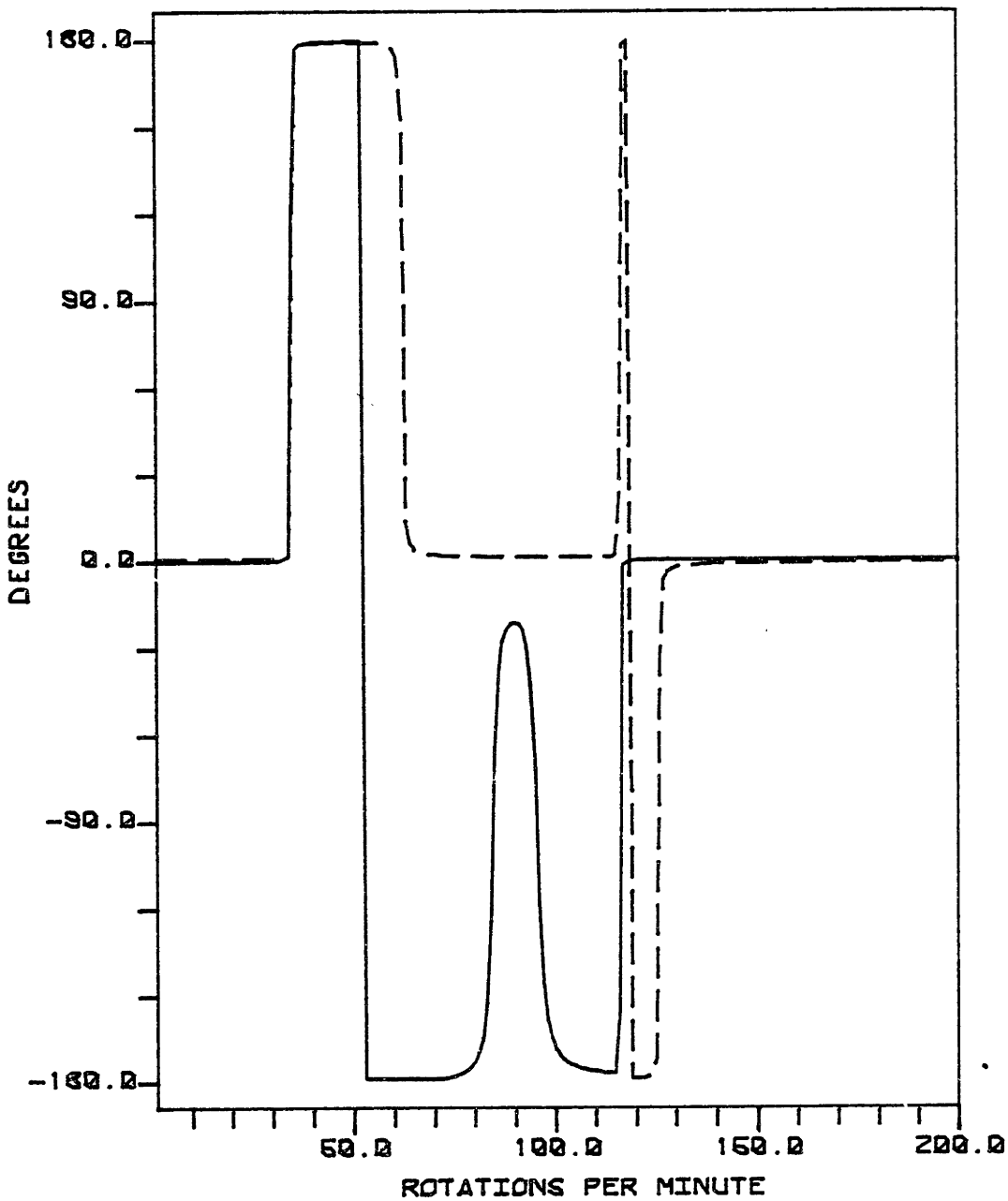

PHASE ANGLE OF FORCE: AT BIT ——
AT STABILIZER — — —

Figure 8.a - Effect of Weight on Bit and
Boundary Conditions at Stabilizer.

W_b = 30000 lbs
c = 1

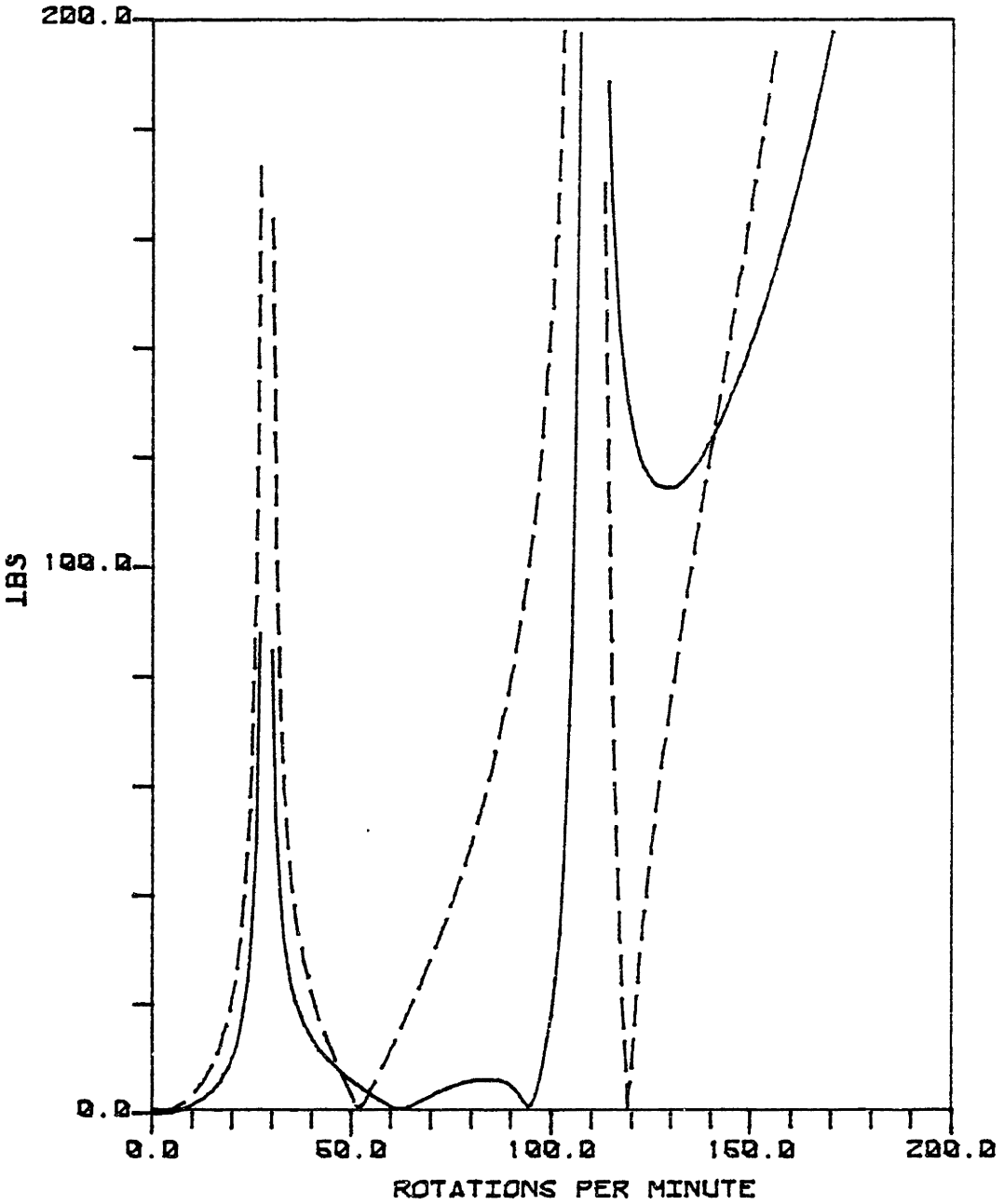

ROTATING SIDE-FORCE: AT BIT ———
AT STABILIZER — — —

Figure 8.b

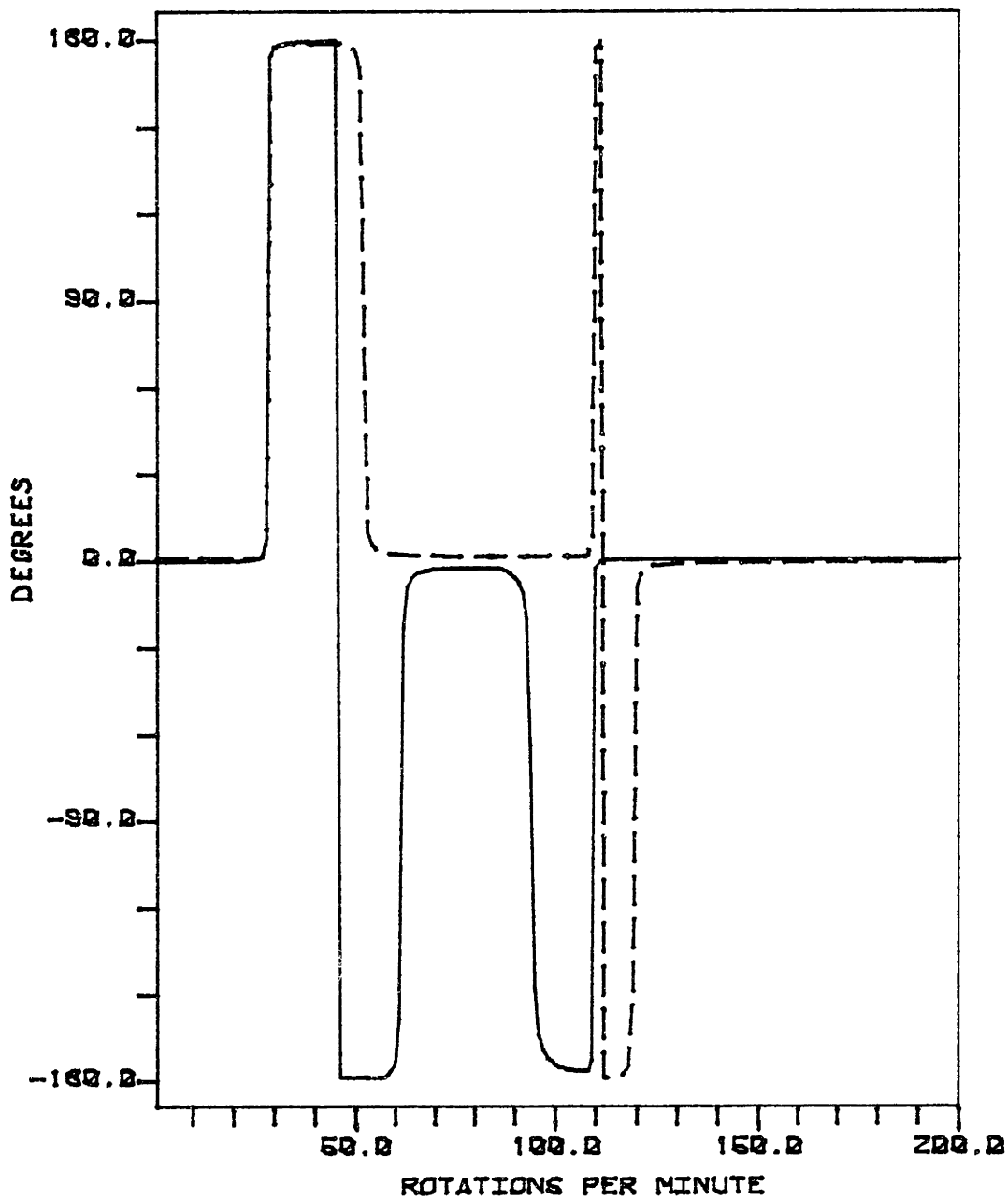

PHASE ANGLE OF FORCE: AT BIT ———
AT STABILIZER — — —

Figure 9.a - Effect of Weight on Bit and

Boundary Conditions at Stabilizer.

W_b = 60000 lbs

c = 1

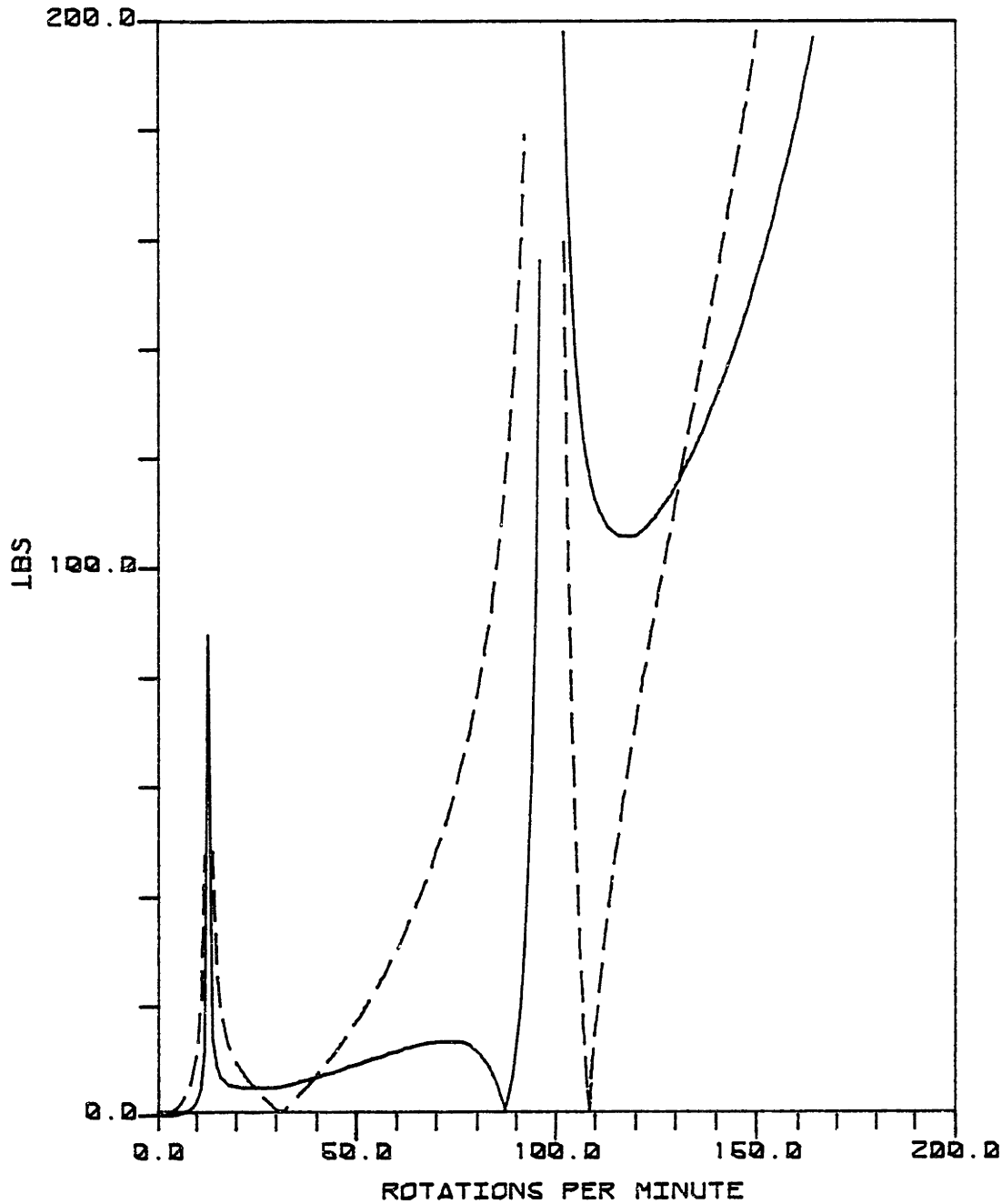

ROTATING SIDE-FORCE: AT BIT ———

AT STABILIZER — — —

Figure 9.b

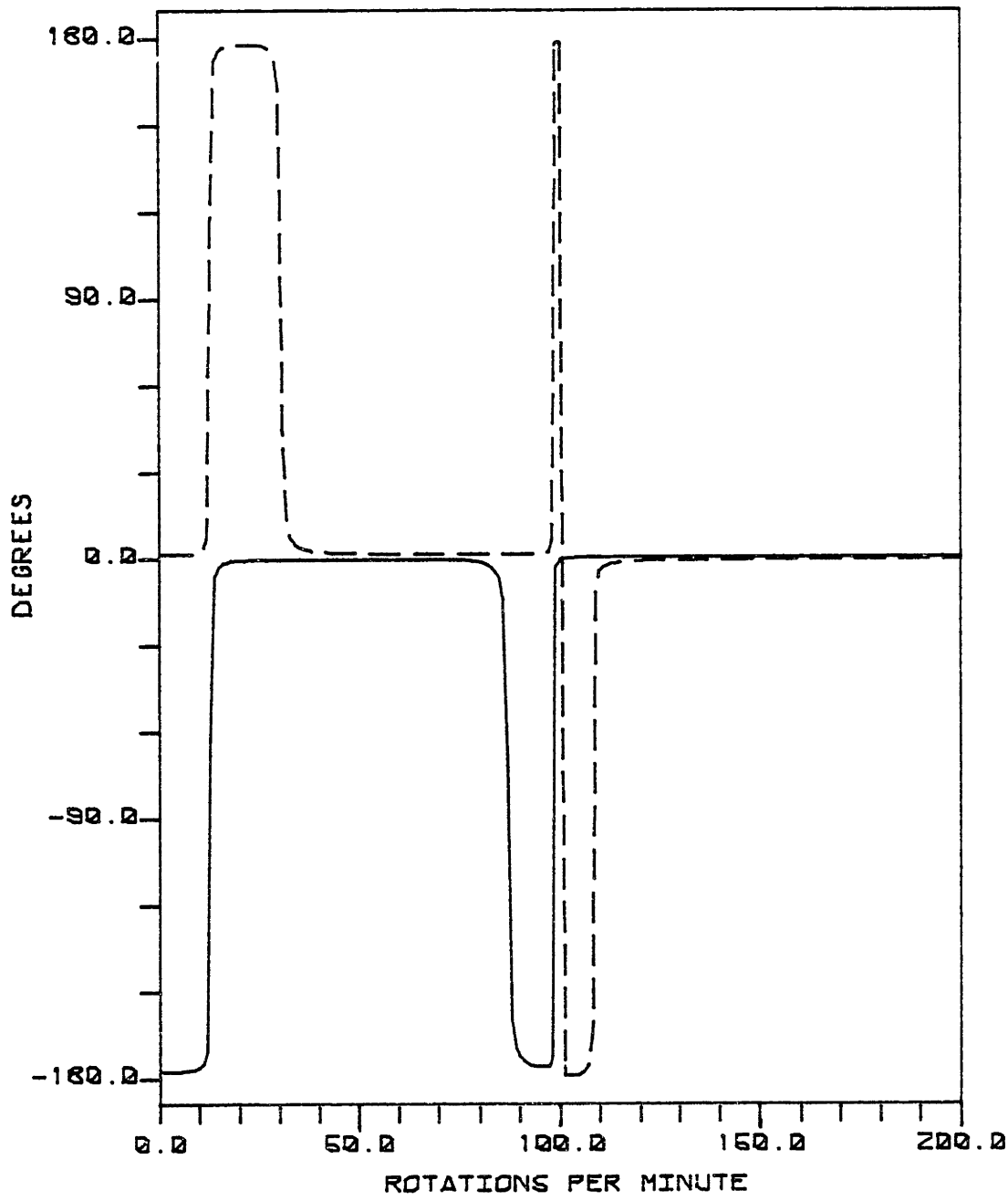
180.0
90.0
0.0
-90.0
-180.0
DEGREES
0.0
50.0
100.0
150.0
200.0
ROTATIONS PER MINUTE
PHASE ANGLE OF FORCE: AT BIT
AT STABILIZER

Figure 10.a - Effect of Weight on Bit and
Boundary Conditions at Stabilizer.

W_b = 10000 lbs

c = 0

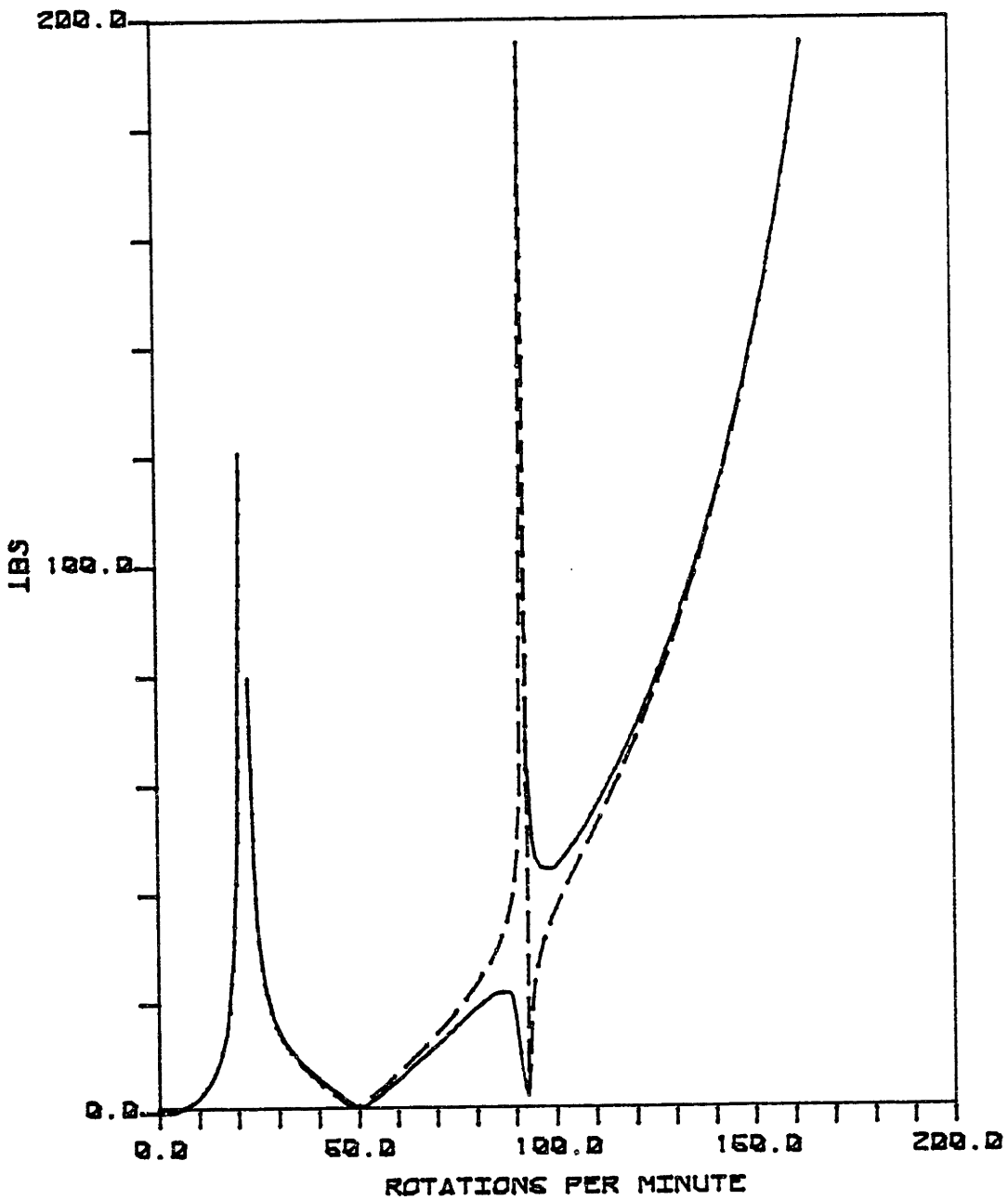

ROTATING SIDE-FORCE: AT BIT ————
AT STABILIZER — — —

Figure 10.b

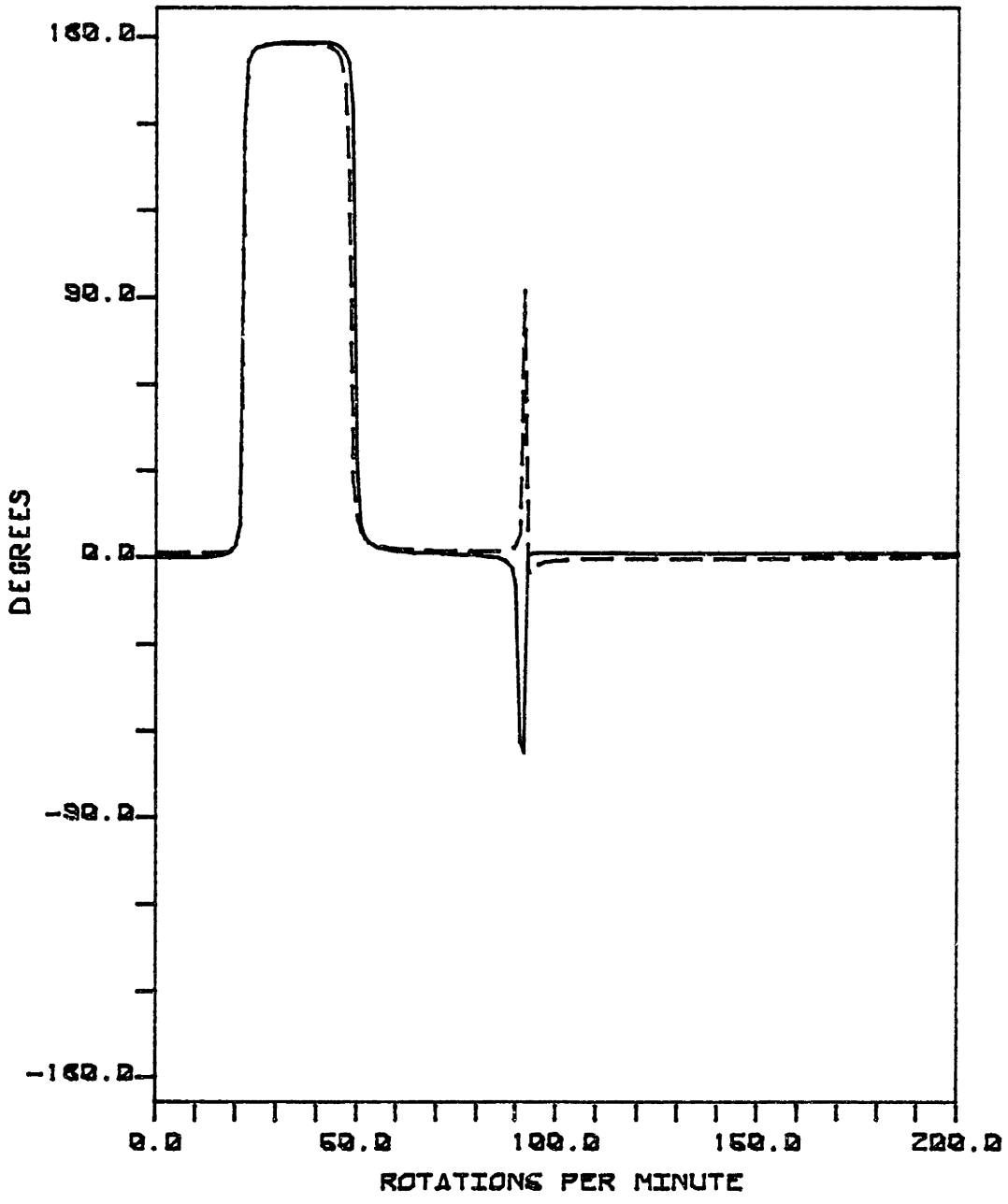

PHASE ANGLE OF FORCE: AT BIT ————
AT STABILIZER — — —

Figure 11.a - Effect of Weight on Bit and
Boundary Conditions at Stabilizer.

W_b = 30000 lbs
c = 0

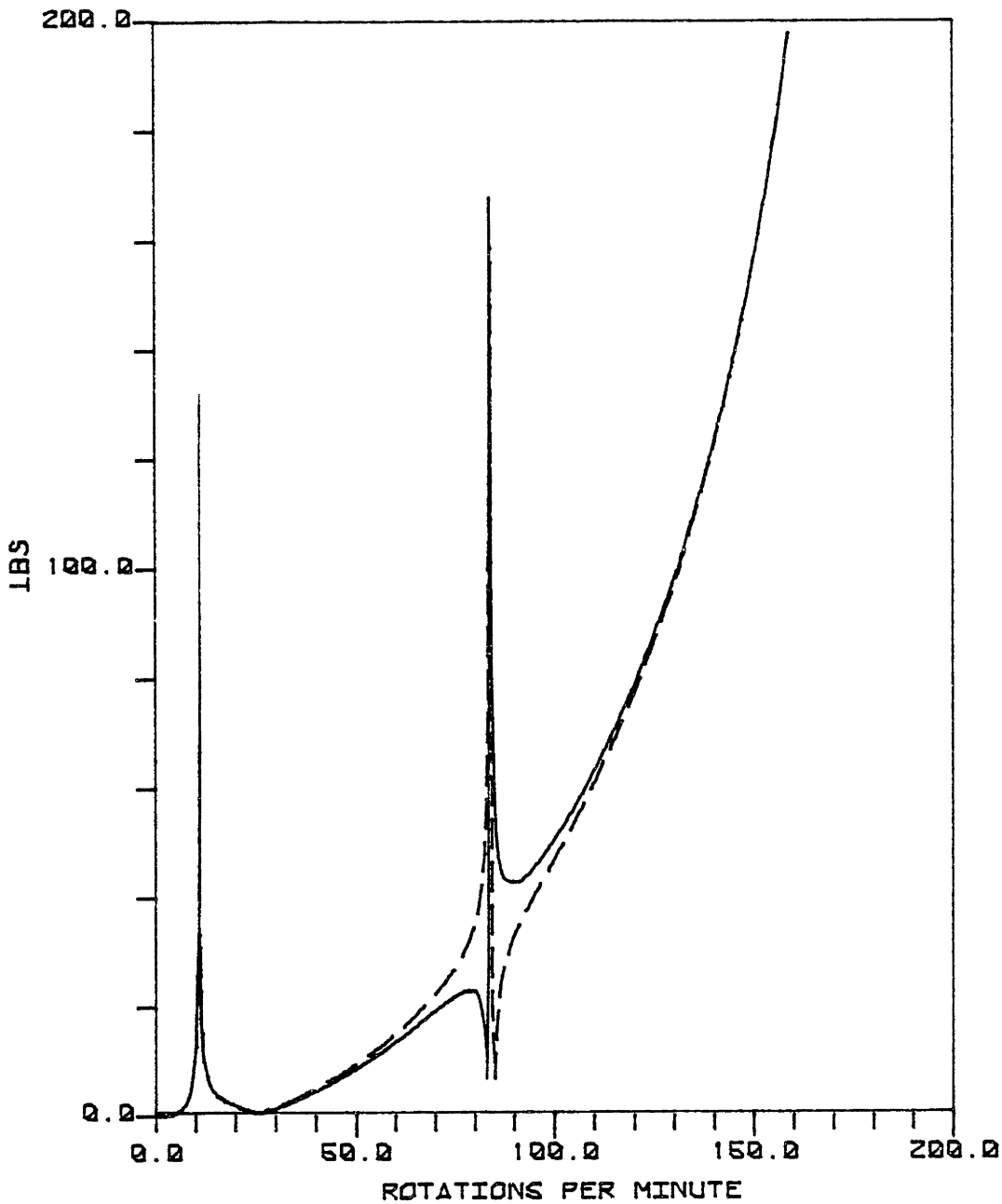

ROTATING SIDE-FORCE: AT BIT ———
AT STABILIZER — — —

Figure 11.b

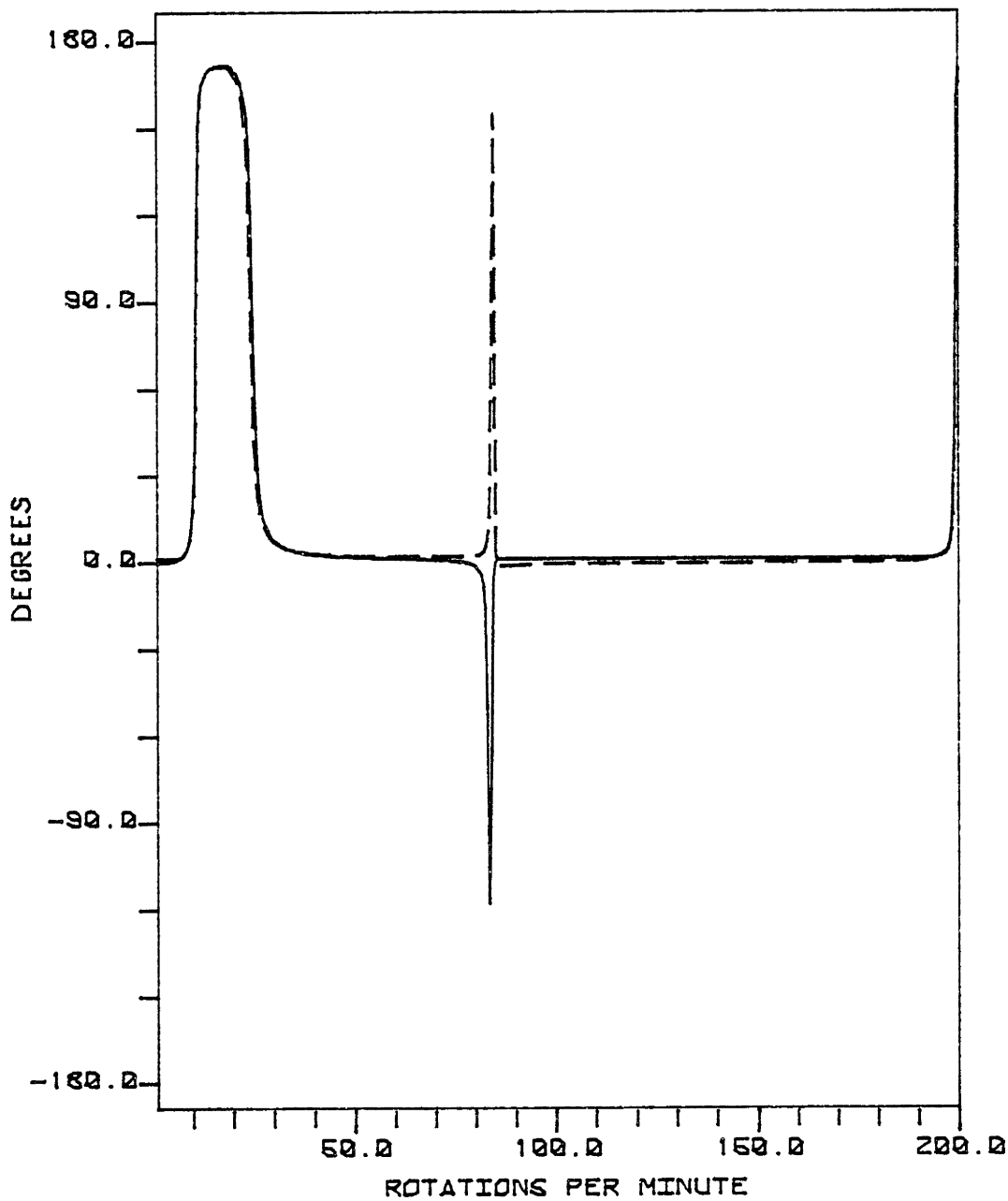

PHASE ANGLE OF FORCE: AT BIT ———
AT STABILIZER — — —

Figure 12.a - Effect of Mud Damping.

C_e = 0.8 lbs/($\frac{ft}{sec}$)/ft of pipe

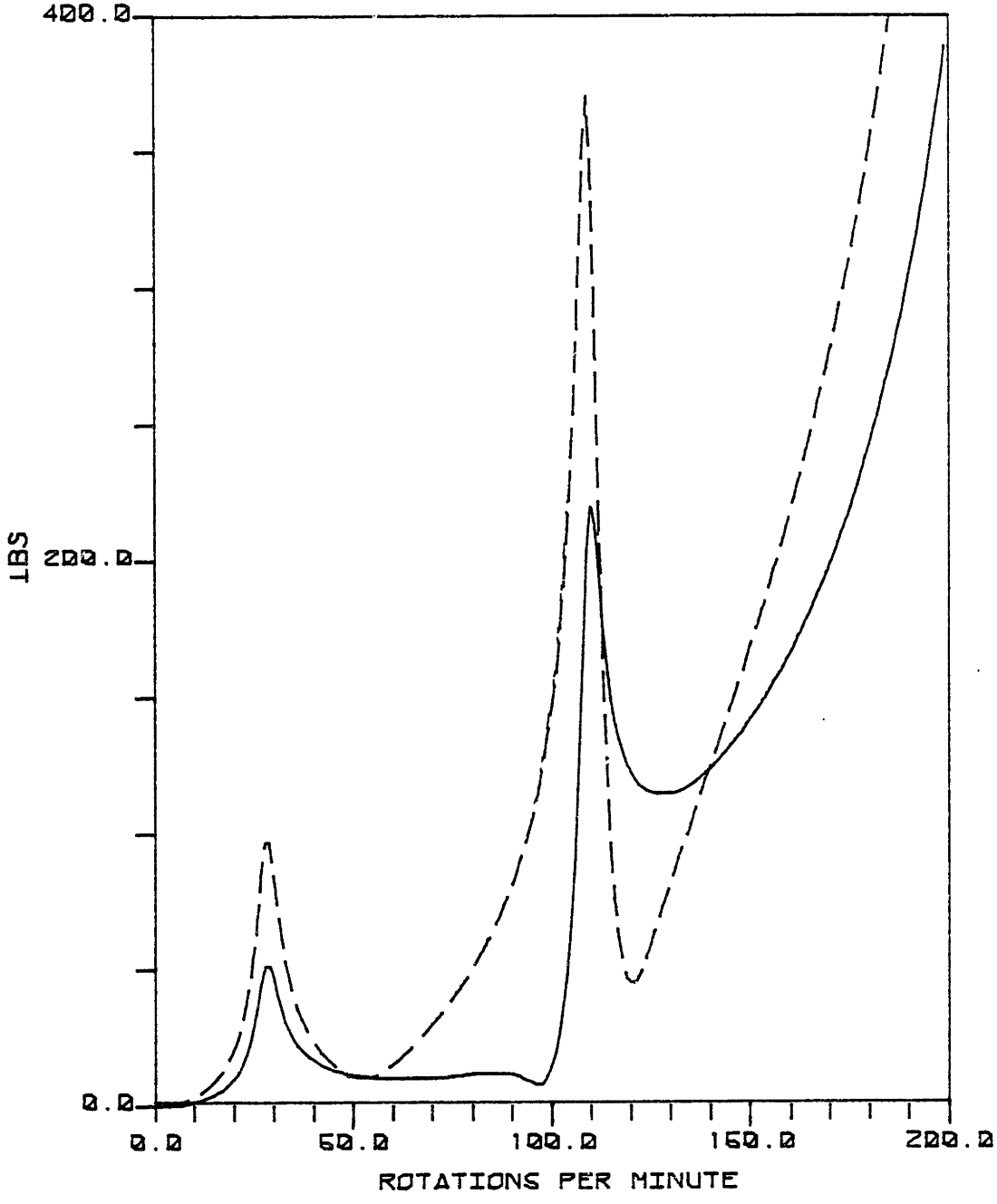

Figure 12.b

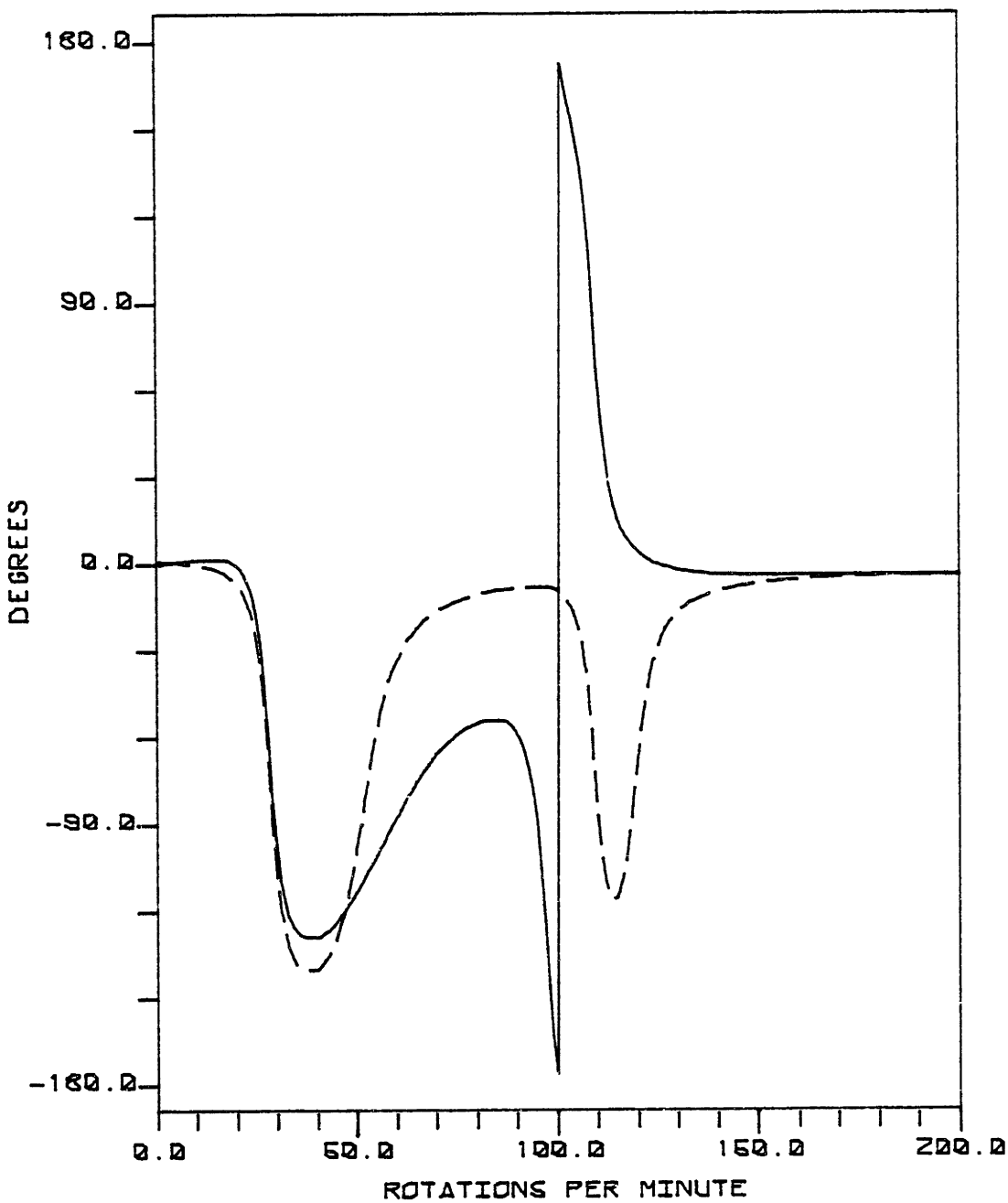

PHASE ANGLE OF FORCE: AT BIT ———
AT STABILIZER — — —

Figure 13.a - Effect of Bit Embedding, k' = 15 inches
W_b = 30000 lbs
c = 0

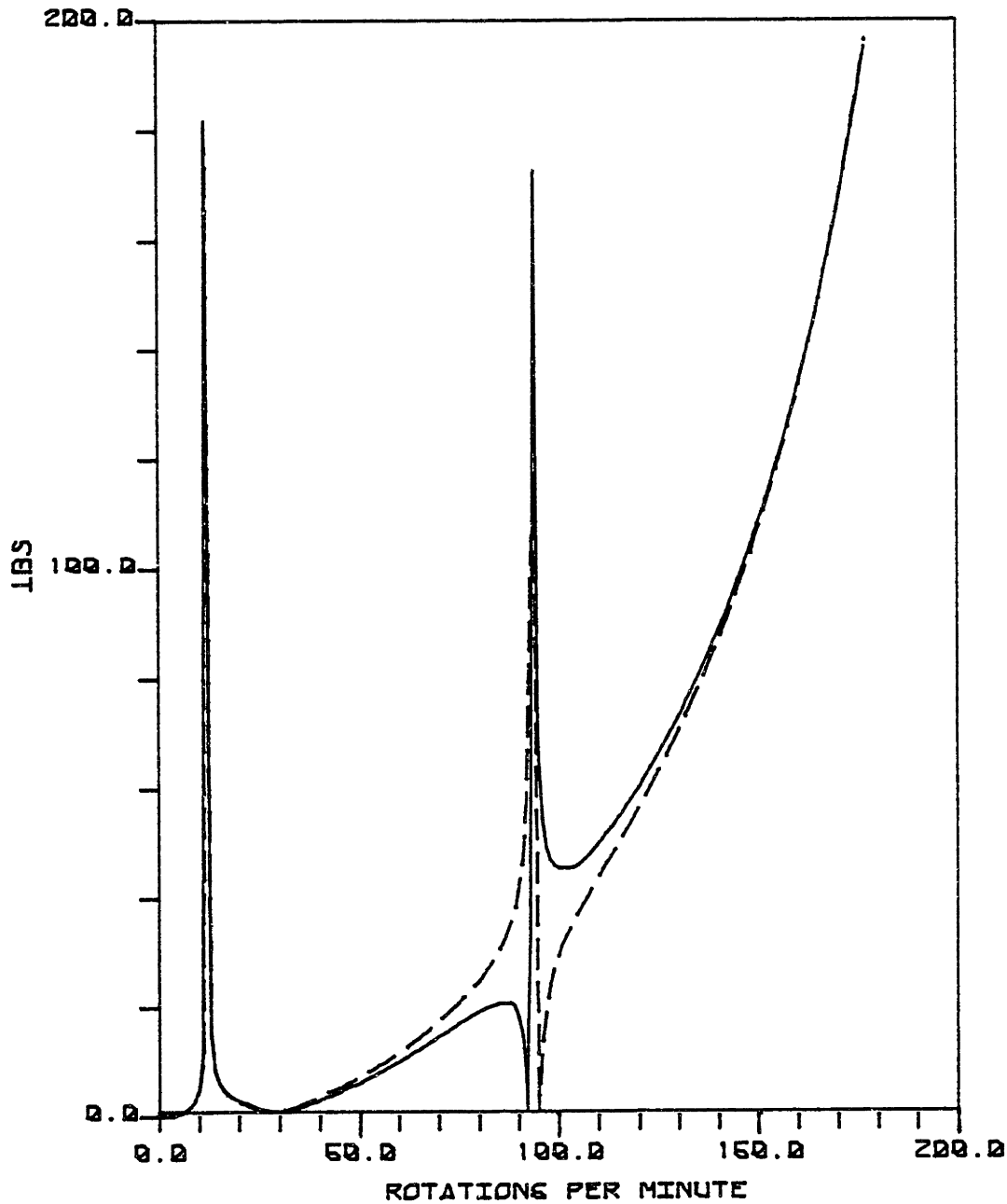

ROTATING SIDE-FORCE: AT BIT ———
AT STABILIZER — — —

Figure 13.b

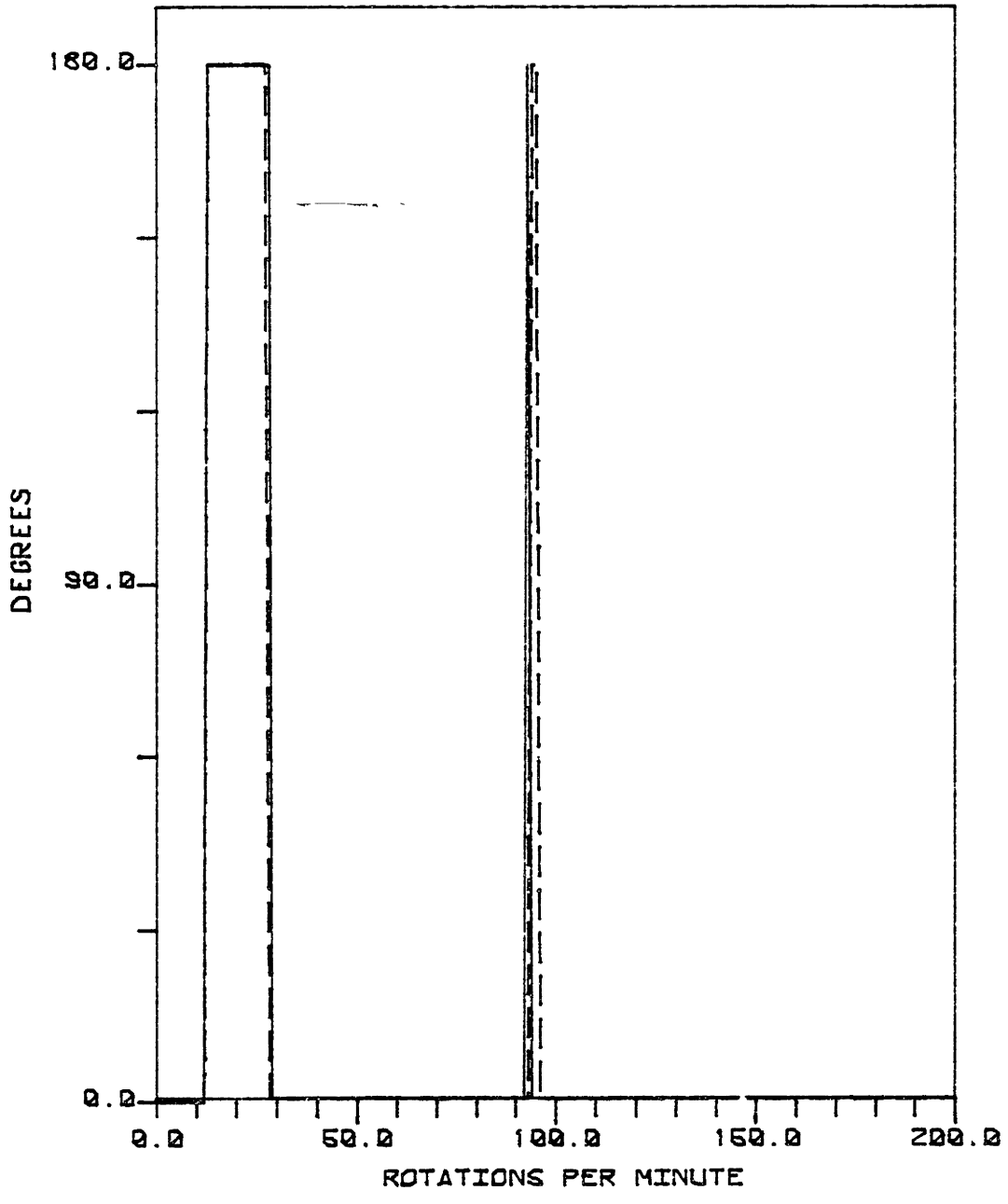

PHASE ANGLE OF FORCE: AT BIT ———
AT STABILIZER — — —

Figure 14.a - Effect of Bit Embedding, k' = 1000 inches
W_b = 30000 lbs
c = 0

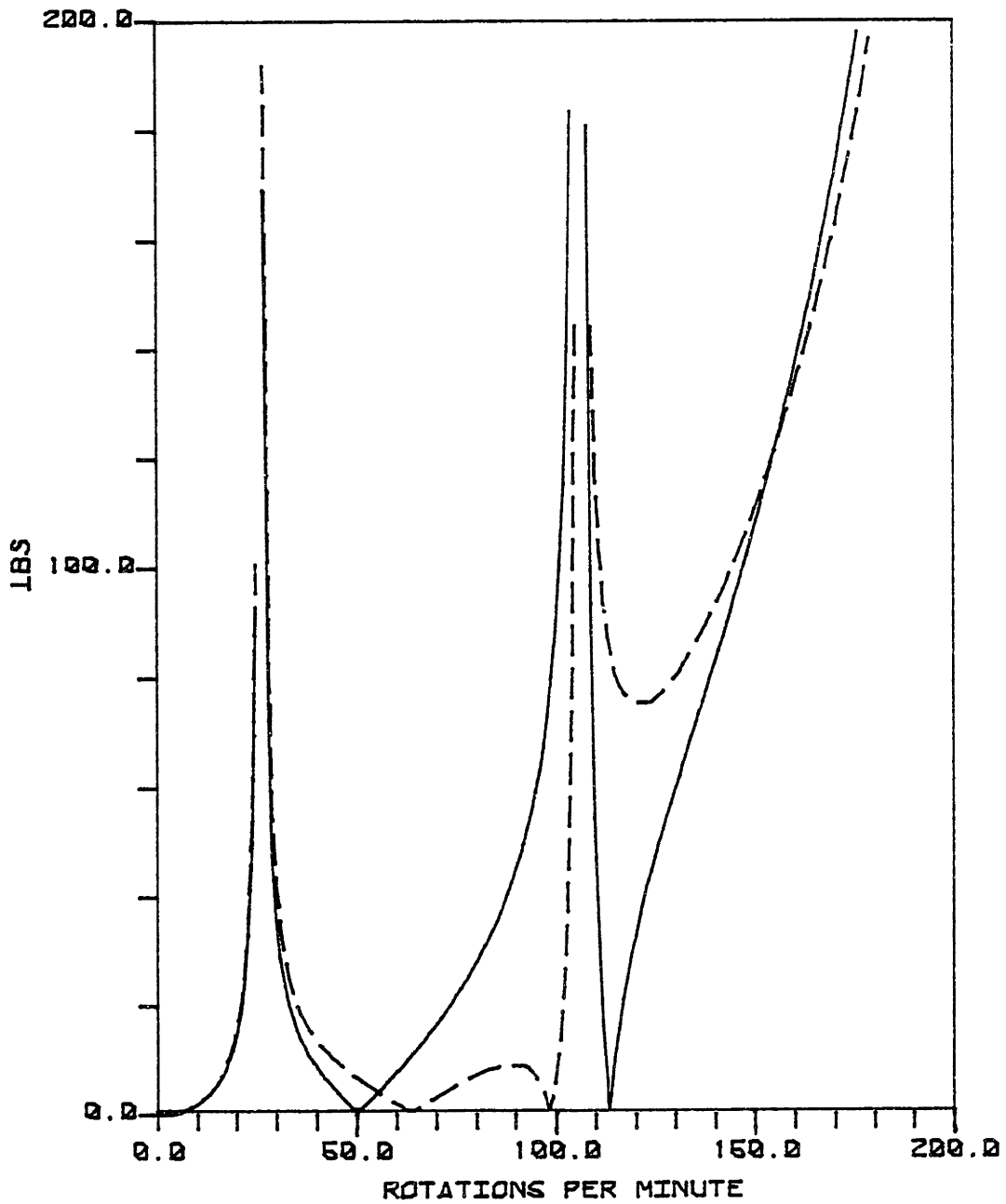

ROTATING SIDE-FORCE: AT BIT ———
AT STABILIZER — — —

Figure 14.b

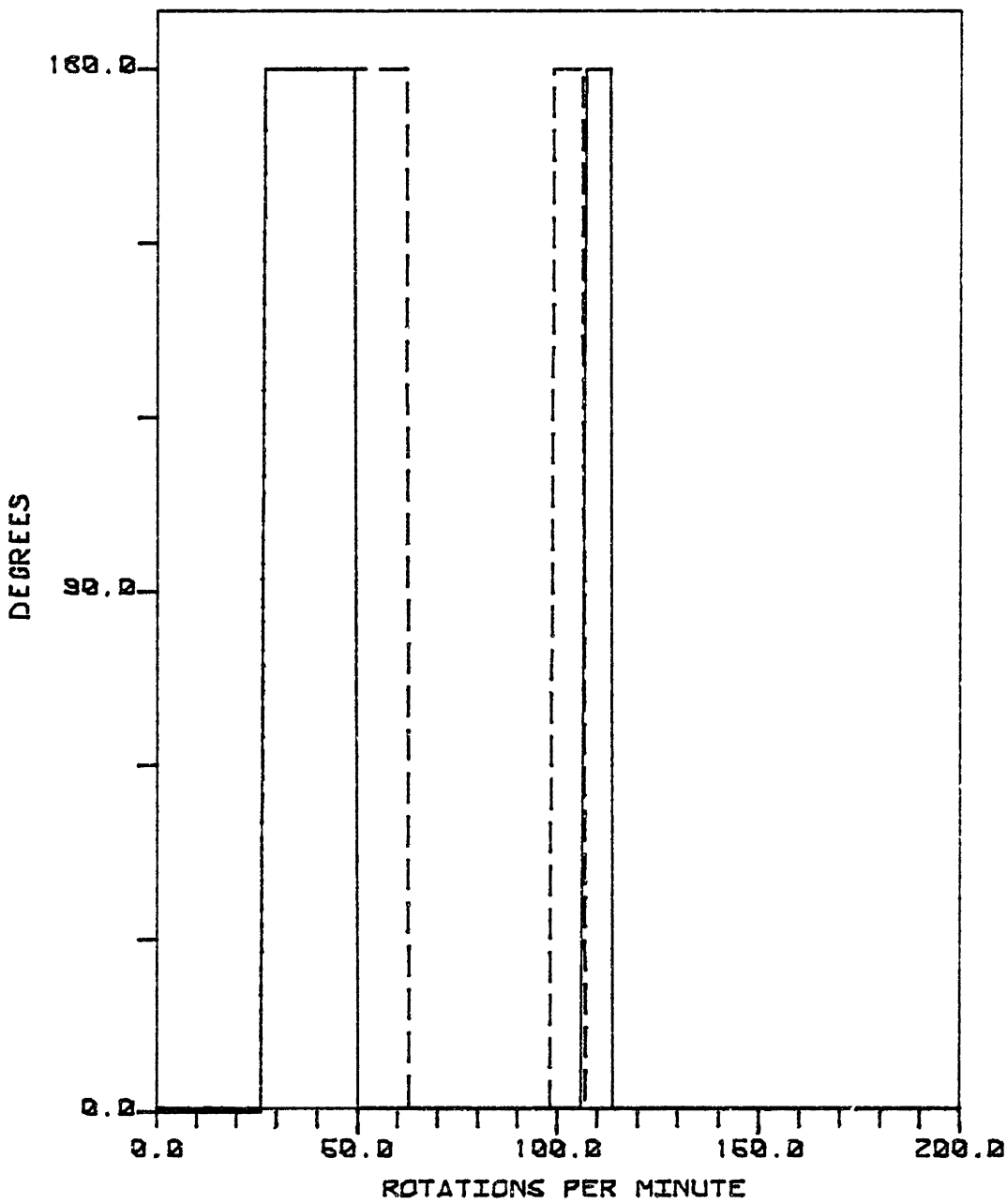
180.0
90.0
0.0
DEGREES
0.0
50.0
100.0
150.0
200.0
ROTATIONS PER MINUTE
PHASE ANGLE OF FORCE: AT BIT
AT STABILIZER

Figure 14.c - Mode Shapes at Resonance.

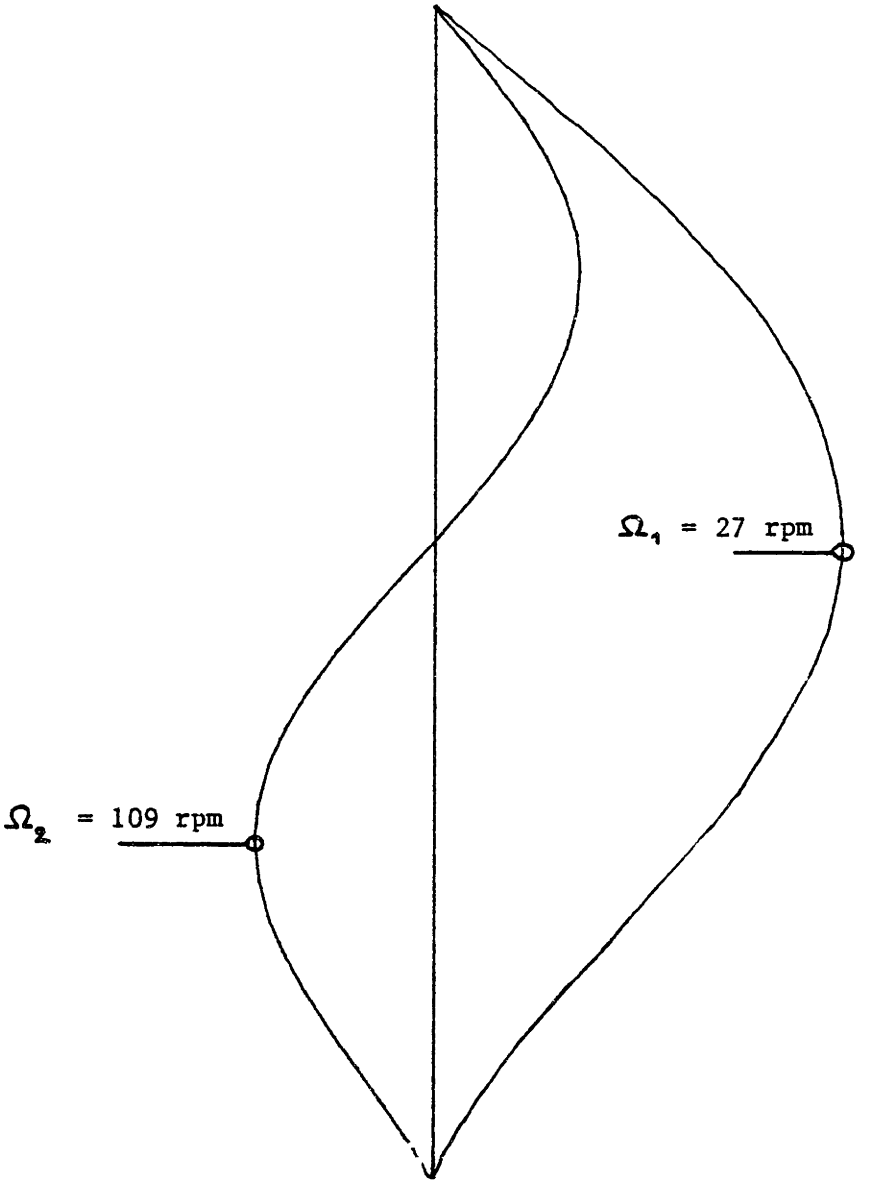

Figure 15.a - Effect of Mass-Eccentricity Distribution.

Same Parameters as in Case 8, except $e'(z) = 0.1"$ $0 \leqslant z < L/2$

$-0.1"$ $L/2 < z \leqslant L$

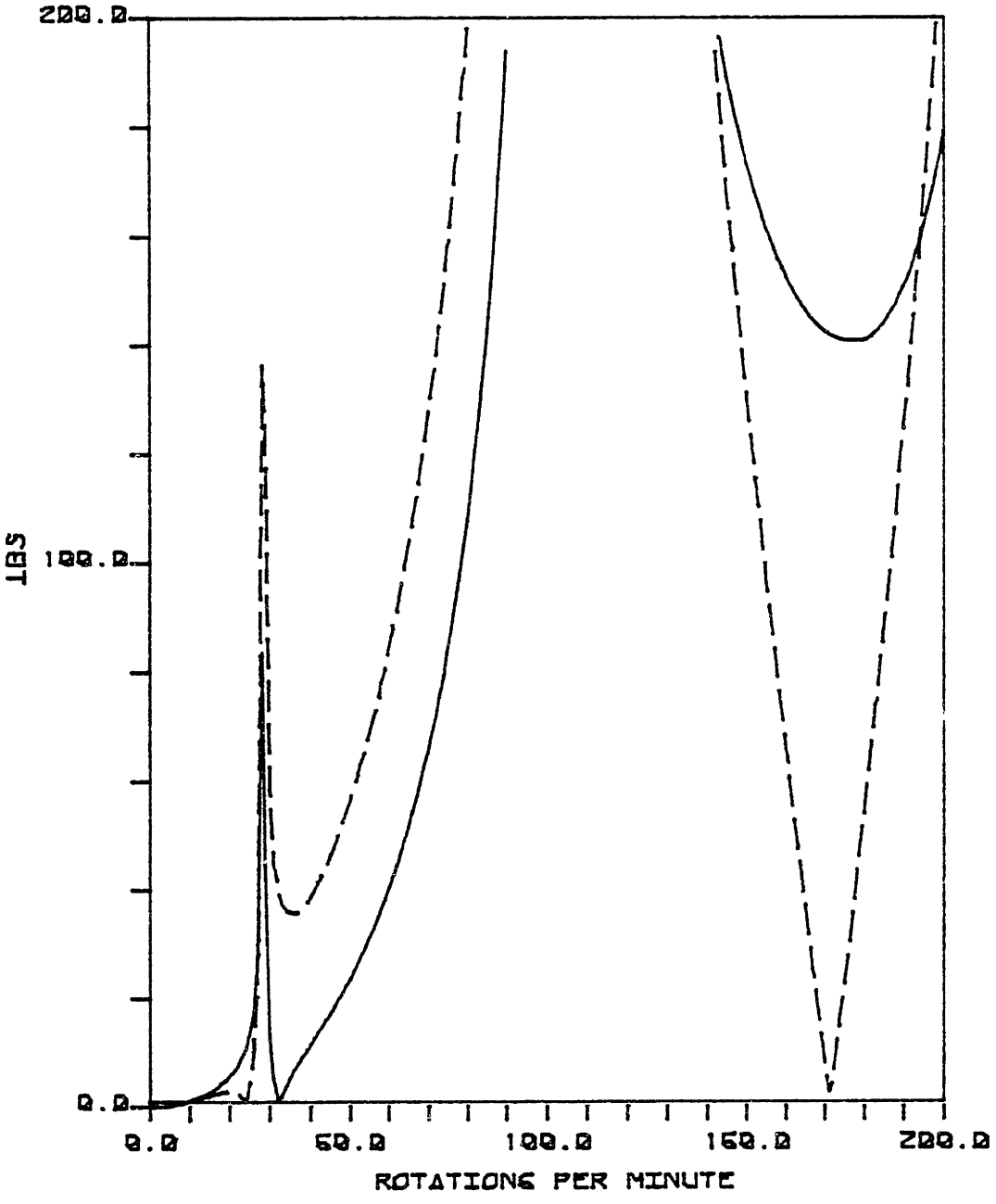

Figure 15.b

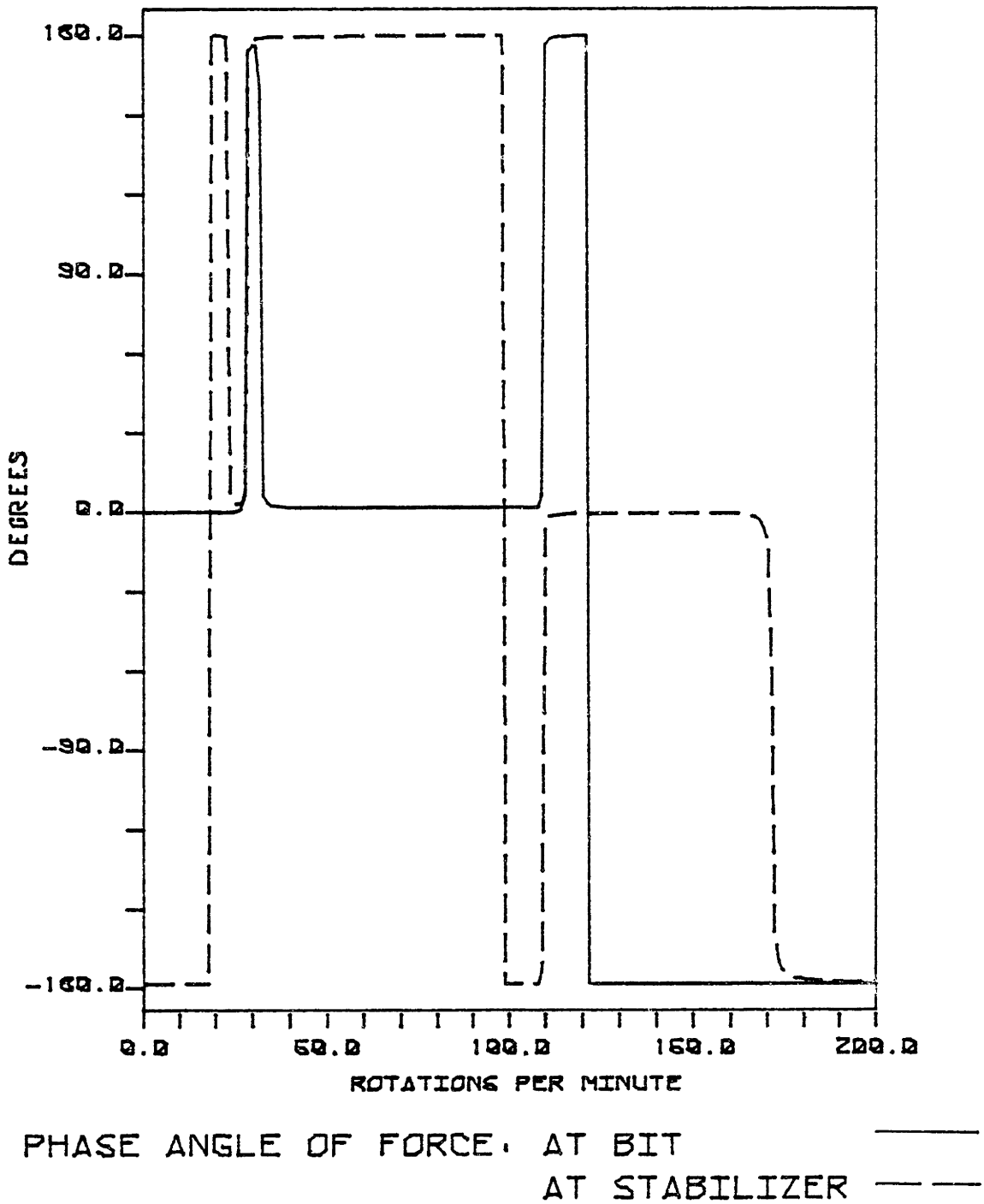
160.0
90.0
0.0
-90.0
-160.0
DEGREES
0.0
60.0
100.0
160.0
200.0
ROTATIONS PER MINUTE
PHASE ANGLE OF FORCE: AT BIT
AT STABILIZER

Figure 16.a - Effect of Mass-Eccentricity Distribution.

Same Parameters as in Case 8, except $e'(z) = 0.1"$ $0 \leq z < 3L/4$

0 elsewhere

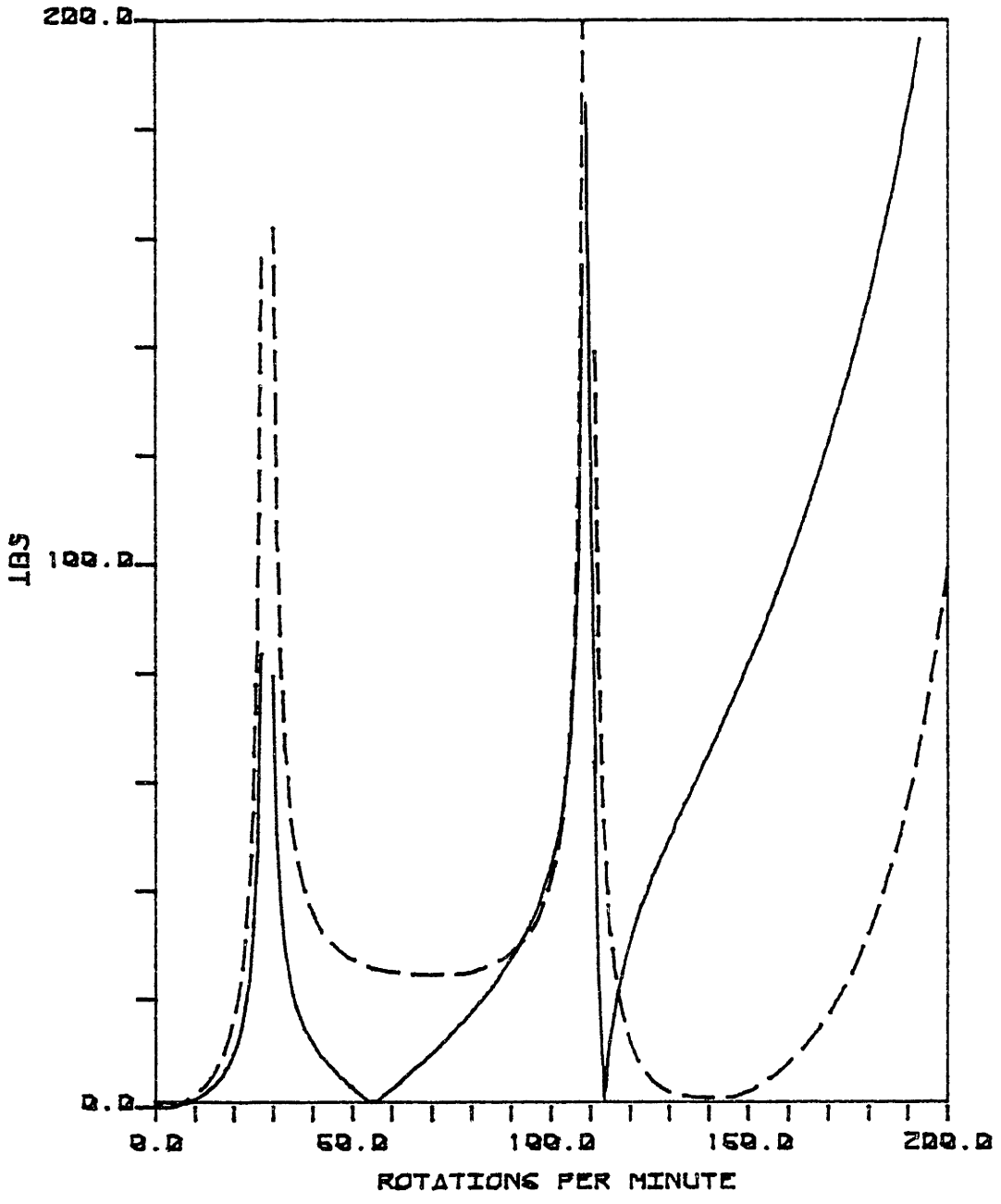

Figure 16.b

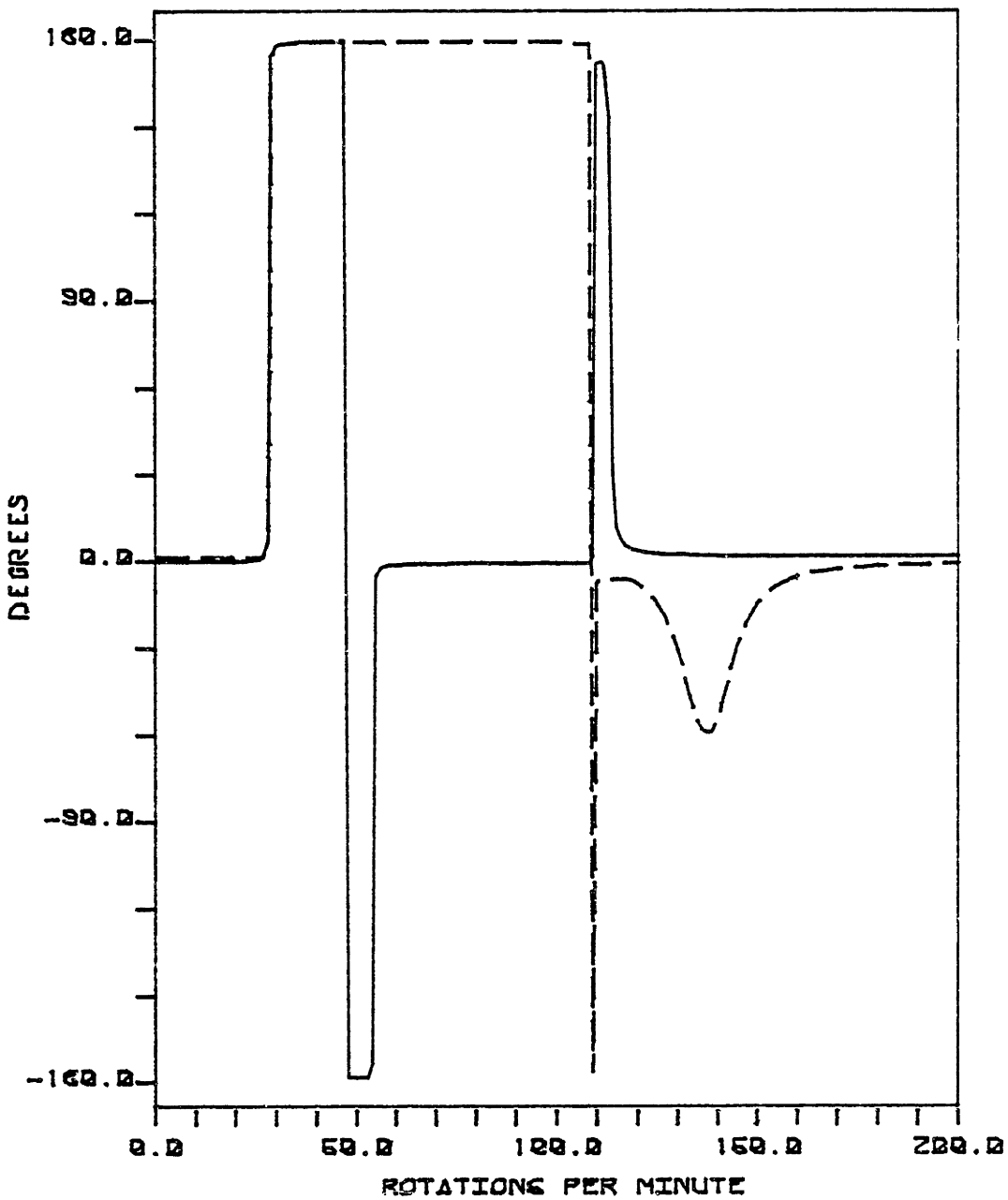
180.0
90.0
0.0
-90.0
-180.0
DEGREES
0.0
60.0
120.0
150.0
200.0
ROTATIONS PER MINUTE
PHASE ANGLE OF FORCE: AT BIT
AT STABILIZER

Figure 17.a - Effect of Mass-Eccentricity Distribution.

Same Parameters as in Case 8, except $e'(z) = 0.1"$ $0 \leq z < L/4$

0 elsewhere

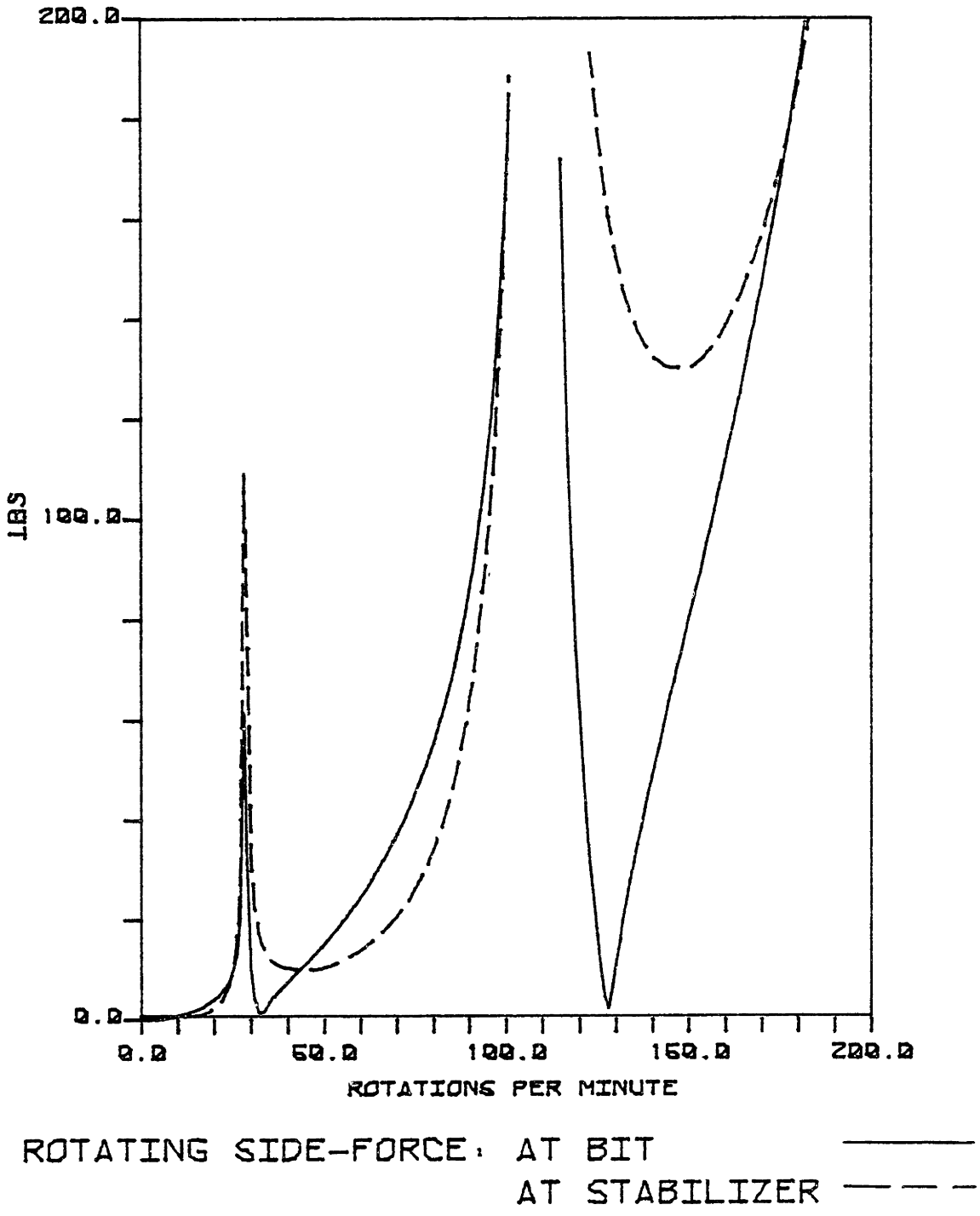

Figure 17.b

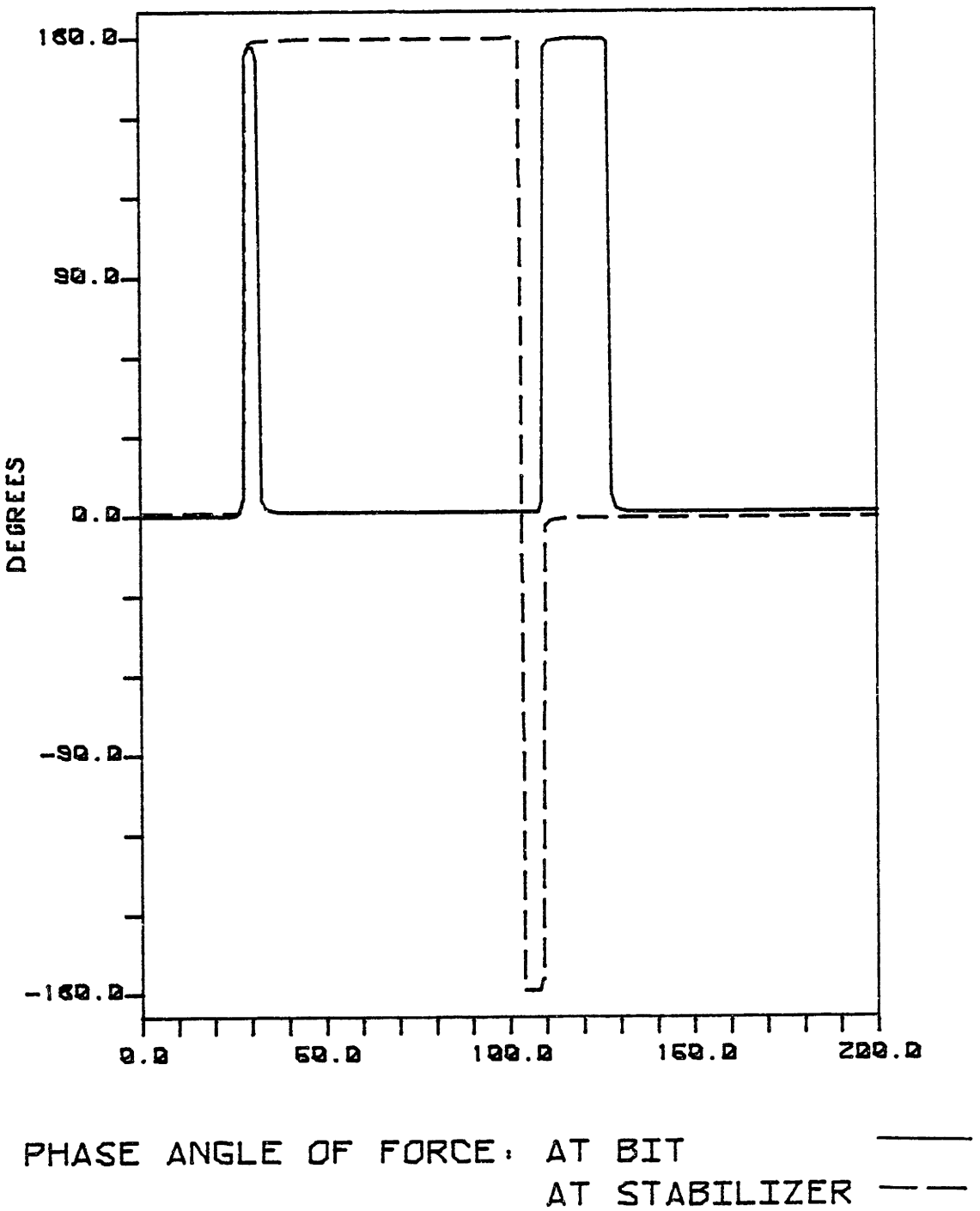
180.0
90.0
0.0
-90.0
-180.0
DEGREES
0.0
50.0
100.0
150.0
200.0
PHASE ANGLE OF FORCE: AT BIT
AT STABILIZER

Figure 18.a - Effect of Mass-Eccentricity Distribution.

Same Parameters as in Case 8, except e'(z) = -0.1" $0 \leqslant z < L/4$

0.1" $L/4 < z \leqslant L$

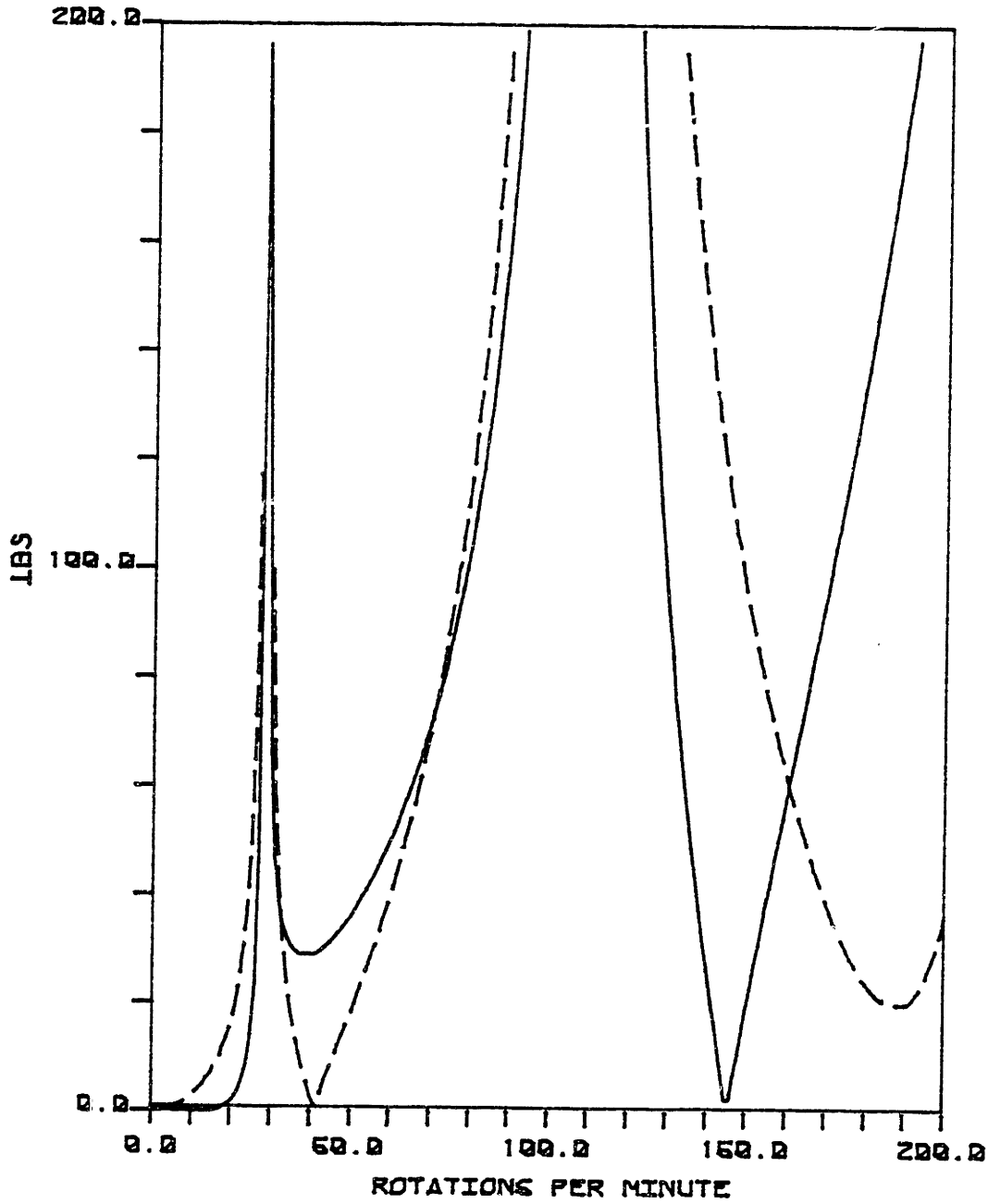

ROTATING SIDE-FORCE: AT BIT ————

AT STABILIZER — — — —

Figure 18.b

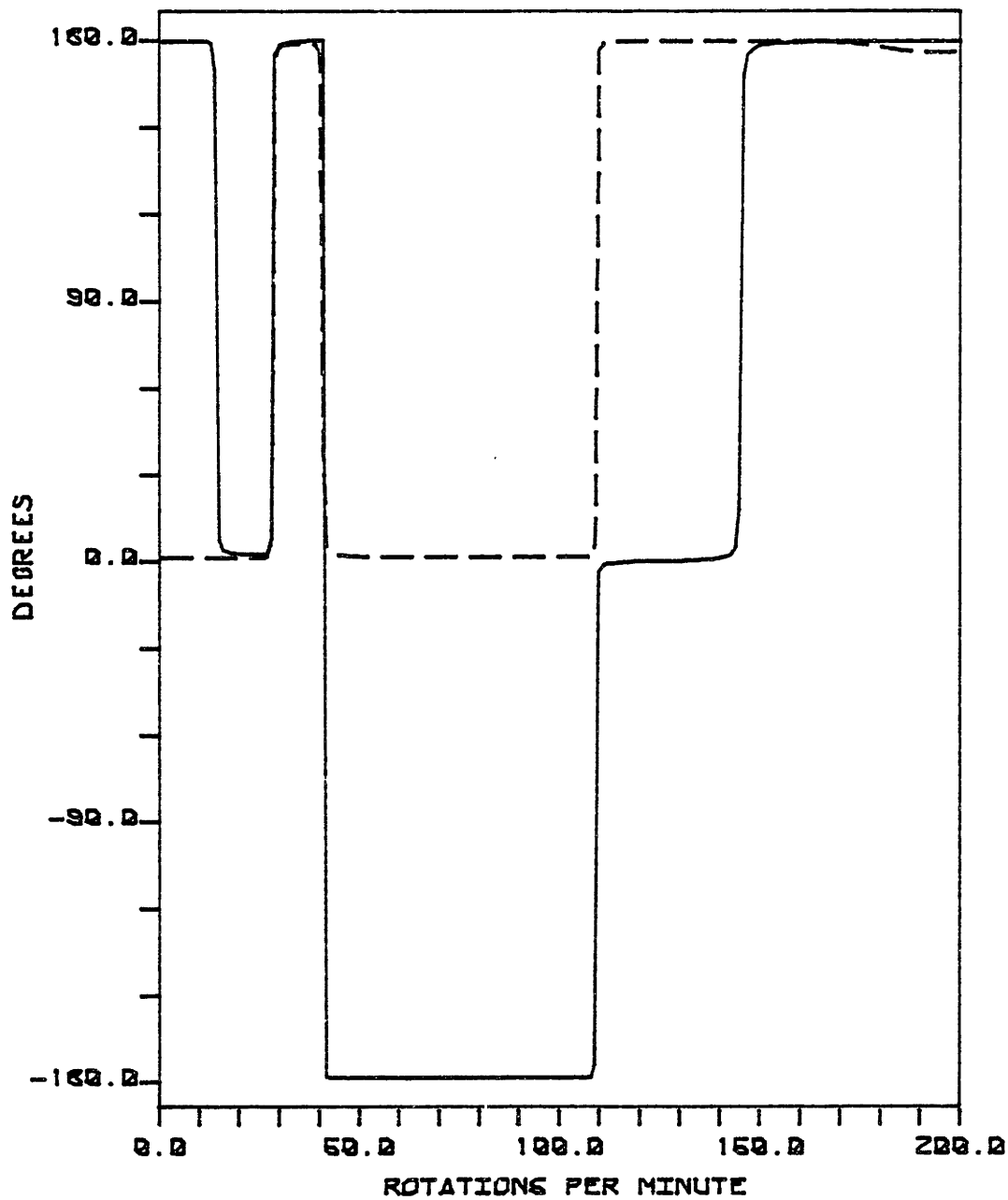

PHASE ANGLE OF FORCE: AT BIT ————
AT STABILIZER — — —

Figure 19.a - Effect of Mass-Eccentricity Distribution.

Same Parameters as in Case 8, except e'(z) = 0 $0 \leq z < L/4$

0.1" $L/4 < z < L/2$

-0.1" $L/2 < z < 3L/4$

0 $3L/4 < z \leq L$

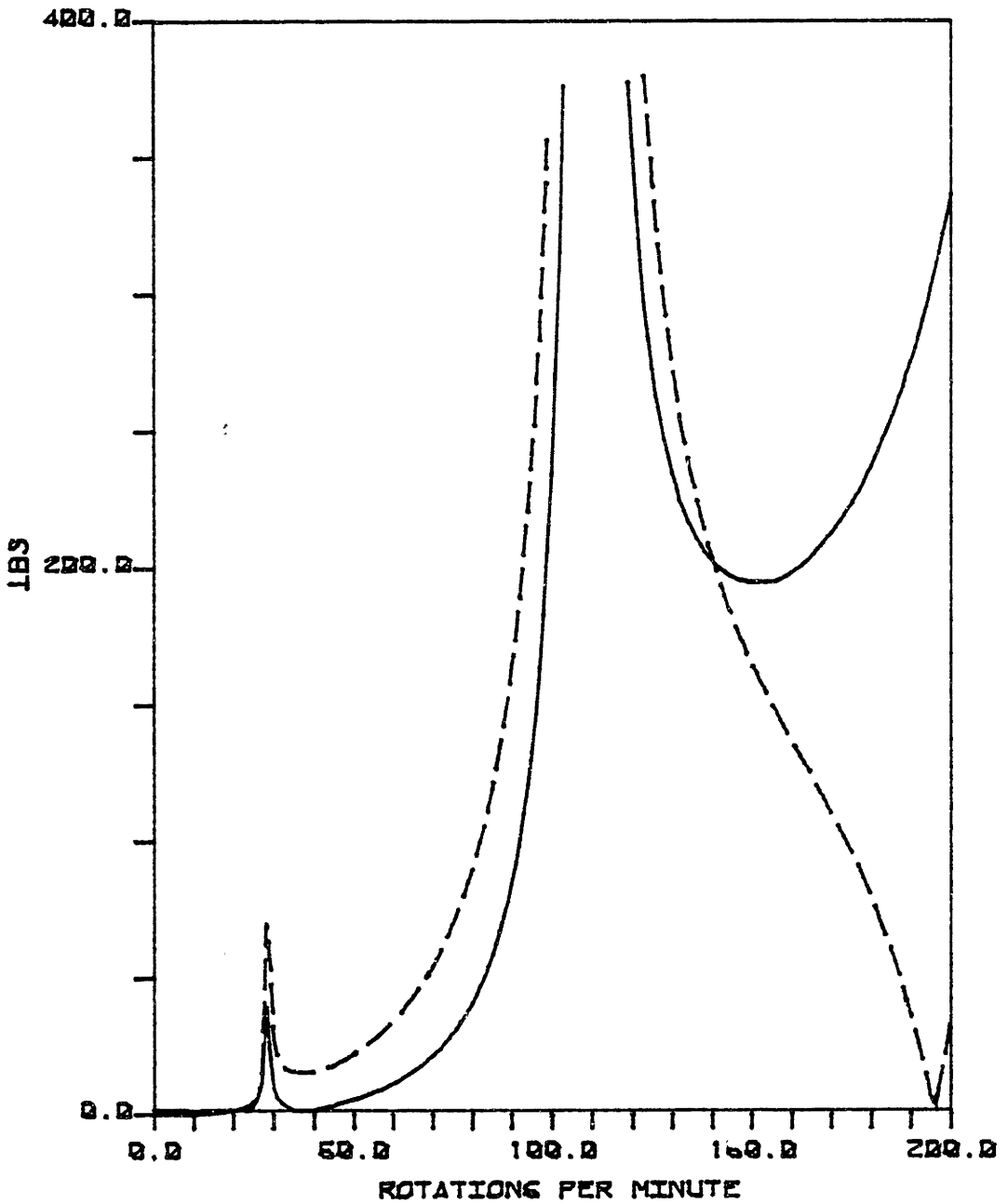

ROTATING SIDE-FORCE: AT BIT ————

AT STABILIZER — — —

Figure 19.b

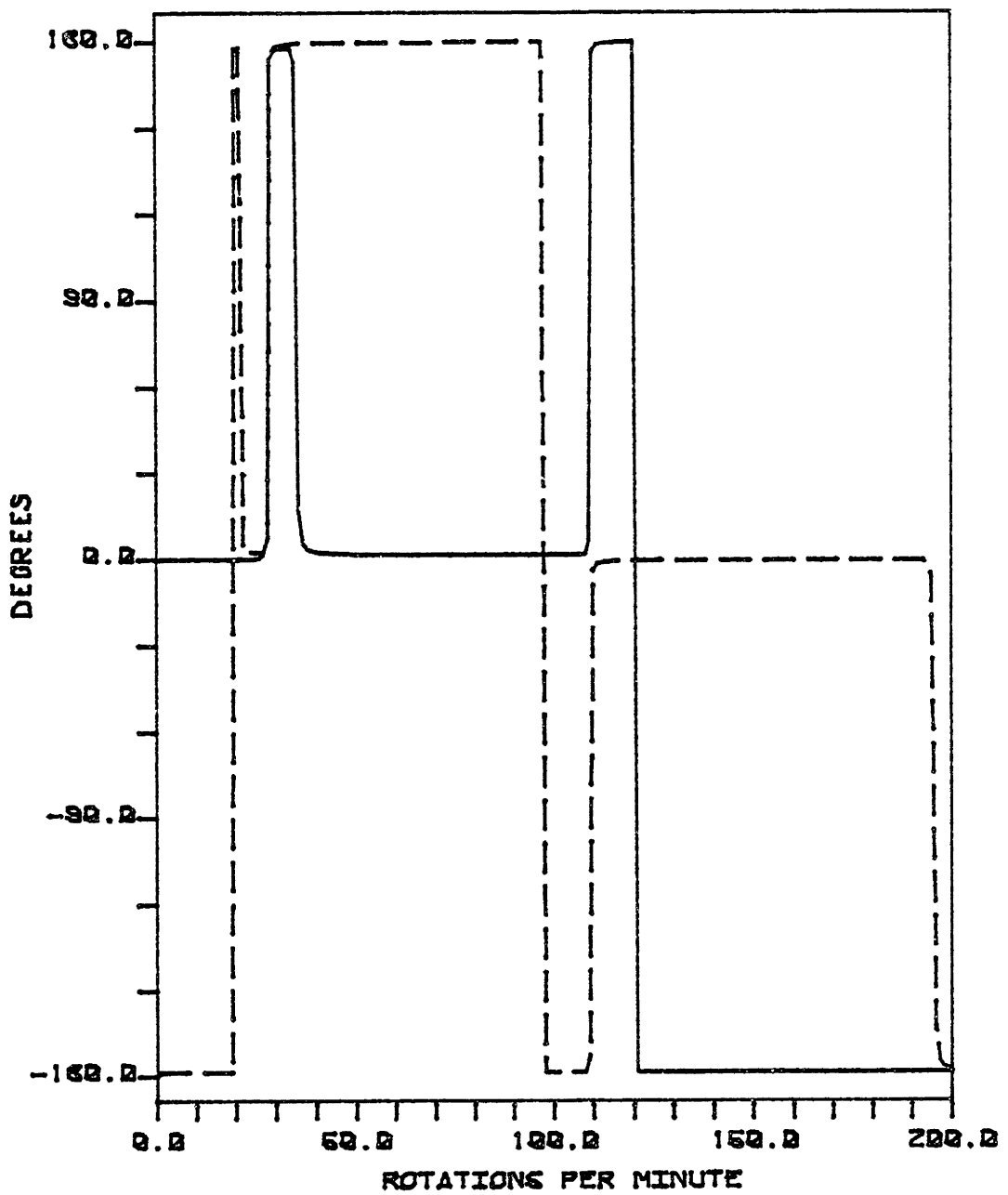
180.0
90.0
0.0
-90.0
-180.0
DEGREES
0.0
60.0
100.0
150.0
200.0
ROTATIONS PER MINUTE
PHASE ANGLE OF FORCE: AT BIT
AT STABILIZER

Figure 20.a - Effect of Mass-Eccentricity Distribution.

Same Parameters as in Case 8, except e'(z) = 0.1" $0 \leq z < L/4$

-0.1" $L/4 < z < L/2$

0.1" $L/2 < z < 3L/4$

-0.1" $3L/4 < z \leq L$

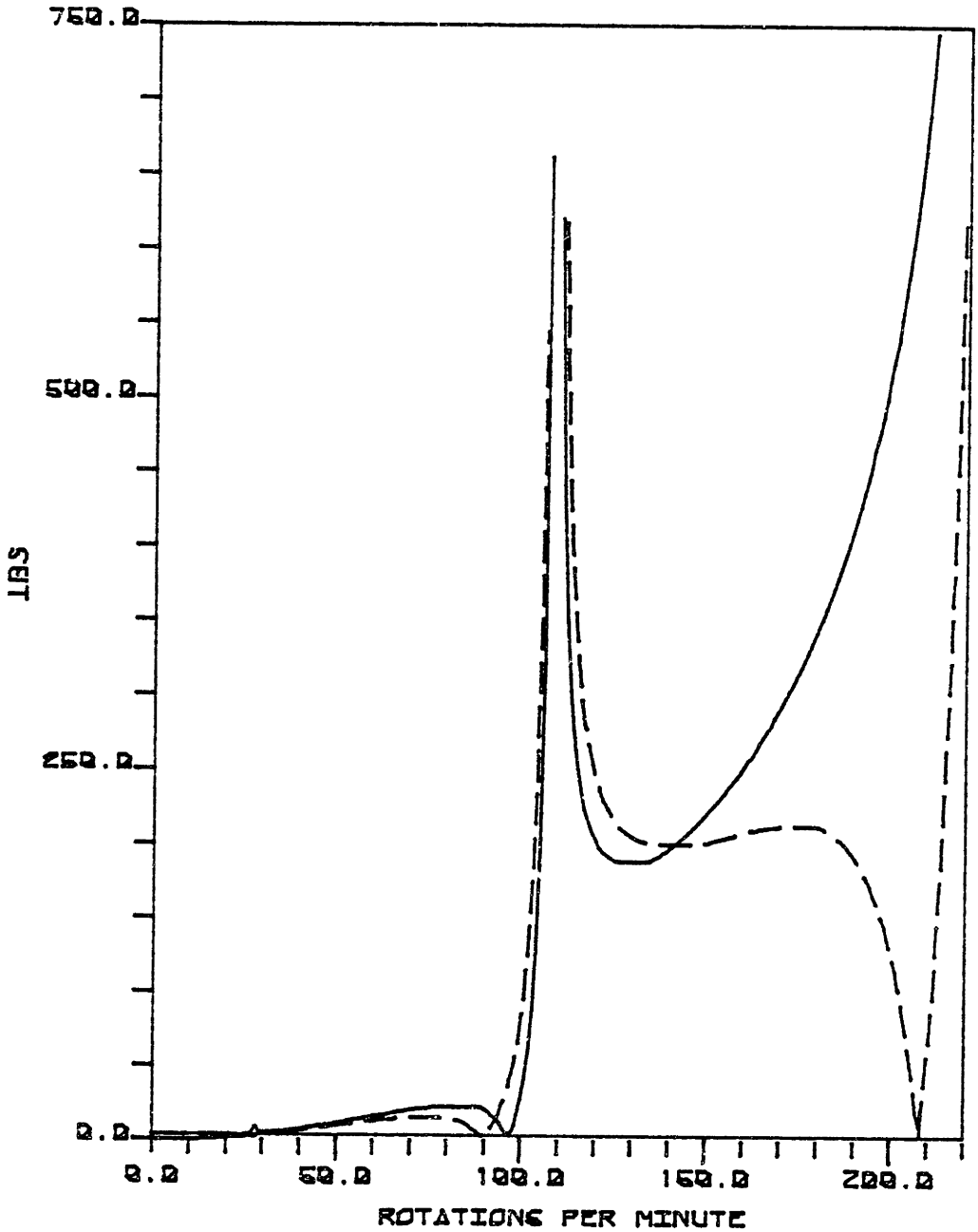

ROTATING SIDE-FORCE: AT BIT ————————

AT STABILIZER — — — —

Figure 20.b

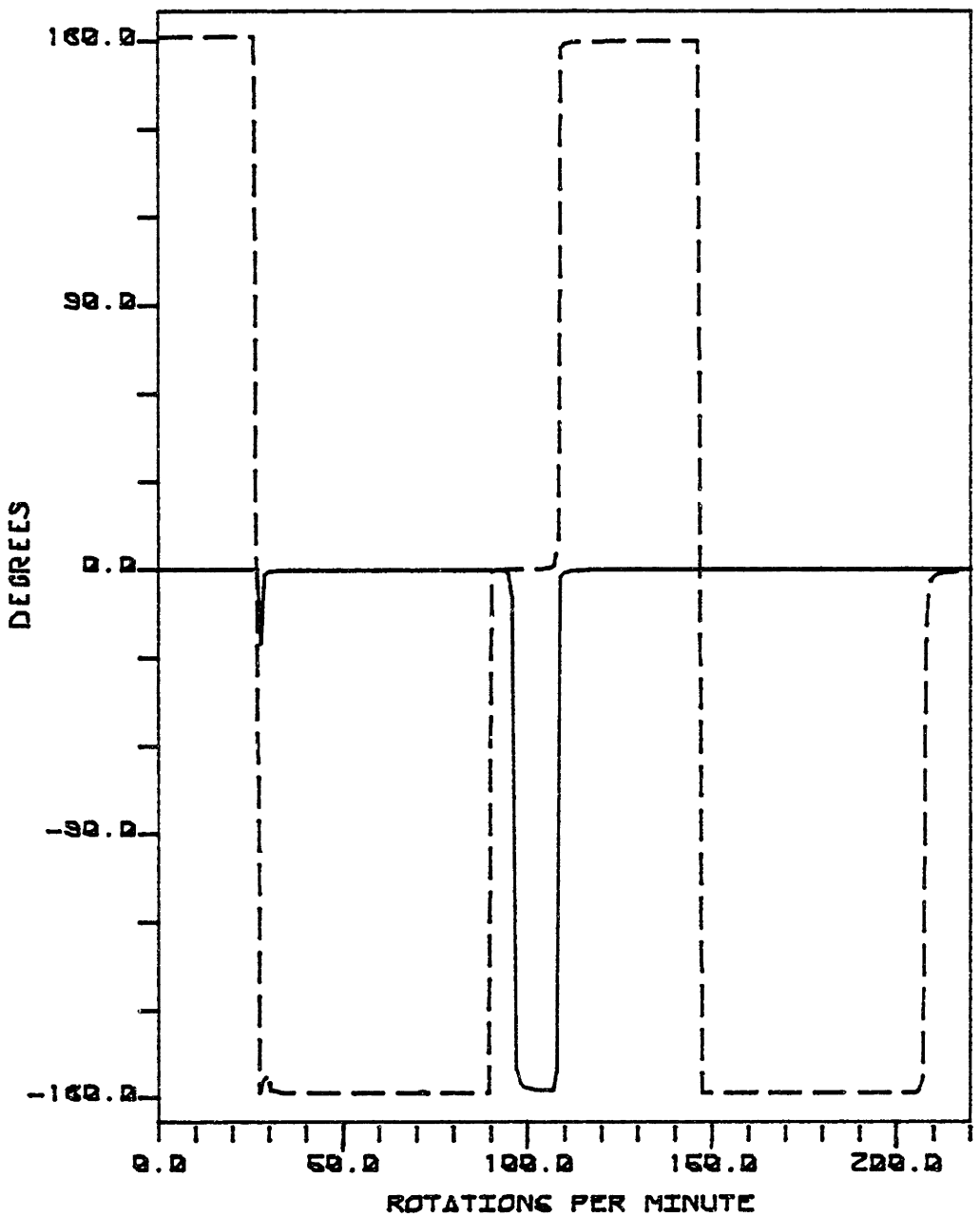

PHASE ANGLE OF FORCE: AT BIT ————
AT STABILIZER — — —

9. Typical Printout from COLLAR.

One considers Case 8 at the "optimum" speed Ω = 119 rpm.

(See Table 1, page 17, and Figure 8.a, page 43).

```
-------------------------------------------------------------------------------

      THE COLLARS HAVE A BIT-STABILIZER LENGTH :      L =   100.00 FEET
              AN INTERNAL DAMPING COEFFICIENT :     Ci =  0.0000E+00 LBS/(FT/S)/FT OF PIPE
                              AN OUTER DIAMETER :     OD =     7.50 INCHES
                              AN INNER DIAMETER :     ID =     2.81 INCHES
       AND ARE ACTED UPON BY A DRIVING TORQUE :      Q = 10000.00 LBS * FT
                        ROTATING AT THE SPEED : OMEGA =   119.00 RPM

      THE HOLE IS OFF THE VERTICAL BY AN ANGLE :    PHI =    10.00 DEGREES
              AND FILLED WITH A MUD OF WEIGHT : RHOMUD =    12.00 LBS / GAL
                   AND OF DAMPING COEFFICIENT :     Ce =  0.0000E+00 LBS/(FT/S)/FT OF PIPE

          THE BIT HAS A CHARACTERISTIC RADIUS :     k' =     0.00 INCHES
                       AND SUPPORTS A NET WEIGHT :     Wb = 30000.00 LBS

                     THE SHAFT IS DISCRETIZED INTO :      N =   19 SEGMENTS  (OF THE TYPE 4M-1)
  THE BOUNDARY VALUE COEF. AT THE STABILIZER IS :      C =  1.0000 (0 = PINNED, 1 = CLAMPED)

    THE MASS ECCENTRICITY IS FOR THE LOWER QUART :    E'1 =  0.100 INCHES AT    0.00 DEGREES
                                  SECOND QUART :    E'2 =  0.100 INCHES AT    0.00 DEGREES
                                   THIRD QUART :    E'3 =  0.100 INCHES AT    0.00 DEGREES
                                   UPPER QUART :    E'4 =  0.100 INCHES AT    0.00 DEGREES

-------------------------------------------------------------------------------

THE DIMENSIONLESS DISPLACEMENTS S AND R ARE :

                    MAGNITUDE      PHASE            MAGNITUDE      PHASE

I =  1 :  S =  0.1099E-02 ,  -89.51 .  R =  0.1227E-04 ,    2.36
I =  2 :  S =  0.2146E-02 ,  -89.55 .  R =  0.1896E-04 ,    2.76
I =  3 :  S =  0.3096E-02 ,  -89.59 .  R =  0.1649E-04 ,    4.08
I =  4 :  S =  0.3911E-02 ,  -89.63 .  R =  0.3546E-05 ,   20.75
I =  5 :  S =  0.4560E-02 ,  -89.67 .  R =  0.1979E-04 ,  176.64
I =  6 :  S =  0.5023E-02 ,  -89.70 .  R =  0.5021E-04 ,  178.97
I =  7 :  S =  0.5287E-02 ,  -89.74 .  R =  0.8410E-04 ,  179.63
I =  8 :  S =  0.5351E-02 ,  -89.77 .  R =  0.1168E-03 ,  179.94
I =  9 :  S =  0.5219E-02 ,  -89.81 .  R =  0.1438E-03 , -179.88
I = 10 :  S =  0.4909E-02 ,  -89.84 .  R =  0.1614E-03 , -179.77
I = 11 :  S =  0.4441E-02 ,  -89.87 .  R =  0.1669E-03 , -179.68
I = 12 :  S =  0.3849E-02 ,  -89.90 .  R =  0.1599E-03 , -179.62
I = 13 :  S =  0.3169E-02 ,  -89.94 .  R =  0.1413E-03 , -179.57
I = 14 :  S =  0.2446E-02 ,  -89.97 .  R =  0.1142E-03 , -179.53
I = 15 :  S =  0.1728E-02 ,  -90.00 .  R =  0.8242E-04 , -179.48
I = 16 :  S =  0.1067E-02 ,  -90.03 .  R =  0.5084E-04 , -179.44
I = 17 :  S =  0.5204E-03 ,  -90.06 .  R =  0.2414E-04 , -179.39
I = 18 :  S =  0.1449E-03 ,  -90.10 .  R =  0.6294E-05 , -179.31

THE FORCES AT THE BIT ARE :

    FIXED COMPONENT     : FB1 =  0.5852E+03  LBS  AT  -89.94  DEGREES
    ROTATING COMPONENT  : FB2 =  0.1295E+03  LBS  AT    0.63  DEGREES

THE FORCES AT THE STABILIZER ARE :

    FIXED COMPONENT     : FS1 =  0.1243E+04  LBS  AT  -90.03  DEGREES
    ROTATING COMPONENT  : FS2 =  0.2678E+01  LBS  AT -148.57  DEGREES
```

CONCLUSION

When stabilizers enforce built-in conditions (c = 1), results seem to indicate that best drilling conditions are immediately after second resonance, when rotating forces are large at bit and small at stabilizer. This holds also when the shaft is only pinned at stabilizer, but in this case, forces are small and too close to each other in magnitude.

However, rigid stabilizers cause large static force at stabilizers and diminish the static component at bit, thus reducing the pendulum effect when the hole is slanted. Therefore, a further study should investigate more precisely the best trade-off between the two following situations at bit:

large static force and small rotating force, or

small static force and large rotating force.

BIBLIOGRAPHY

1. Bishop, R. E. D., and Gladwell, G. M. L. 1959a "The Vibrations of Rotating Shafts," J. Mech. Eng. and Sci., Vol 1, No 1, pp 50-65.

2. Bishop, R. E. D., and Gladwell, G. M. L. 1959b "The Vibration and Balancing of an Unbalanced Flexible Rotor," J. Mech. Eng. and Sci., Vol 1, No 1, pp 66-77.

3. Drilco 1982, Drilling Assembly Handbook, P.O.Box 60068, Houston, Texas 77205.

4. Dubigeon, Serge 1973 "The Movement of Long Vertical Shafts," Journal of Sound and Vibration, Vol 26, No 3, pp 337-352.

5. Eshleman, R. L., and Eubanks, R. A. 1969 "On the Critical Speeds of a Continuous Rotor," Transactions of the ASME, Journal of Engineering for Industry, B 91, pp 1180-1188.

6. Golomb, M., and Rosemberg, R. M. 1961 "Critical Speeds of Uniform Shafts Under Axial Torque," Proceedings of the U.S. National Congress of Applied Mechanics, New York.

7. "Unique Drill Collar Limits Angle With High Bit Loads," World Oil June 1971, pp 91-92.

8. "Unbalanced Drill Collar Increases Penetration Rates," World Oil January 1978.

APPENDIX A

DERIVATION OF GOVERNING PARTIAL DIFFERENTIAL EQUATION

A.1 Methodology

The two sets of axes used are shown in Figure A.1. The fixed rectangular right-hand coordinate system is referred to as OXYZ, where the origin O is the center of the lower face of the bit. Z intersects the centerline of the pipe at the bit and at the stabilizers. (OY,OZ) defines a vertical plane that contains the acceleration of gravity g.

The rotating set of axes is referred to as OUVZ.

The method adopted is to isolate a infinitesimal slice of the shaft and apply Newton's second law:

$$m\vec{\gamma} = \sum \vec{F} \qquad \text{(A.1)}$$

where:

- m not only represents the mass of the slice, but also accounts for the added mass of mud,
- $\vec{\gamma}$ is the acceleration of the center of gravity G of the slice,
- $\sum \vec{F}$ is the sum of the differential transverse forces. As we suppose the displacements small, superposition holds and we can address the different contribution separately: effects of flexural stiffness, driving torque, damping, mud, gravity, tensile force.

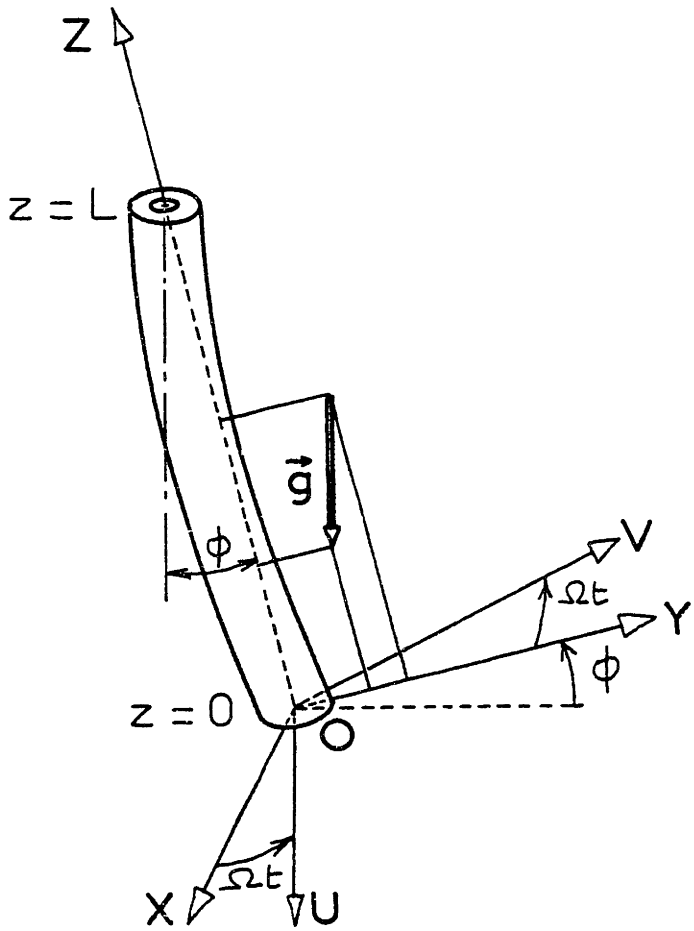

Figure A.1 - Coordinate Systems Definition.

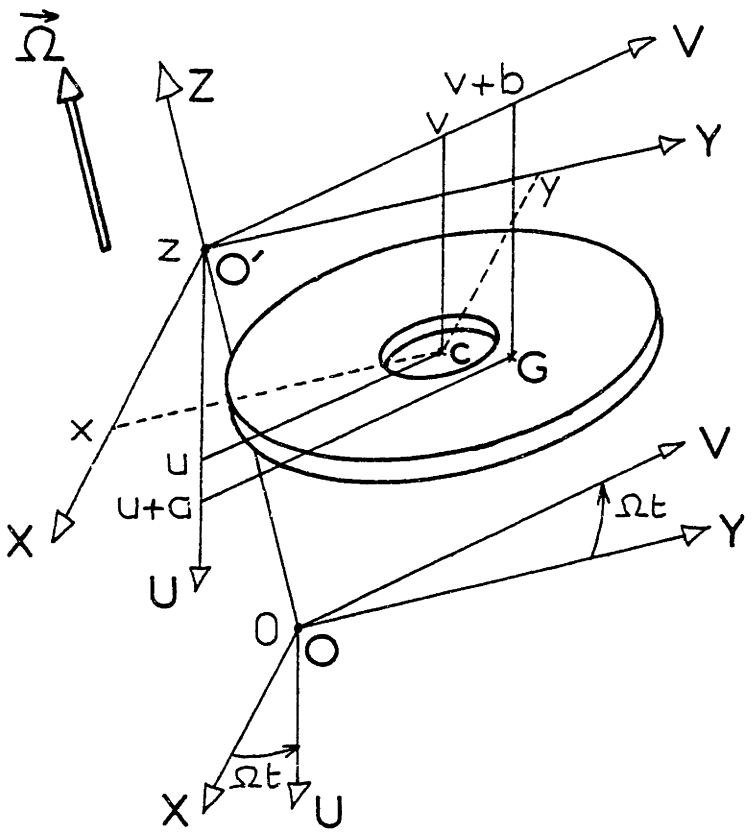

Figure A.2 - Coordinate Notations.

As seen in Figure A.2, the coordinates of the center of surface C are:

$u(z,t)$, $v(z,t)$, z in OUVZ,

$x(z,t)$, $y(z,t)$, z in OXYZ.

G denoting the center of gravity of the slice, the components of the offset vector CG are time-independent in OUVZ:

$$\overrightarrow{CG} = a(z)\ \vec{U} + b(z)\ \vec{V} \qquad (A.2)$$

Before addressing systematically each force involved, let us derive the expression of the acceleration :

$$\vec{\gamma} = \frac{d^2\overrightarrow{OG}}{dt^2} = \frac{d^2\overrightarrow{OO'}}{dt^2} + \frac{d^2\overrightarrow{O'G}}{dt^2} \qquad (A.3)$$

It is considered that the bit buries itself into the soil slowly and steadily. Therefore, the trihedral OXYZ bound to the bit undergoes a translation along Z and is galilean.

$\frac{d^2\overrightarrow{OO'}}{dt^2} = \frac{d^2z}{dt^2}\ \vec{Z}$ is neglected.

In OXYZ, $\overrightarrow{O'G}$ and $\frac{d^2\overrightarrow{O'G}}{dt^2}$ are:

$$\overrightarrow{O'G} = \begin{vmatrix} x + a\cos\Omega t \\ y + b\sin\Omega t \\ 0 \end{vmatrix}_{OXYZ} \quad (A.3) \quad ; \quad \frac{d^2\overrightarrow{O'G}}{dt^2} = \begin{vmatrix} \ddot{x} - a\Omega^2\cos\Omega t \\ \ddot{y} - b\Omega^2\sin\Omega t \\ 0 \end{vmatrix}_{OXYZ} \quad (A.4)$$

A.2 Effect of Flexural Stiffness.

Sign conventions are shown in Figure A.3.

Neglecting the rotatory inertia of the slice about any

diametral axis, the equilibrium in the plane OYZ reads:

$$0.\vec{X} = \vec{M}_x + d\vec{M}_x - \vec{M}_x + dz\ \vec{Z} \wedge (S_y + dS_y)\ \vec{Y}$$

$$\vec{0} = d\vec{M}_x + dz\ S_y\ \vec{Z} \wedge \vec{Y}$$

$$= dM_x\ \vec{X} + dz\ S_y\ (-\vec{X})$$

Scalar multiplication by $\vec{X}$ gives $S_y = \frac{dM_x}{dz}$

and the net force acting onto the slice is $dS_y = \frac{d^2M_x}{dz^2}\,dz$

Substituting for $M_x = -EI\ \frac{d^2y}{dz^2}$

(positive when the curvature in y is negative), one eventually gets

$$dS_y = -EI\ \frac{d^4y}{dz^4}\,dz$$

With the sign conventions of Figure A.4, equilibrium in plane OZX reads:

$$0.\vec{Y} = \vec{M}_y + d\vec{M}_y - \vec{M}_y + dz\ \vec{Z} \wedge (S_x + dS_x)\ \vec{X}$$

$$\vec{0} = d\vec{M}_y + dz\ S_x\ \vec{Z} \wedge \vec{X}$$

$$= dM_y\ \vec{Y} + dz\ S_x\ \vec{Y}$$

Scalar multiplication by $\vec{Y}$ yields $S_x = -\frac{dM_y}{dz}$

and the net force acting onto the slice is $dS_x = -\frac{d^2M_y}{dz^2}\,dz$

Substituting for $M_y = EI\ \frac{d^2x}{dz^2}$

(positive when the curvature in x is positive), one finds

$dS_x = -EI\ \frac{d^4x}{dz^4}\,dz$, and

$$\vec{M}_{bend.} = EI \begin{vmatrix} - d^2y/dz^2 \\ d^2x/dz^2 \\ 0 \end{vmatrix}_{oxyz} \quad \text{creates} \quad \vec{F}_{stiff.} = -EI\,dz \begin{vmatrix} \frac{d^4x}{dz^4} \\ \frac{d^4y}{dz^4} \\ 0 \end{vmatrix}_{oxyz} \qquad (A.5)$$

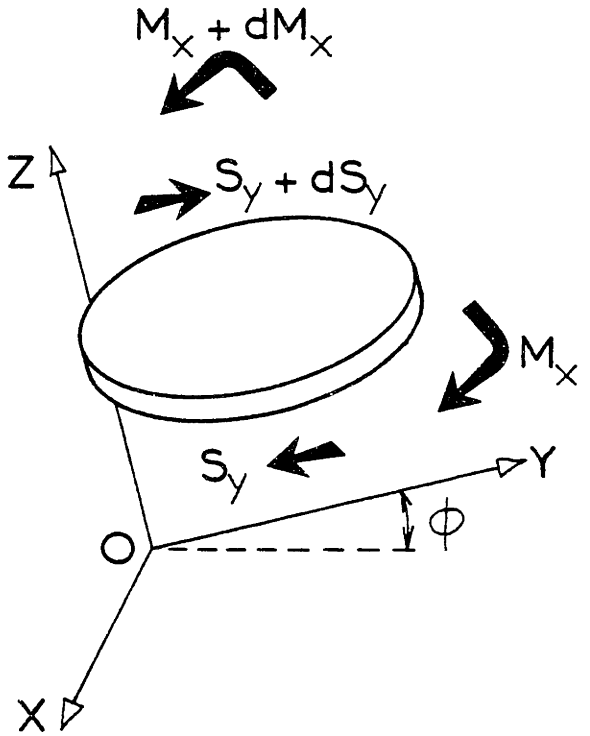

Figure A.3 - Sign Conventions in Plane OYZ.

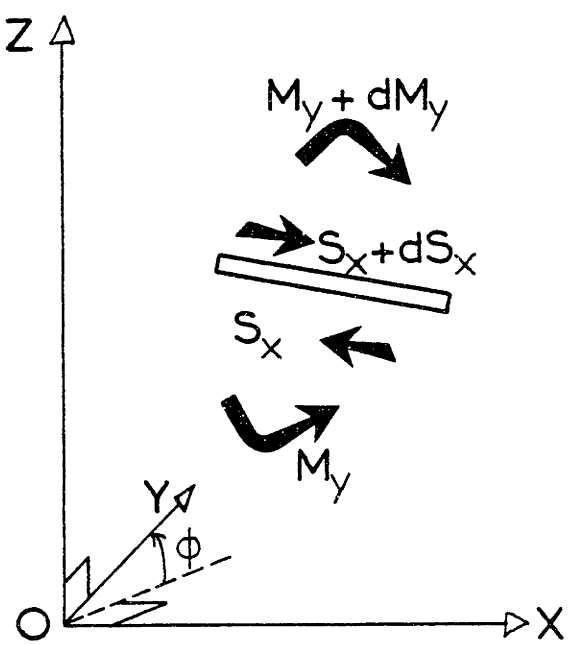

Fifure A.4 - Sign Conventions in Plane OZX.

A.3 Effect of Coupling Torque-Bending.

The very fact that the shaft is bent makes the driving torque contribute to bending the shaft somewhat further. An intuitive insight of the phenomenon may be easily reached as follows:

Take a bar made of rubber and hold it with hands, say, three feet apart. Then, without giving it any initial curvature, twist it: apart from some superficial helicoidal deformation, the center line of the bar remains straight (Figure A.5).

However, if one gives the bar an initial curvature, as shown in Figure A.6, one clearly sees on Figure A.7 that the twisting moment causes the bar to bend out of plane. This time, the centerline of the bar itself assumes a helicoidal shape.

The actual situation is shown on Figure A.8.

The driving torque $\vec{Q}$ is decomposed in $\vec{Q} = \vec{Q}_n + \vec{Q}_p$

where

$\vec{Q}_n$ is the true axial driving torque,

$\vec{Q}_p$ is the component in the plane of the slice.

$\vec{Q}_n$ is obtained by $\vec{Q}_n = \vec{n} \wedge (\vec{Q} \wedge \vec{n})$, where $\vec{n}$ is the tangent vector:

$$\vec{Q}_p = \begin{vmatrix} \frac{dx}{dz} \\ \frac{dy}{dz} \\ 1 \end{vmatrix} \wedge \left(\begin{vmatrix} 0 \\ 0 \\ Q \end{vmatrix} \wedge \begin{vmatrix} \frac{dx}{dz} \\ \frac{dy}{dz} \\ 1 \end{vmatrix} \right) = Q \begin{vmatrix} -\frac{dx}{dz} \\ -\frac{dy}{dz} \\ 0 \end{vmatrix}_{OXYZ}$$

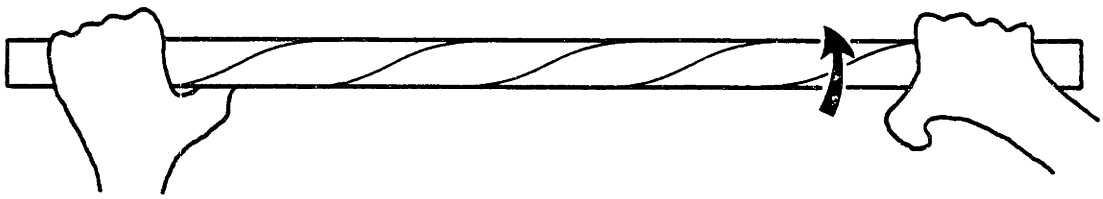

Figure A.5 - Twisting of a Straight Bar.

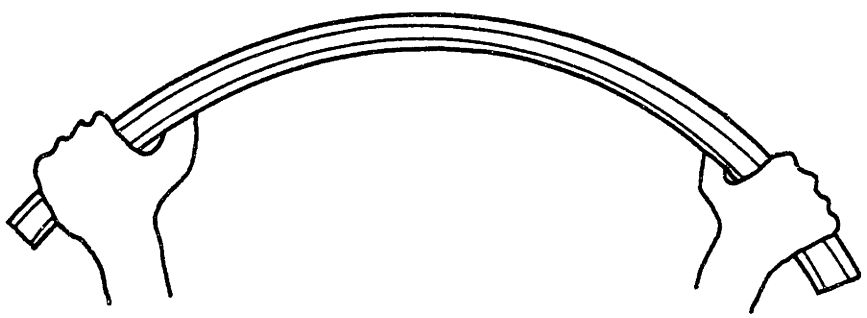

Figure A.6 - The Bar With Initial Curvature.

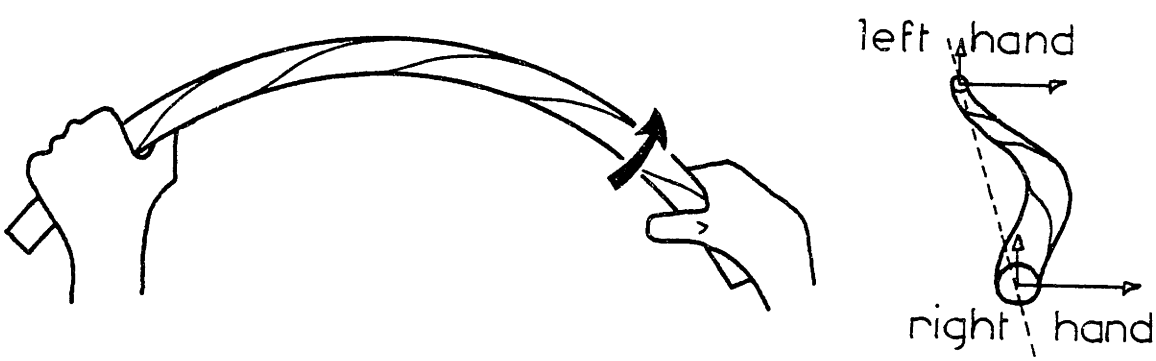

Figure A.7 - Interaction Between Bending and Twisting.

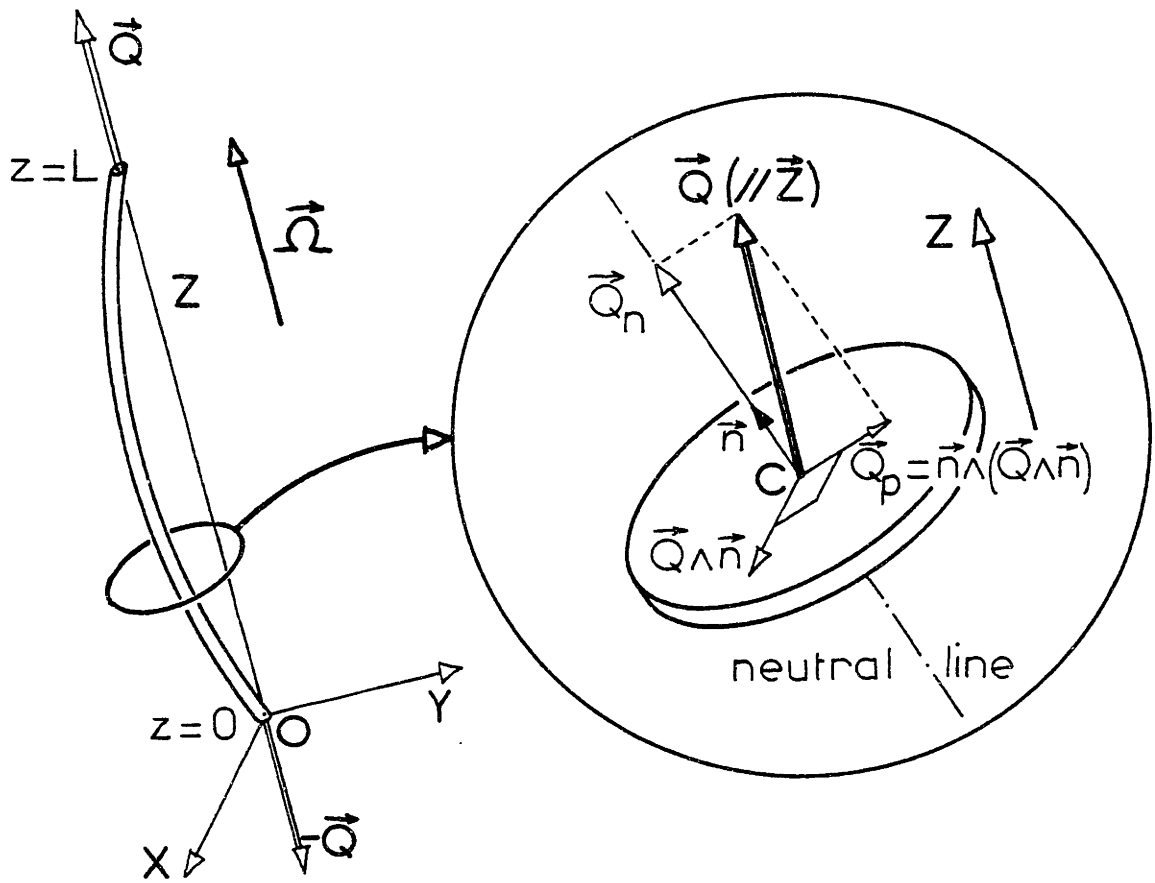

Figure A.8 - Vector Decomposition of Driving Torque.

In much the same way $\vec{M}_{bend}$ created $\vec{F}_{stiff}$,

$$\vec{Q}_p \quad \text{creates} \quad \vec{F}_{torq} = -Q\,dz \Big|_{OXYZ} \begin{vmatrix} -\frac{\partial^3 y}{\partial z^3} \\ \frac{\partial^3 x}{\partial z^3} \\ 0 \end{vmatrix} \qquad (A.6)$$

A.4 Effect of External and Internal Damping.

According to Bishop and Gladwell (1959a), damping can be apprehended in two coexistent ways:

a. External damping.

The drilling pipe is surrounded by mud, both inside and outside. This medium creates a force against the slice that is assumed to be

$$\vec{F}_{ext.\,damp.} = -C_e \cdot \left(\begin{matrix} \text{transverse} \\ \text{absolute} \\ \text{velocity of C} \end{matrix} \right) dz$$

that is

$$\vec{F}_{ext.\,damp.} = -C_e\,dz \Big|_{OXYZ} \begin{vmatrix} \dot{x} \\ \dot{y} \\ 0 \end{vmatrix} \qquad (A.7)$$

b. Internal damping.

The steel from which the pipe is rolled dissipates energy as well. This structural damping depends only on the motion of the pipe as seen by an observer tied to the rotating frame; the solid rotational motion imposed to the pipe has no influence. Therefore,

$$\vec{F}_{int.\,damp.} = -C_i \left(\begin{matrix} \text{transverse} \\ \text{relative} \\ \text{velocity of C} \end{matrix} \right) dz$$

that is

$$\vec{F}_{\text{int. damp.}} = - C_i \, dz \Big|_{oxyz} \begin{vmatrix} \dot{x} + \Omega y \\ \dot{y} - \Omega x \\ 0 \end{vmatrix} \qquad (A.8)$$

A.5 Effect of Transverse Mud Thrust.

In the field, except at the bit, the slice is subjected to the pressure of the mud along its sides only. However, in order to avoid clumsy calculations, we shall consider the slice to be completely immersed into mud, and then substract the hydrostatic forces exerted onto the two material cross-sections (Figure A.9).

Let $\vec{n_1}$ = vector orthogonal to the upper side of the slice, origin C_1

$\vec{n_2}$ = vector orthogonal to the lower side of the slice, origin C_2

$\vec{z_1}$ = vertical ascendent axis (figure A.10),

h_1 = distance from C_1 to the surface (rig),

h_2 = distance from C_2 to the surface (rig).

In the case of complete immersion, the thrust is the displaced weight of mud.

$$\vec{F}_{mud} = A \rho_m g \, dz \, \vec{z_1} + A \rho_m g h_1 \vec{n_1} + A \rho_m g h_2 \vec{n_2} \qquad (A.10)$$

where

$$\vec{z_1} = \begin{vmatrix} 0 \\ \sin\phi \\ \cos\phi \end{vmatrix}_{oxyz} ; \quad \vec{n_1} = \begin{vmatrix} (\partial x/\partial z)_{z+\frac{dz}{2}} \\ (\partial y/\partial z)_{z+\frac{dz}{2}} \\ 1 \end{vmatrix}_{oxyz} ; \quad \vec{n_2} = \begin{vmatrix} -(\partial x/\partial z)_{z-\frac{dz}{2}} \\ -(\partial y/\partial z)_{z-\frac{dz}{2}} \\ -1 \end{vmatrix}_{oxyz}$$

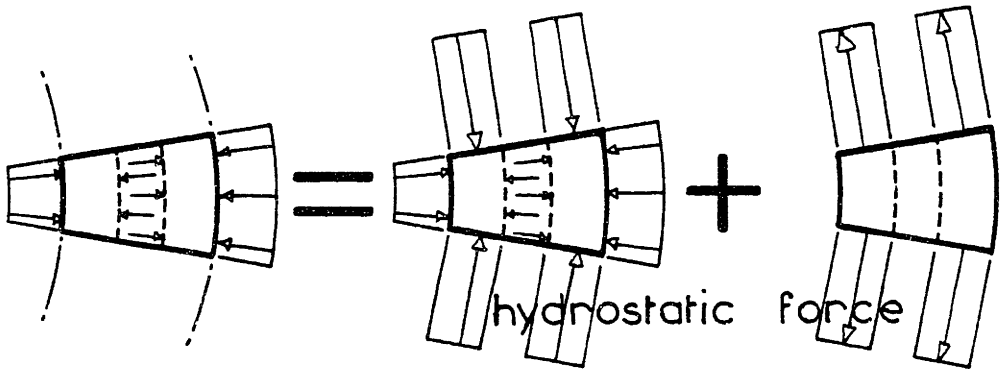

Figure A.9 - Calculation of Mud Forces.

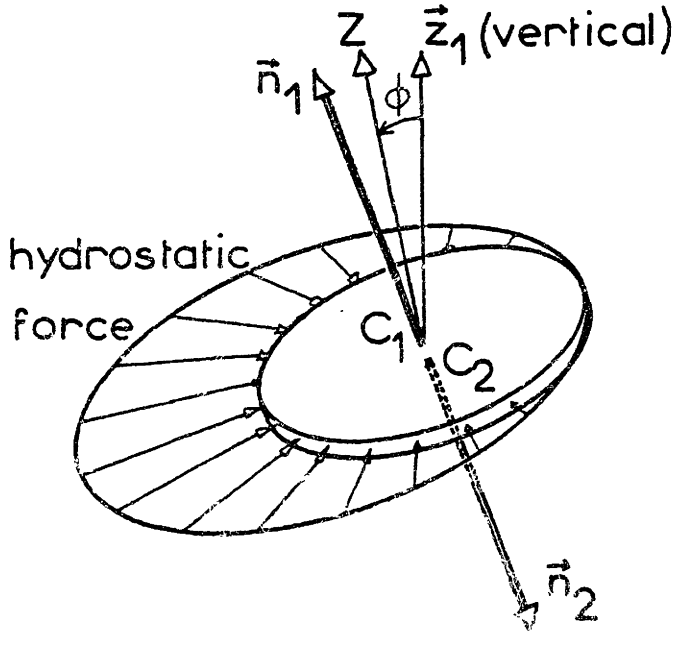

Figure A.10 - Notations for Action of Hydrostatic Pressure.

$$h_2 - h_1 = \overrightarrow{C_2 C_1} \cdot \vec{z}_1 = dz \begin{vmatrix} (\partial x/\partial z) \\ (\partial y/\partial z) \\ 1 \end{vmatrix} \cdot \begin{vmatrix} 0 \\ \sin\phi \\ \cos\phi \end{vmatrix} = \left[\sin\phi \frac{\partial y}{\partial z} + \cos\phi \right] dz$$

$$\vec{F}_{mud} = A\rho_m g \left\{ \vec{z}_1 dz + h_1 \vec{n}_1 + \left[h_1 + (h_2 - h_1) \right] \vec{n}_2 \right\}$$

$$= A\rho_m g \left\{ \vec{z}_1 dz + h_1 (\vec{n}_1 + \vec{n}_2) + \left(\sin\phi \frac{\partial y}{\partial z} + \cos\phi \right) \vec{n}_2 \, dz \right\}$$

$$\vec{F}_{mud} = A\rho_m g \, dz \begin{vmatrix} h_1 \frac{\partial^2 x}{\partial z^2} - \cos\phi \frac{\partial x}{\partial z} \\ \sin\phi + h_1 \frac{\partial^2 y}{\partial z^2} - \cos\phi \frac{\partial y}{\partial z} \\ \cos\phi - \cos\phi - \sin\phi \frac{\partial y}{\partial z} \end{vmatrix}_{OXYZ}$$

Now, with Figure A.11, let us write h_1 in terms of z, and the depth D of the bit:

For $0 \leqslant z \leqslant L$, we have $h_1 = D - z\cos\phi - y\sin\phi$

$$\sim D - z\cos\phi$$

$$\vec{F}_{mud} = A\rho_m g \, dz \begin{vmatrix} (D - z\cos\phi) \frac{\partial^2 x}{\partial z^2} - \cos\phi \frac{\partial x}{\partial z} \\ (D - z\cos\phi) \frac{\partial^2 y}{\partial z^2} - \cos\phi \frac{\partial y}{\partial z} + \sin\phi \\ -\sin\phi \frac{\partial y}{\partial z} \end{vmatrix}_{OXYZ} \quad (A.11)$$

A.6 Effect of gravity.

Since

$$\vec{g} = -g \begin{vmatrix} 0 \\ \sin\phi \\ \cos\phi \end{vmatrix}_{OXYZ},$$

the weight of the slice of mass $A\rho\,dz$ is:

$$\vec{F}_{gravity} = -A\rho g \, dz \begin{vmatrix} 0 \\ \sin\phi \\ \cos\phi \end{vmatrix}_{OXYZ} \quad (A.12)$$

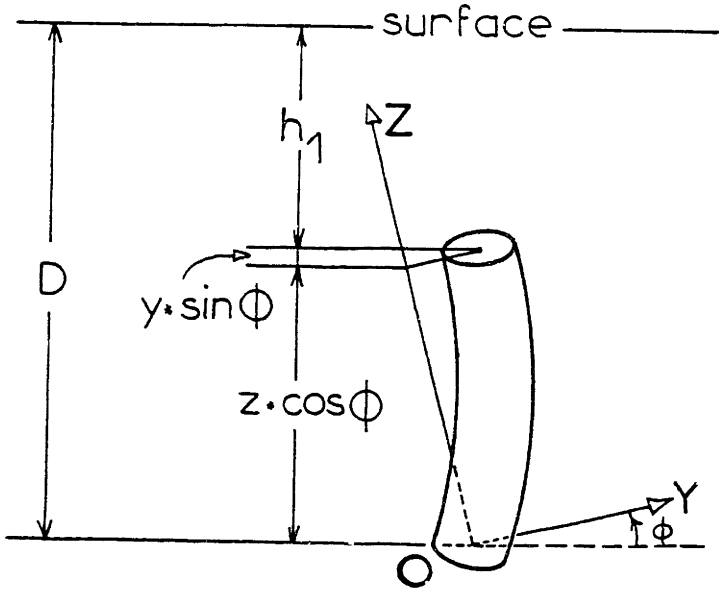

Figure A.11 - Depth of Section in Terms of D, z, y, ϕ.

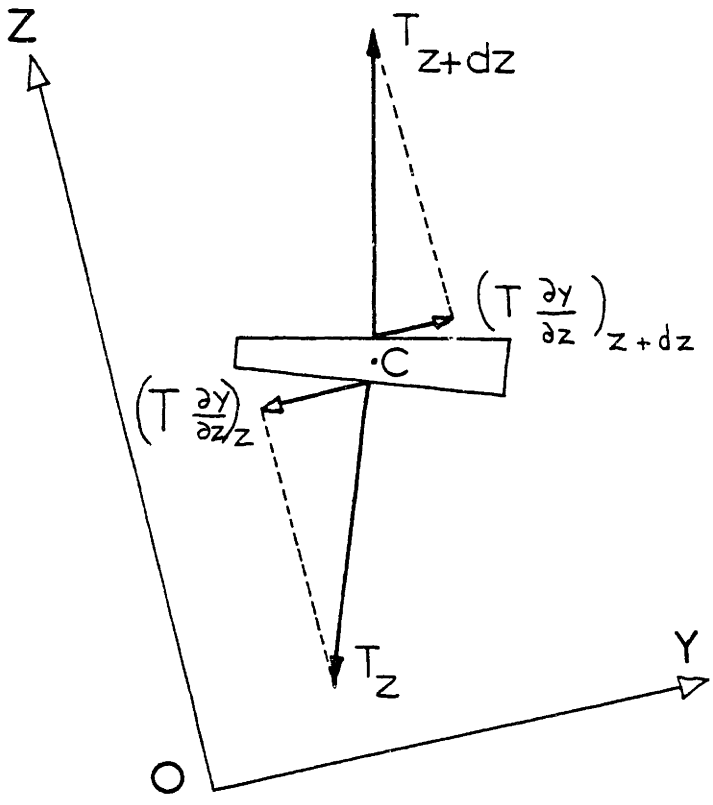

Figure A.12 - Contribution of Tensile Force to Net Side-Force.

A.7 Effect of Coupling Compression-Bending.

The exact location of the point where the tensile force is applied doesn't matter. However, Figure A.12 considers that it is located at the centroid.

Actually, the shaft is most likely to be in compression, so T is usually negative.

The net Y-force is $\left(T\frac{\partial y}{\partial z}\right)_{z+dz} - \left(T\frac{\partial y}{\partial z}\right)_{z} = \frac{\partial}{\partial z}\left(T\frac{\partial y}{\partial z}\right)dz$

Similarly, the net X-force is $\frac{\partial}{\partial z}\left(T\frac{\partial x}{\partial z}\right)dz$

To reach the normal tension T, the forces $\overrightarrow{T}_{z+dz}$, $\overrightarrow{T}_{z}$, $\overrightarrow{F}_{mud}$ and $\overrightarrow{F}_{gravity}$ are projected along Z, and the acceleration along this axis is equated to zero:

$$0 = T_{z+dz} - T_z - A\rho_m g\, dz \sin\phi \frac{\partial y}{\partial z} - A\rho g\, dz \cos\phi$$

$$\frac{dT}{dz} = A g\left[\rho_m \sin\phi \frac{\partial y}{\partial z} + \rho\cos\phi\right]$$

$$T(z) = A g\left[\rho_m.\sin\phi.y + \rho.\cos\phi.z\right] - T_o$$

where T_o is the true compression exerted onto the lower face of the bit. According to the assumptions stated in the introduction, y remains small compared to z and doesn't exceed 20 degrees, so we are perfectly justified in writing:

$$T(z) = A\rho g.\cos\phi.z - T_o \qquad (A.13)$$

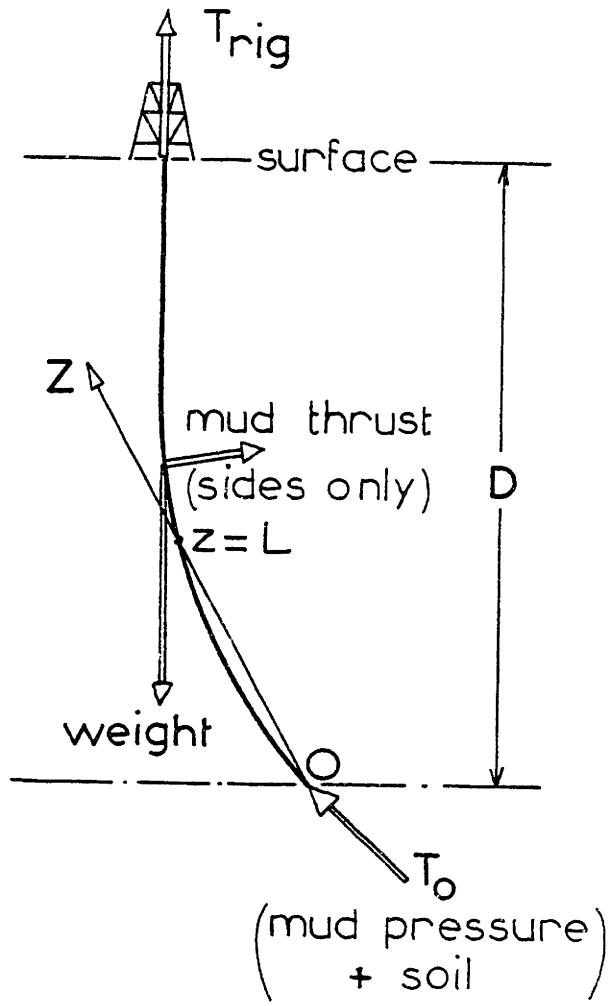

Figure A.13 - Forces Exerted on the Entire Drill String.

T_o can be reached by static analysis: Figure A.13 shows that beside T_o, the entire drill string is submitted to its own weight W, the mud thrust, the tension T_{rig}, and the side-forces due to all the various bearings along the pipe (stabilizers, shock absorbers, etc.). It is assumed that these bearings have no axial contribution.

To make calculations easier, Figure A.14 shows how the hydrostatic force is introduced and then substracted.

The mud thrust along the sides of the pipe together with the hydrostatic pressure at the bit yields the standard vertical buoyant force, equal to the weight of mud displaced by the entire string. Projecting the forces along Z:

$$0 = \left\{T_{rig} - W(1 - \rho_m/\rho)\right\} \cos\phi + T_o - \rho_m g D A$$

$$T_o = \rho_m g D A + \left\{W(1 - \rho_m/\rho) - T_{rig}\right\} \cos\phi \quad (A.14)$$

If one considers the case where the string is vertical and the rig supports entirely the apparent weight of the pipe, one has:

$$T_{rig} = W(1 - \rho_m/\rho) .$$

Although the drill string is suspended and the bit doesn't touch the soil, one still has the hydrostatic compression, and indeed $T_o = \rho_m g D A$.

However, as will be seen later, the effective compression that appears in the final equations is the reaction of the soil, namely: $\left\{W(1 - \rho_m/\rho) - T_{rig}\right\} \cos\phi$.

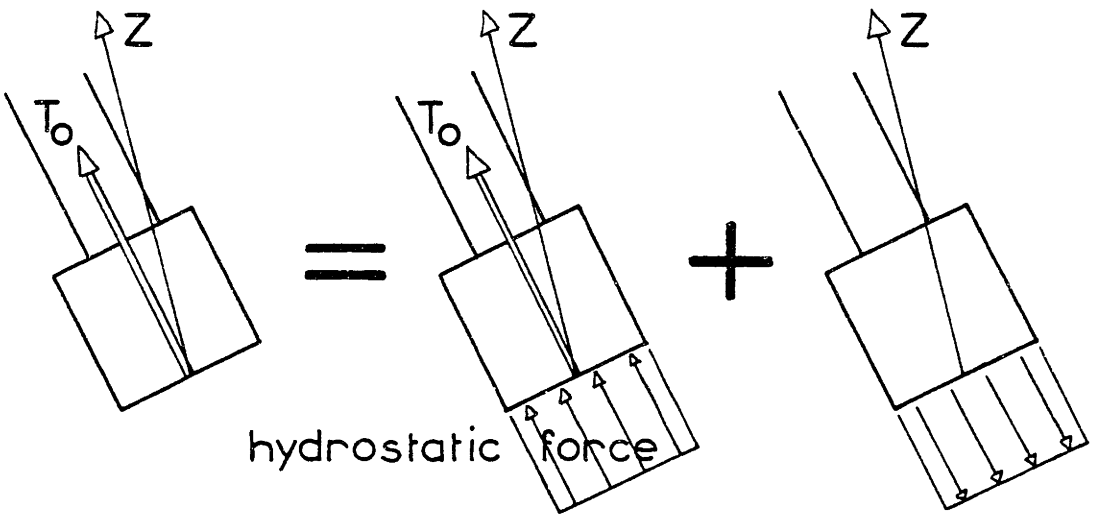

Figure A.14 - Calculation of Forces on the Bit.

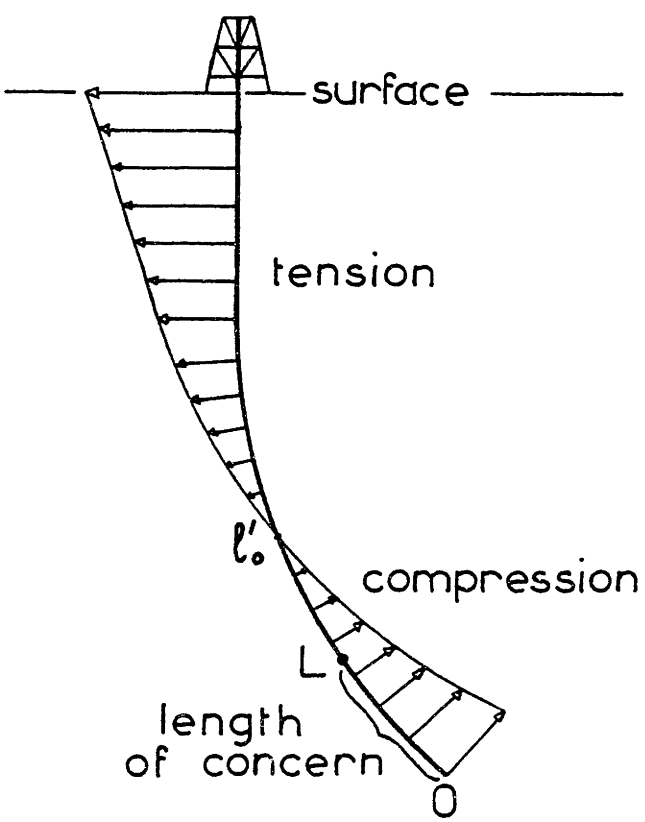

Figure A.15 - Tension Variation Along the String.

Introducing $\ell'_o = \frac{T_o}{A\rho g \cos\phi}$, we have

$$T(z) = A\rho g \cos\phi \,(z - \ell'_o) \qquad \text{(A.15)}$$

l'_o is a characteristic length of compression (Figure A.15).

Strictly speaking, l'_o is not the exact length over which the collars are in compression, because the cross-section A and the angle ϕ usually decrease toward the top, thus affecting the local mean rate of change of tension $A\rho g \cos\phi$.

We finally get

$$\vec{F}_{comp.} = -A\rho g \cos\phi \, dz \begin{vmatrix} \frac{\partial}{\partial z}\left[(\ell'_o - z)\frac{\partial x}{\partial z}\right] \\ \frac{\partial}{\partial z}\left[(\ell'_o - z)\frac{\partial y}{\partial z}\right] \\ -1 \end{vmatrix}_{oxyz} \qquad \text{(A.16)}$$

A.8 Dimensional Partial Differential Equation:

a. In the Static Frame.

Recollecting the different contributions, equation (A.1) becomes

$$m\frac{d^2\overrightarrow{O'G}}{dt^2} = \vec{F}_{stiff.} + \vec{F}_{torq.} + \vec{F}_{\substack{ext.\\damp.}} + \vec{F}_{\substack{int.\\damp.}} + \vec{F}_{mud} + \vec{F}_{gravity} + \vec{F}_{comp} \qquad \text{(A.17)}$$

where m = mass of steel + added mass of mud = $A\rho C_M dz$.

Projecting along X and Y only and dividing through by dz:

$$A\rho C_M\left[\ddot{x} - a\Omega^2\cos\Omega t\right] = -EI\frac{\partial^4 x}{\partial z^4} - Q\left(-\frac{\partial^3 y}{\partial z^4}\right) - C_e\dot{x} - C_i\left(\dot{x} + \Omega y\right)$$

$$+ A\rho_m g(D - z\cos\phi)\frac{\partial^2 x}{\partial z^2} - A\rho_m g\cos\phi\frac{\partial x}{\partial z} - A\rho g\cos\phi(\ell'_o - z)\frac{\partial^2 x}{\partial z^2} + A\rho g\cos\phi\frac{\partial x}{\partial z}$$

- $$A\rho C_M\left[\ddot{y} - b\Omega^2 \sin\Omega t\right] = -EI\frac{\partial^4 y}{\partial z^4} - Q\frac{\partial^3 x}{\partial z^3} - C_e\dot{y} - C_i(\dot{y} - \Omega x)$$

$$+ A\rho_m g(D - z\cos\phi)\frac{\partial^2 y}{\partial z^2} - A\rho_m g\cos\phi\frac{\partial y}{\partial z} - A\rho g\cos\phi(l'_o - z)\frac{\partial^2 y}{\partial z^2}$$

$$+ A\rho g\cos\phi\frac{\partial y}{\partial z} - A(\rho - \rho_m)g\sin\phi .$$

Using $T_o = A\rho g l'_o \cos\phi$:

- $$A\rho C_M\left[\ddot{x} - a\Omega^2\cos\Omega t\right] = -EI\frac{\partial^4 x}{\partial z^4} + Q\frac{\partial^3 y}{\partial z^3} - C_i\Omega y - (C_e + C_i)\dot{x}$$

$$+ \frac{\partial^2 x}{\partial z^2}\left[Agz\cos\phi(\rho - \rho_m) - (T_o - \rho_m g DA)\right] + A(\rho - \rho_m)g\cos\phi\frac{\partial x}{\partial z}$$

- $$A\rho C_M\left[\ddot{y} - b\Omega^2\sin\Omega t\right] = -EI\frac{\partial^4 y}{\partial z^4} - Q\frac{\partial^3 x}{\partial z^3} + C_i\Omega x - (C_e + C_i)\dot{y}$$

$$+ \frac{\partial^2 y}{\partial z^2}\left[Agz\cos\phi(\rho - \rho_m) - (T_o - \rho_m g DA)\right] + A(\rho - \rho_m)g\cos\phi\frac{\partial y}{\partial z}$$

$$- A(\rho - \rho_m)g\sin\phi$$

Here appears the quantity

$$T_o - \rho_m g DA = \left\{W(1 - \rho_m/\rho) - T_{riz}\right\}\cos\phi \equiv T_1$$

Introducing $h = 1 - \rho_m/\rho$

and $$l'_1 = \frac{T_1}{A\rho g h\cos\phi} \qquad \text{(A.18)}$$

the coefficient of the second order derivatives becomes

$$A\rho g h \cos\phi \left(z - \ell_1'\right)$$

Reordering the terms:

$$\cdot\ A\rho C_M \ddot{x} + (C_e + C_i)\dot{x} + C_i \Omega y + EI \frac{\partial^4 x}{\partial z^4} - Q \frac{\partial^3 y}{\partial z^3}$$

$$+ A\rho g h \cos\phi \left\{ (\ell_1' - z) \frac{\partial^2 x}{\partial z^2} - \frac{\partial x}{\partial z} \right\} = A\rho C_M a \Omega^2 \cos \Omega t$$

$$\cdot A\rho C_M \ddot{y} + (C_e + C_i)\dot{y} - C_i \Omega x + EI \frac{\partial^4 y}{\partial z^4} + Q \frac{\partial^3 x}{\partial z^3}$$

$$+ A\rho g h \cos\phi \left\{ (\ell_1' - z) \frac{\partial^2 y}{\partial z^2} - \frac{\partial y}{\partial z} \right\} = A\rho C_M b \Omega^2 \sin \Omega t - A\rho g h \sin\phi$$

This equation can be conveniently handled if we work in a complex plane located at the running cut z. Then, introducing

$e'(z) = a(z) + i\ b(z)$ (e as in eccentricity)

$s'(z,t) = x(z,t) + i\ y(z,t)$ (s as in static frame)

and dividing through by $A\rho C_M$, one finally obtains:

$$\ddot{s}' + \frac{C_e + C_i}{A\rho C_M} \dot{s}' + \frac{EI}{A\rho C_M} \frac{\partial^4 s'}{\partial z^4} + i \frac{Q}{A\rho C_M} \frac{\partial^3 s'}{\partial z^3}$$

$$+ \frac{g h \cos\phi}{C_M} \left[(\ell_1' - z) \frac{\partial^2 s'}{\partial z^2} - \frac{\partial s'}{\partial z} \right] - i \frac{C_i \Omega}{A\rho C_M} s' \qquad \text{(A.19)}$$

$$= \Omega^2 e'(z)\, e^{i\Omega t} - i \frac{g h \sin\phi}{C_M}$$

The contribution of Q is multiplied by i, which expresses the out-of-plane effect of Q on the bending. If we set

$\rho_m = 0$ (so $C_M = 1$ and $h = 1$)

$Q = 0$

$\phi = \pi/2$, we obtain:

$$\ddot{s}' + \frac{c_e + c_i}{A\rho}\dot{s}' + \frac{EI}{A\rho}\frac{\partial^4 s'}{\partial z^4} - i\frac{c_i \Omega}{A\rho}s' = \Omega^2 e'(z)\, e^{i\Omega t} - i g$$

which is the equation derived by Bishop and Gladwell (1959b, page 75, equation 76).

b. In the Rotating Frame.

An alternative form of (A.19) can be obtained in the rotating frame;

Let $s'(z,t) = r'(z,t).e^{i\Omega t}$, where $r' = u + i\,v$ (r as in rotating frame), one has

$$\dot{s}' = (\dot{r}' + i\Omega r').e^{i\Omega t}$$

$$\ddot{s}' = (\ddot{r}' + 2i\Omega \dot{r}' - \Omega^2 r').e^{i\Omega t}$$

Substituting for s', $\dot{s}'$ and $\ddot{s}'$ into (A.19) yields

$$\ddot{r}' + \left[\frac{c_e + c_i}{A\rho c_M} + 2i\Omega\right]\dot{r}' + \frac{EI}{A\rho c_M}\frac{\partial^4 r'}{\partial z^4} + i\frac{Q}{A\rho c_M}\frac{\partial^3 r'}{\partial z^3} + \frac{g h \cos\phi}{c_M}\left[(\ell_1' - z)\frac{\partial^2 r'}{\partial z^2} - \frac{\partial r'}{\partial z}\right] - \left[\Omega^2 - i\frac{c_e \Omega}{A\rho c_M}\right]r' = \Omega^2 e'(z) - \frac{g h \sin\phi}{c_M}\, e^{-i\Omega t} \qquad (A.20)$$

A.9 Boundary Conditions and External Torques.

a. At Bit.

First, we assume that the bit remains centered about the center of the hole:

$$s'(0,t) = 0$$

An attempt has been made to account for a restoring moment resulting from the embedding of the bit into the soil. The total compression at the bit is T_o, but T_o includes the hydrostatic thrust against the lower face of the bit, which clearly cannot cause any moment (Figure A.16).

The magnitude of this restoring moment is taken equal to

$$M_{rest} = k' T_1 \alpha$$

where T_1 = reaction of the soil only

$= A \rho g h l_1' \cos\phi$, according to (A.18),

and k' = dimensional characteristic radius of the bit.

k' depends essentially on two parameters, the shape of the bit (Figure A.17) and the nature of the soil being drilled through (Figure A.18): if the bit drills through an infinitely hard soil, it cannot bite into the bottom of the hole, and k' is equal to the radius of the bit. On the other hand, a very soft soil has a small stiffness and can hardly apply a restoring moment: in this case, k' is intuitively very small.

Figure A.19 helps derive the analytical expression for $\overrightarrow{M}_{rest}$.

When $\frac{\partial x}{\partial z} = 0$ and $\frac{\partial y}{\partial z} > 0$, one has a positive X-borne moment.

When $\frac{\partial x}{\partial z} < 0$ and $\frac{\partial y}{\partial z} = 0$, one gets a positive Y-borne moment.

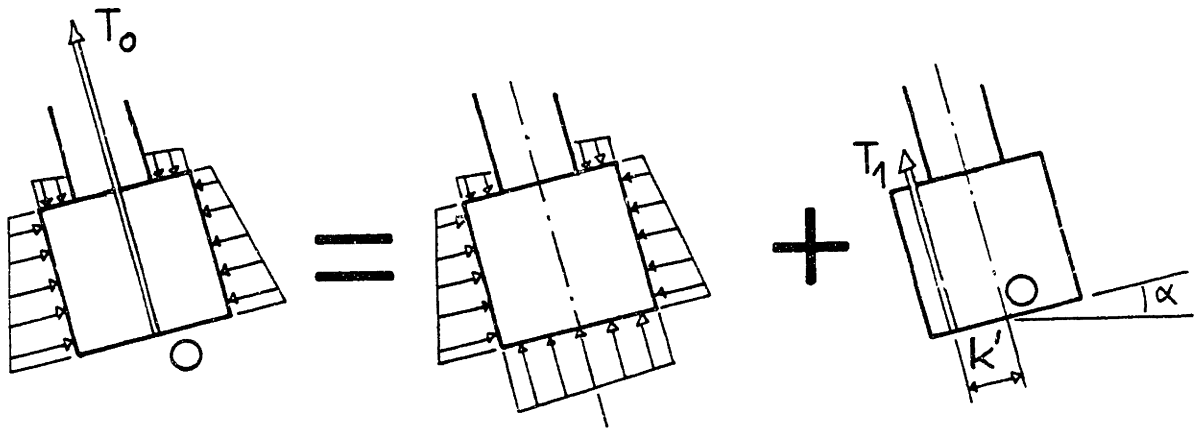

Figure A.16 - Computation of the Soil Contact Force, T_1.

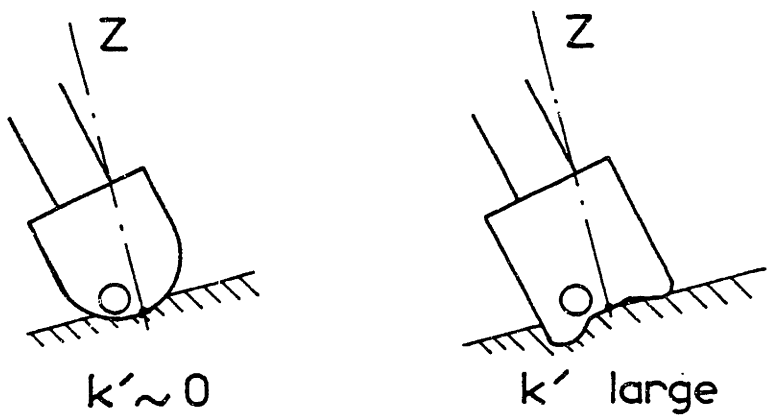

Figure A.17 - Dependence of k' on the Shape of the Bit.

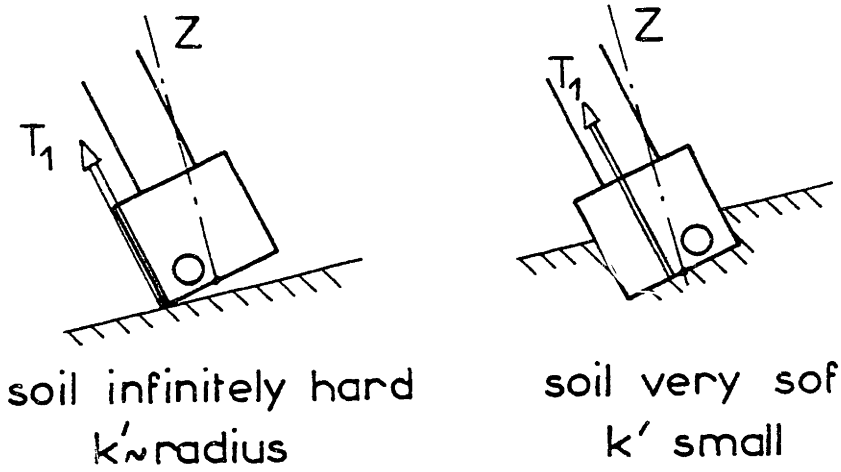

Figure A.18 - Dependence of k' on the Soil Properties.

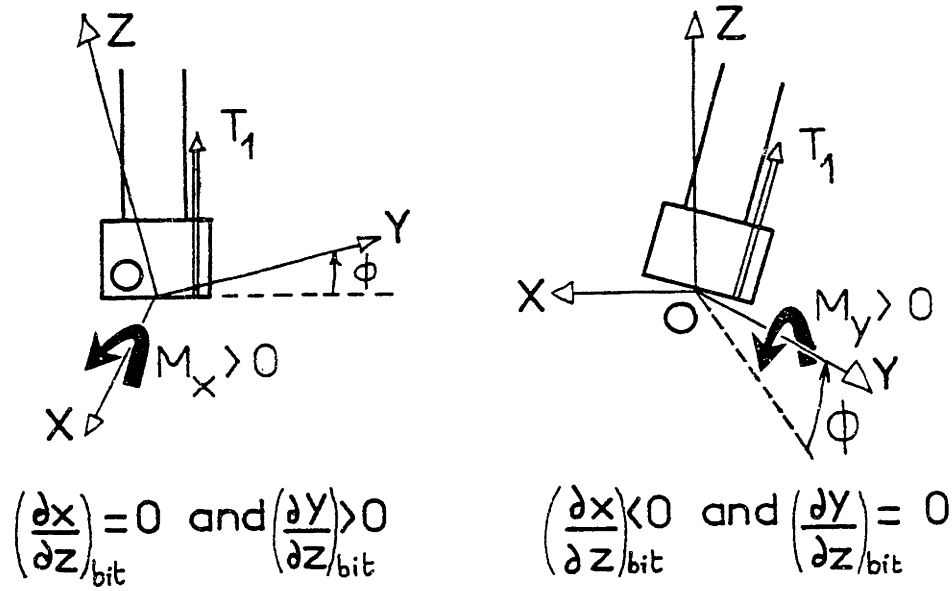

Figure A.19 - Sign Considerations for Expressing the Restoring Moment, $\overrightarrow{M}_{rest}$.

$$\vec{M}_{rest} = k' T_1 \Big|_{oxyz} \begin{vmatrix} \frac{\partial y}{\partial z} \\ -\frac{\partial x}{\partial z} \\ 0 \end{vmatrix} \qquad \text{(A.21)}$$

The rate of change of momentum is neglected, therefore the relationship between the externally applied torque Q_{bit} and EI is provided by the usual approximation in strength material theory:

$$\vec{Q}_{bit} \wedge \vec{n}_{bit} = EI \frac{\partial^2 \vec{OC}}{\partial z^2} \qquad \text{(A.22)}$$

But $\vec{Q}_{bit} = -Q\,\vec{Z} + \vec{M}_{rest}$ ($-Q\,\vec{Z}$ is the reaction of the soil)

$$\vec{Q}_{bit} = \Big|_{oxyz} \begin{vmatrix} k' T_1 \frac{\partial y}{\partial z} \\ -k' T_1 \frac{\partial x}{\partial z} \\ -Q \end{vmatrix}$$

Substituting for $\vec{n} = \Big|_{oxyz} \begin{vmatrix} \partial x/\partial z \\ \partial y/\partial z \\ 1 \end{vmatrix}$,

relation (A.22) reads:

$$\begin{cases} EI \frac{\partial^2 x}{\partial z^2} = Q \frac{\partial y}{\partial z} - k' T_1 \frac{\partial x}{\partial z} \\ EI \frac{\partial^2 y}{\partial z^2} = -Q \frac{\partial x}{\partial z} - k' T_1 \frac{\partial y}{\partial z} \end{cases}$$

As a conclusion one gets:

Externally applied torque

$$\vec{Q}_{bit} = -i k' T_1 \left(\frac{\partial s'}{\partial z}\right)_{z=0} - Q \vec{Z} \qquad (A.23)$$

Boundary conditions

$$\begin{cases} s'(0,t) = 0 \\ \left(\frac{\partial^2 s'}{\partial z^2}\right)_{(0,t)} = -\frac{k' T_1 + i Q}{EI} \left(\frac{\partial s'}{\partial z}\right)_{(0,t)} \end{cases} \qquad (A.24)$$

b. At Stabilizers.

Firstly, let us consider the case of a fully built-in condition.

Let $\vec{Q}_{sta}$ = externally applied moment = $\begin{vmatrix} Q_x \\ Q_y \\ Q \end{vmatrix}$.

Substituting for $\vec{n}_{sta} = \begin{vmatrix} 0 \\ 0 \\ 1 \end{vmatrix}_{oxyz}$ into relation (A.22):

$$\left(\begin{vmatrix} Q_x \\ Q_y \\ Q \end{vmatrix}_{oxyz} \wedge \begin{vmatrix} 0 \\ 0 \\ 1 \end{vmatrix}_{oxyz} \right) = \begin{vmatrix} Q_y \\ -Q_x \\ 0 \end{vmatrix}_{oxyz} \equiv EI \begin{vmatrix} \frac{\partial^2 x}{\partial z^2} \\ \frac{\partial^2 y}{\partial z^2} \\ 0 \end{vmatrix}_{oxyz}$$

whence $\vec{Q}_{sta} = \begin{vmatrix} Q_x = -EI \frac{\partial^2 y}{\partial z^2} \\ Q_y = EI \frac{\partial^2 x}{\partial z^2} \\ Q \end{vmatrix}_{oxyz}$

As a conclusion $\vec{Q}_{sta} = i EI \frac{\partial^2 s'}{\partial z^2}_{(L,t)} + Q \vec{Z}$

Boundary conditions $\begin{cases} s'(L,t) = 0 \\ \left(\frac{\partial s'}{\partial z}\right)_{(L,t)} = 0 \end{cases}$

Then let us address the case of a pinned end.

$$\vec{Q}_{sta} = \vec{Q} = \begin{vmatrix} 0 \\ 0 \\ Q \end{vmatrix}_{oxyz} \quad , \quad \text{and} \quad \vec{n}_{sta} = \begin{vmatrix} \frac{\partial x}{\partial z} \\ \frac{\partial y}{\partial z} \\ 1 \end{vmatrix}_{oxyz}$$

The boundary conditions stem from relation (A.22):

Hence

$$\vec{Q}_{sta} = Q \vec{Z}$$

Boundary conditions

$$\begin{cases} \delta'_{(L,t)} = 0 \\ \left(\frac{\partial^2 \delta'}{\partial z^2}\right)_{(L,t)} = i \frac{Q}{EI} \left(\frac{\partial \delta'}{\partial z}\right)_{(L,t)} \end{cases}$$

Now, we can allow for an end condition somewhere in between clamped and pinned. To this end, a continuous parameter c is introduced, such that

c = 0 for a pinned end,

c = 1 for a clamped end.

The actual effect of c on reality is investigated in appendix B.1.2.b. and in Figures B.2 and B.3.

Thus

$$\vec{Q}_{sta} = i c EI \left(\frac{\partial^2 \delta'}{\partial z^2}\right)_{(L,t)} + Q \vec{Z} \qquad (A.25)$$

with the corresponding end conditions:

$$\begin{cases} \delta'_{(L,t)} = 0 \\ (1-c) \left(\frac{\partial^2 \delta'}{\partial z^2}\right)_{(L,t)} - i \frac{Q}{EI} \left(\frac{\partial \delta'}{\partial z}\right)_{(L,t)} = 0 \end{cases} \qquad (A.26)$$

A.10 Non-Dimensionalization of the Problem.

Introducing

$$\omega_o^2 = EI / A\rho C_M L^4$$

$$\tau = \omega_o t$$

$$w = z/L$$

$$\delta(w,\tau) = \delta'(z,t)/L \qquad \left(\frac{\partial \delta}{\partial \tau} \equiv \dot{\delta} \,,\ \frac{\partial^2 \delta}{\partial \tau^2} \equiv \ddot{\delta} \right)$$

$$e(w) = e'(z)/L$$

$$l_1 = l_1'/L$$

$$k = k'/L \,,$$

the equation in the static frame becomes

$$\ddot{\delta} + \frac{C_e + C_i}{A\rho C_M \omega_o} \dot{\delta} + \frac{\partial^4 \delta}{\partial w^4} + i \frac{QL}{EI} \frac{\partial^3 \delta}{\partial w^3} + \frac{h}{C_M} \frac{g\cos\phi}{L\omega_o^2} \left[(l_1 - w) \frac{\partial^2 \delta}{\partial w^2} - \frac{\partial \delta}{\partial w} \right] - i \frac{C_i \Omega}{A\rho C_M \omega_o^2} \delta = \frac{\Omega^2}{\omega_o^2} e(w) e^{i \frac{\Omega}{\omega_o} \tau} - i \frac{h}{C_M} \frac{g \sin\phi}{L\omega_o^2} \tag{A.27}$$

with the associated end conditions:

$$\text{Bit} \begin{cases} r(0,\tau) = 0 \\ \left(\frac{\partial^2 r}{\partial w^2} \right)_{(0,\tau)} = -\left(\frac{h}{C_M} \frac{g\cos\phi}{L\omega_o^2} k l_1 + i \frac{QL}{EI} \right) \left(\frac{\partial r}{\partial w} \right)_{(0,\tau)} \end{cases}$$

(A.28)

$$\text{Stabilizer} \begin{cases} r(1,\tau) = 0 \\ (1-c) \left(\frac{\partial^2 r}{\partial w^2} \right)_{(1,\tau)} - i \frac{QL}{EI} \left(\frac{\partial r}{\partial w} \right)_{(1,\tau)} = 0 \end{cases}$$

Setting

$$C_i = 0$$

$$C_M = 1$$

$$\phi = 0$$

$e(w) = 0$, one gets

$$\ddot{s} + \frac{Ce}{A\rho\omega_0}\dot{s} + \frac{\partial^4 s}{\partial w^4} + i\frac{QL}{EI}\frac{\partial^3 s}{\partial w^3} + \frac{gh}{L\omega_0^2}\left[(\ell_1 - w)\frac{\partial^2 s}{\partial w^2} - \frac{\partial s}{\partial w}\right] = 0 ,$$

which is to be identified with the results of Dubigeon (1973, page 340, equation D) where it is to be noticed that the conventions of this author are different and cause a sign shift for the term $\frac{gh}{L\omega_0^2}$. Likewise, the dimensionless problem in the rotating trihedral becomes:

$$\ddot{r} + \left[\frac{Ce+Ci}{A\rho C_M \omega_0} + 2i\frac{\Omega}{\omega_0}\right]\dot{r} + \frac{\partial^4 r}{\partial w^4} + i\frac{QL}{EI}\frac{\partial^3 r}{\partial w^3}$$

$$+ \frac{h}{C_M}\frac{g\cos\phi}{L\omega_0^2}\left[(\ell_1 - w)\frac{\partial^2 r}{\partial w^2} - \frac{\partial r}{\partial w}\right] - \left[\frac{\Omega^2}{\omega_0^2} - i\frac{Ce\,\Omega}{A\rho C_M \omega_0^2}\right] r \qquad (A.29)$$

$$= \frac{\Omega^2}{\omega_0^2}e(w) - i\frac{h}{C_M}\frac{g\sin\phi}{L\omega_0^2}e^{-i\frac{\Omega}{\omega_0}\tau}$$

with the similar end conditions

$$\text{Bit} \begin{cases} r(0,\tau) = 0 \\ \left(\frac{\partial^2 r}{\partial w^2}\right)_{(0,\tau)} = -\left(\frac{h}{C_M}\frac{g\cos\phi}{L\omega_0^2}k\ell_1 + i\frac{QL}{EI}\right)\left(\frac{\partial r}{\partial w}\right)_{(0,\tau)} \end{cases} \qquad (A.30)$$

$$\text{Stabilizer} \begin{cases} r(1,\tau) = 0 \\ (1-c)\left(\frac{\partial^2 r}{\partial w^2}\right)_{(1,\tau)} - i\frac{QL}{EI}\left(\frac{\partial r}{\partial w}\right)_{(1,\tau)} = 0 \end{cases}$$

A.11 Ultimate Dimensionless Formulation in Terms of Ordinary Differential Equations.

As shown in parts B.1.4 and B.2.2, the forces at the bit and the stabilizer are easily obtained when the displacements are known. Since the purpose of this study is to get these forces in the fixed trihedral, let us focus our attention on equation (A.27).

Although one of the coefficients in (A.27) is not a constant, the equation is linear and the principle of superposition holds. Therefore, we can proceed as follows:

$$s = s_h + s_e + s_\phi \qquad (A.31)$$

where:

s_h = general (transient) solution of the homogeneous equation corresponding to (A.27). The shaft is assumed to be stable, so s_h decays and vanishes.

s_e = particular (steady-state) solution of (A.27) with forcing term $\frac{\Omega^2}{\omega_o^2} e(w).e^{i\frac{\Omega}{\omega_o}\tau}$ only. s_e is cast under the form $s_e(w,\tau) = r_e(w).e^{i\frac{\Omega}{\omega_o}\tau}$, so r_e is the solution of (A.29) with $\dot{r} = \ddot{r} = 0$.

s_ϕ = particular (steady-state) solution of (A.27) with forcing term $-i\frac{h}{c_M}\frac{gain\,\phi}{L\omega_o^2}$ only. Since this term is time-independent, s_ϕ is sought under the form $s_\phi(w,\tau) \equiv s_\phi(w)$, so s_ϕ the is solution of equation (A.27) with $\dot{s} = \ddot{s} = 0$.

As a conclusion, the solution for the displacements is given by :

$$s_{\substack{\text{steady}\\\text{state}}}(w,t) = s_\phi(w) + r_e(w).e^{i\Omega t} \qquad (A.32)$$

where s_ϕ is the particular solution of the ordinary differential equation

$$\frac{d^4 s_\phi}{dw^4} + i\frac{QL}{EI}\frac{d^3 s_\phi}{dw^3} + \frac{h}{c_M}\frac{g\cos\phi}{L\omega_o^2}\left[(l_1 - w)\frac{d^2 s_\phi}{dw^2} - \frac{d s_\phi}{dw}\right] - i\frac{c_i \Omega}{A\rho c_M \omega_o^2} s_\phi = -i\frac{h}{c_M}\frac{g\sin\phi}{L\omega_o^2} \qquad (A.33)$$

and r_e is the particular solution of the ordinary differential equation

$$\frac{d^4 r_e}{dw^4} + i\frac{QL}{EI}\frac{d^3 r_e}{dw^3} + \frac{h}{c_M}\frac{g\cos\phi}{L\omega_o^2}\left[(l_1 - w)\frac{d^2 r_e}{dw^2} - \frac{d r_e}{dw}\right] - \left[\frac{\Omega^2}{\omega_o^2} - i\frac{c_e \Omega}{A\rho c_M \omega_o^2}\right] r_e = \frac{\Omega^2}{\omega_o^2} e(w) \qquad (A.34)$$

Both s_ϕ and r_e satisfy the boundary conditions:

Bit
$$\begin{cases} q(0) = 0 \\ \left(\frac{d^2 q}{dw^2}\right)_{(0)} = -\left(\frac{h}{c_M}\cdot\frac{g\cos\phi}{L\omega_o^2}\cdot k l_1 + i\frac{QL}{EI}\right)\left(\frac{dq}{dw}\right)_{(0)} \end{cases} \qquad (A.35)$$

Stabilizer
$$\begin{cases} q(1) = 0 \\ (1-c)\left(\frac{\partial^2 q}{\partial w^2}\right)_{(1)} - i\frac{QL}{EI}\left(\frac{\partial q}{\partial w}\right)_{(1)} = 0 \end{cases}$$

APPENDIX B

IMPLEMENTATION OF COMPUTER PROGRAM COLLAR

B.1 Calculation of Solution s_ϕ.

1.1 Finite-Difference Formulation.

For ease of notation, the following coefficients are defined:

$$a_1 = i \frac{QL}{EI}$$

$$a_2 = \frac{h}{c_M} \frac{g\cos\phi}{L\omega_o^2}$$

$$a_3 = -i \frac{c_i \Omega}{A\rho c_M \omega_o^2}$$

$$a_4 = -i \frac{h}{c_M} \frac{g\sin\phi}{L\omega_o^2}$$

$$a_5 = -\frac{\Omega^2}{\omega_o^2} + i \frac{c_e \Omega}{A\rho c_M \omega_o^2}$$

$$a_6 = \frac{\Omega^2}{\omega_o^2}$$

$$a_7 = -\left(\frac{h}{c_M} \frac{g\cos\phi}{L\omega_o^2} \cdot k\ell_1 + i \frac{QL}{EI}\right) = -a_1 - a_2 k\ell_1$$

The equations to solve now read:

$$\frac{d^4 s_\phi}{dw^4} + a_1 \frac{d^3 s_\phi}{dw^3} + a_2 (\ell_1 - w) \frac{d^2 s_\phi}{dw^2} - a_2 \frac{d s_\phi}{dw} + a_3 s_\phi = a_4 \qquad (B.1)$$

$$\frac{d^4 r_e}{dw^4} + a_1 \frac{d^3 s}{dw^3} + a_2 (\ell_1 - w) \frac{d^2 r_e}{dw^2} - a_2 \frac{d r_e}{dw} + a_5 r_e = a_6\, e(w) \qquad (B.2)$$

with the end conditions

$$\text{Bit} \begin{cases} q(0) = 0 & \text{(B.3)} \\ \left(\frac{d^2q}{dw^2}\right)_{(0)} = a_7 \left(\frac{dq}{dw}\right)_{(0)} & \text{(B.4)} \end{cases}$$

$$\text{Stabilizer} \begin{cases} q(1) = 0 & \text{(B.5)} \\ (1-c)\left(\frac{d^2q}{dw^2}\right)_{(1)} - a_1 \left(\frac{dq}{dw}\right)_{(1)} = 0 & \text{(B.6)} \end{cases}$$

The method implemented is the finite-difference method, which is a numerical method that easily applies to any type of boundary value problem. It consists in breaking up the dimensionless shaft into N segments of length 1/N (figure B.1). Strictly speaking, equations (B.1) and (B.2) as they stand only apply to $0 < w < 1$: clearly, at w = 0 and w = 1, the side forces from the fulcra have to be taken into account.

We start by solving for s_ϕ. From now on, s_ϕ will be referred to as s. Making use of the following approximations,

$$\left(\frac{ds}{dw}\right)_j = \frac{N}{2}\left[-s_{j-1} + s_{j+1} \right] + O(1/N^2)$$

$$\left(\frac{d^2s}{dw^2}\right)_j = N^2\left[s_{j-1} - 2s_j + s_{j+1} \right] + O(1/N^2)$$

$$\left(\frac{d^3s}{dw^3}\right)_j = \frac{N^3}{2}\left[-s_{j-2} + 2s_{j-1} - 2s_{j+1} + s_{j+2} \right] + O(1/N^2)$$

$$\left(\frac{d^4s}{dw^4}\right)_j = N^4\left[s_{j-2} - 4s_{j-1} + 6s_j - 4s_{j+1} + s_{j+2} \right] + O(1/N^2)$$

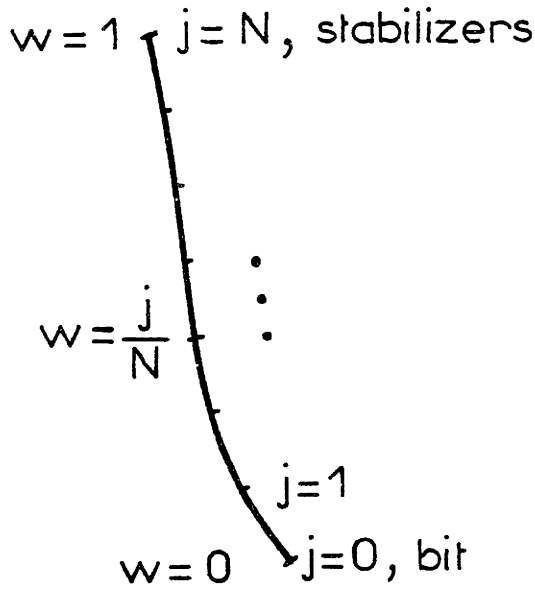

Figure B.1 - Discretization of the Dimensionless Shaft.

we can come up with a set of linear equations and solve for s at every intermediate station j, where $1 \leqslant j \leqslant N-1$.

Unknowns: The N-1 unknowns are $s_1, s_2, \ldots, s_{N-1}$.

Equations: Applying (B.1) at j = 1, ... , N-1 provides N-1 equations involving $s_{-1}, s_0, s_1, \ldots, s_{N-1}, s_N, s_{N+1}$. From equations (B.3) and (B.5), $s_0 = s_N = 0$, and we are left with N+1 unknowns only. At last, equations (B.4) and (B.6) allow us to write s_{-1} in terms of s_1 and s_{N+1} in terms of s_{N-1}, so indeed we get a set of N-1 equations with N-1 unknowns.

1.2 Boundary Conditions.

a. At Bit.

The bit of the dimensionless shaft is at w = j = 0. Equations (B.3) and (B.4) become

$$\begin{cases} \delta_0 = 0 \\ N^2(\delta_{-1} - 2\delta_0 + \delta_1) = a_7 \frac{N}{2}(-\delta_{-1} + \delta_1) \end{cases}$$

Let

$$a_8 = \frac{a_7 - 2N}{a_7 + 2N}$$

We obtain $\begin{cases} s_o = 0 \\ s_{-1} = a_8 \, s_1 \end{cases}$

b. At Stabilizers.

The set of stabilizers of the dimensionless shaft is located at w = 1, or j = N. Equations (B.5) and (B.6) become

$$\begin{cases} \delta_N = 0 \\ (1-c)N^2\left(\delta_{N-1} - 2\delta_N + \delta_{N+1}\right) - a_1 \frac{N}{2}\left(-\delta_{N-1} + \delta_{N+1}\right) = 0 \end{cases}$$

Let

$$a_9 = \frac{a_1 + 2(1-c)N}{a_1 - 2(1-c)N}$$

We obtain

$$\begin{cases} \delta_N = 0 \\ \delta_{N+1} = a_9 \, \delta_{N-1} \end{cases}$$

In order to get a physical understanding of the boundary condition parameter c, let us investigate the effect of c on the coefficient a_9. Plugging in $a_1 = i \frac{QL}{EI}$ into a_9,

$$a_9 = -\frac{4(1-c)^2N^2 - \left(\frac{QL}{EI}\right)^2}{4(1-c)^2N^2 + \left(\frac{QL}{EI}\right)^2} - i\frac{4\frac{QL}{EI}(1-c)N}{4(1-c)^2N^2 + \left(\frac{QL}{EI}\right)^2}$$

$$= -i \cdot \exp\left\{ i \cdot \mathrm{Atan}\left[\frac{(QL/EI)^2 - 4(1-c)^2N^2}{4\frac{QL}{EI}(1-c)N}\right]\right\}$$

As seen in Figure B.2, $a_9(c)$ describes almost entirely the lower half of the unit circle in the complex plane. The effect of c on reality is described in Figure B.3.

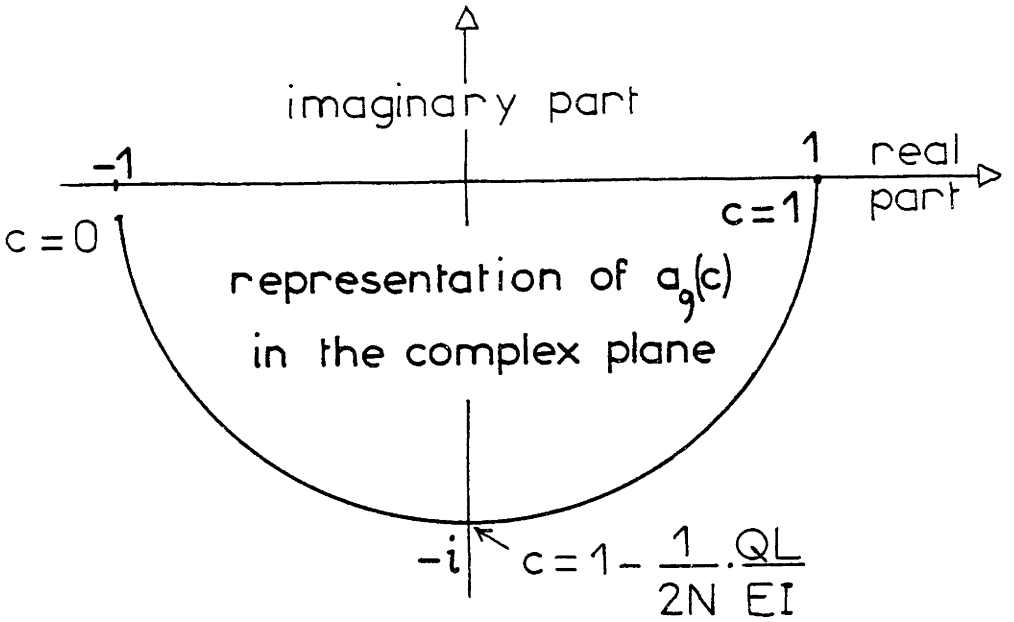

Figure B.2 - Representation of $a_g(c)$ in the Complex Plane.

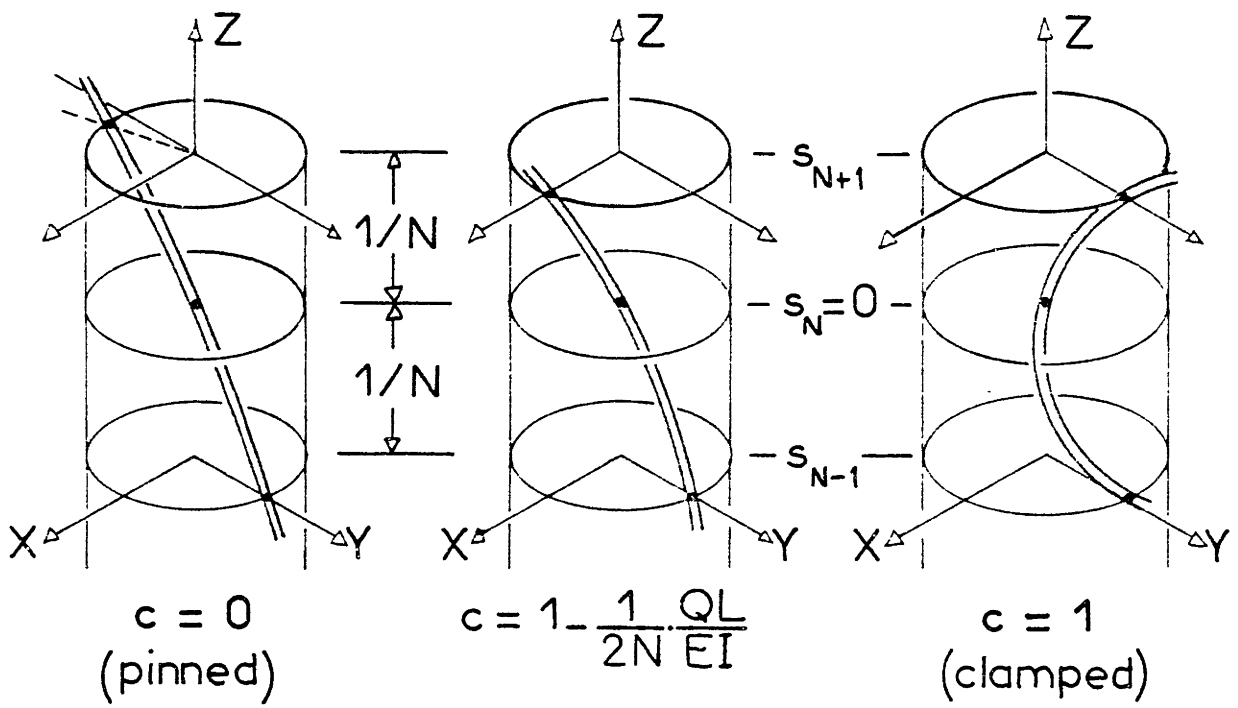

Figure B.3 - Boundary Condition Model at the Stabilizer.

1.3 Construction of the Finite-Difference Matrix.

a. Differential Equation at j, $3 \leq j \leq N-3$.

With $w_j = j/N$, one obtains:

$$
\begin{aligned}
& s_{j-2}\left[N^4 - \frac{a_1}{2} N^3\right] \\
+\ & s_{j-1}\left[-4N^4 + a_1 N^3 + a_2 \ell_1 N^2 - a_2\left(j - \tfrac{1}{2}\right) N\right] \\
+\ & s_j \left[6N^4 - 2a_2 \ell_1 N^2 + 2a_2 jN + a_3\right] \\
+\ & s_{j+1}\left[-4N^4 - a_1 N^3 + a_2 \ell_1 N^2 - a_2\left(j + \tfrac{1}{2}\right) N\right] \\
+\ & s_{j+2}\left[N^4 + \frac{a_1}{2} N^3\right] = a_4
\end{aligned}
$$

b. Differential Equation at j = 1.

$s_{j-2} = s_{-1}$ is replaced by $a_8 \cdot s_1$, and $s_{j-1} = s_0 = 0$.

$$
\begin{aligned}
& s_1\left[a_8\left(N^4 - \frac{a_1}{2} N^3\right) + 6N^4 - 2a_2 \ell_1 N^2 + 2a_2 N + a_3\right] \\
+\ & s_2\left[-4N^4 - a_1 N^3 + a_2 \ell_1 N^2 - a_2\left(1 + \tfrac{1}{2}\right) N\right] \\
+\ & s_3\left[N^4 + \frac{a_1}{2} N^3\right] = a_4
\end{aligned}
$$

c. Differential Equation at j = 2.

Here, $s_{j-2} = s_0 = 0$.

$$\begin{aligned}
&\delta_1\left[-4N^4 + a_1 N^3 + a_2 \ell_1 N^2 - a_2\left(2-\tfrac{1}{2}\right)N\right] \\
&+\delta_2\left[6N^4 - 2a_2\ell_1 N^2 + 4a_2 N + a_3\right] \\
&+\delta_3\left[-4N^4 - a_1 N^3 + a_2\ell_1 N^2 - a_2\left(2+\tfrac{1}{2}\right)N\right. \\
&+\delta_4\left[N^4 + \frac{a_1}{2} N^3\right] \qquad = a_4
\end{aligned}$$

d. Differential Equation at j = N-2.

$s_{N+2} = s_N = 0$.

$$\begin{aligned}
&\delta_{N-4}\left[N^4 - \frac{a_1}{2} N^3\right] \\
&+\delta_{N-3}\left[-4N^4 + a_1 N^3 + a_2\ell_1 N^2 - a_2\left(N-2-\tfrac{1}{2}\right)N\right] \\
&+\delta_{N-2}\left[6N^4 - 2a_2\ell_1 N^2 + 2a_2(N-2)N + a_3\right] \\
&+\delta_{N-1}\left[-4N^4 - a_1 N^3 + a_2\ell_1 N^2 - a_2\left(N-2+\tfrac{1}{2}\right)N\right] \qquad = a_4
\end{aligned}$$

e. Differential Equation at j = N-1.

Now, $s_{j+1} = s_N = 0$, and $s_{j+2} = s_{N+1} = a_9 \cdot s_{N+1}$.

$$\begin{aligned}
&\delta_{N-3}\left[N^4 - \frac{a_1}{2} N^3\right] \\
&+\delta_{N-2}\left[-4N^4 + a_1 N^3 + a_2\ell_1 N^2 - a_1\left(N-1-\tfrac{1}{2}\right)N\right] \\
&+\delta_{N-1}\left[a_9\left(N^4 + \frac{a_1}{2} N^3\right) + 6N^4 - 2a_2\ell_1 N^2 + 2a_2(N-1)N + a_3\right] = a_4
\end{aligned}$$

We get a pentadiagonal matrix.

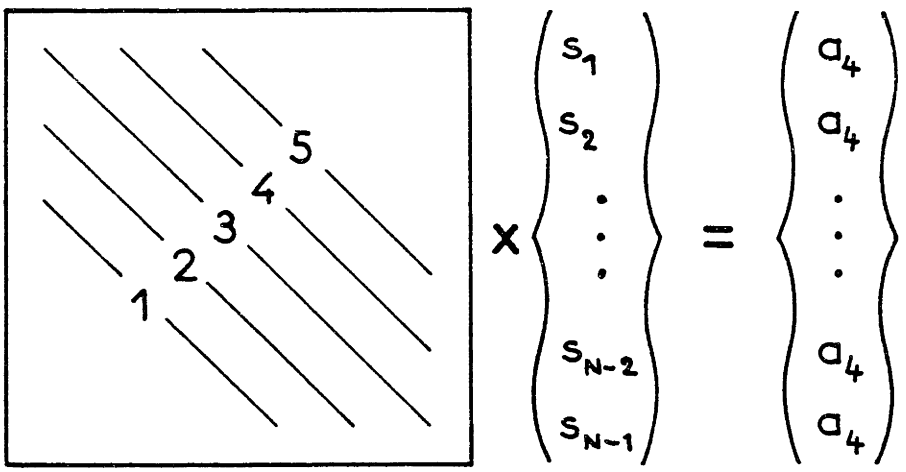

Figure B.4 - Numerotation of the Diagonals.

c_3+2a_2N $+c_1a_8$	c_4-a_2N	c_5				
c_2-2a_2N	c_3+4a_2N	c_4-2a_2N	c_5			
c_1	c_2-3a_2N	c_3+6a_2N	c_4-3a_2N	c_5		
	c_1	$\ddots$	$\ddots$	$\ddots$	c_5	
		c_1	c_2-a_2jN	c_3+2a_2jN	c_4-a_2jN	c_5
			c_1	$\ddots$	$\ddots$	$\ddots$
				c_1	$c_2-a_2(N-2)N$	$c_3+2a_2(N-2)N$
					c_1	$c_2-a_2(N-1)N$

c_5
$c_4-a_2(N-2)N$
$c_3+2a_2(N-1)N$ $+c_5a_9$

Figure B.5 - The Pentadiagonal Complex-Conjugate Finite-Difference Matrix.

Let

$$
\begin{aligned}
c_1 &= N^4 - \frac{a_1}{2} N^3 \\
c_2 &= -4N^4 + a_1 N^3 + a_2 \ell_1 N^2 + \frac{1}{2} a_2 N \\
c_3 &= 6N^4 - 2 a_2 \ell_1 N^2 + a_3 \\
c_4 &= -4N^4 - a_1 N^3 + a_2 \ell_1 N^2 - \frac{1}{2} a_2 N \\
c_5 &= N^4 + \frac{a_1}{2} N^3
\end{aligned}
$$

c_m is the constant part of the coefficients of the matrix in the m-th diagonal, the numerotation being explained in Figure B.4. The matrix is shown in Figure B.5.

It is to be noticed that diagonals 1 and 5 for one hand, and 2 and 4 for the other are complex conjugate with respect to main diagonal 3.

1.4 Dimensional Forces at Bit and Stabilizers.

Once we get the displacements, we can have access to the two side-forces F_{b1}(bit) and F_{s1}(stabilizer) as follows (we are still solving the problem for s_ϕ ; when we get involved in solving for r_e, we shall call the corresponding forces F_{b2} and F_{s2}). The solution s corresponds to a static solution in the fixed set of axes OXYZ. Figure B.6 shows the collars subjected to:

- dimensional forces $-\vec{F}_{b1}$ and $-\vec{F}_{s2}$. $\vec{F}_{b1}$ and $\vec{F}_{s1}$ are the forces exerted by the collars onto the borehole,
- distributed force $-A\rho g\, h \sin\phi\, dz\, \vec{Y} \equiv -i\, A\rho g\, h \sin\phi\, dz$,

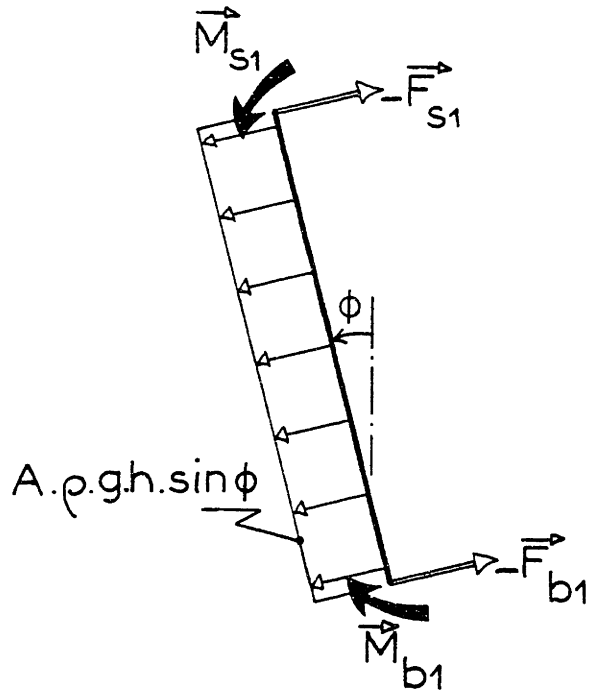

Figure B.6 - Static Equilibrium of the Drill Collars.

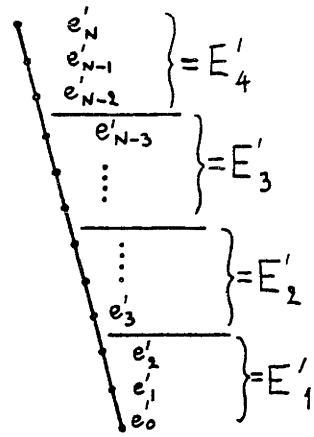

Figure B.7 - Discretization of the Mass-Eccentricity Distribution.

- dimensional moments

$$\begin{cases} \vec{M}_{b_1} = -ik' T_1 \left(\frac{ds'}{dz}\right)_{(0)} - Q\vec{Z} & (A.23) \\ \vec{M}_{s_1} = ic\, EI \left(\frac{d^2 s'}{dz^2}\right)_{(1)} + Q\vec{Z} & (A.25) \end{cases}$$

F_{b1} and F_{s1} denoting the complex forces, the two vector equations of equilibrium read:

$$\begin{cases} -F_{s_1} - F_{b_1} - i\, A\rho g h \sin\phi \int_0^L dz = 0 \\ ic\, EI\left(\frac{d^2 s'}{dz^2}\right)_{(1)} - ik'T_1\left(\frac{ds'}{dz}\right)_{(0)} - iLF_{s_1} + A\rho g h \sin\phi \int_0^L z\, dz = 0 \end{cases}$$

or

$$\begin{cases} F_{s_1} = -\frac{k'T_1}{L}\left(\frac{ds'}{dz}\right)_{(0)} + c\,\frac{EI}{L}\left(\frac{d^2 s'}{dz^2}\right)_{(1)} - iA\rho g h \frac{L}{2}\sin\phi \\ F_{b1} = -iA\rho g h L \sin\phi \;-\; F_{s1} \end{cases}$$

Substituting for

$$\begin{cases} k'/L = k \\ \left(\frac{ds'}{dz}\right)_{(0)} = \frac{N}{2}\left[-s_{-1} + s_1\right] = \frac{N}{2}\left(1 - a_g\right) s_1 \\ \left(\frac{d^2 s'}{dz^2}\right)_{(1)} = \frac{N^2}{L}\left[s_{N-1} + s_{N+1}\right] = \frac{N^2}{L}\left(1 + a_g\right) s_{N-1} \end{cases}$$

the expressions for the dimensional forces corresponding to s become:

$$\begin{cases} F_{s_1} = -kT_1 \frac{N(1-a_g)}{2} s_1 + c\,\frac{EI}{L^2} N^2 (1+a_g) s_{N-1} - iA\rho g h \frac{L}{2}\sin\phi \\ F_{b1} = -iA\rho g h L \sin\phi \;-\; F_{s1} \end{cases}$$

B.2 Calculation of Solution r_e.

2.1 Modification of the Finite-Difference Matrix.

As before, we shall refer to r_e as r. If we replace s by r, the foregoing reasoning holds entirely up to the two following modifications:

- In the pentadiagonal matrix, a_3 has to be replaced by a_5. This modifies the main diagonal only, where c_3 is now $$c_3 = 6N^4 - 2a_2 l_1 N^2 + a_5$$
- The right-hand side excitation vector $\begin{vmatrix} a_4 \\ \vdots \\ a_4 \end{vmatrix}$ must be replaced by $\begin{vmatrix} a_6\, e(1) \\ \vdots \\ a_6\, e(N-1) \end{vmatrix}$ where e(j) refers to the dimensionless eccentricity at $w_j = j/N$.

2.2 Dimensional Forces at the Bit and the Stabilizer.

Having solved for $(r_1, r_2, \ldots, r_{N-1})$, we can now obtain the forces $\vec{F}_{b2}$ and $\vec{F}_{s2}$. An observer tied to the rotating frame always views the collars at rest. However, his trihedral is not galilean: although every slice is at rest, they all are submitted to the dimensional acceleration $-\Omega^2 [r'_{(z)} + e'_{(z)}]$. If he considers now that each slice undergoes the fictitious force $A\rho C_M \Omega^2 (r'+e') dz$, his trihedral becomes galilean and he can safely make use of ordinary static analysis. He sees the immobile collars subjected to:

- dimensional forces $-\vec{F}_{b2}$ and $-\vec{F}_{s2}$,
- distributed force $A \rho C_M \Omega^2 (r' + e')\, dz$,
- dimensional moments

$$\begin{cases} \vec{M}_{b2} = -i k' T_1 \left(\frac{dr'}{dz}\right)_{(0)} - Q\vec{Z} & \text{(Analog to A.23)} \\ \vec{M}_{s2} = i c EI \left(\frac{d^2 r'}{dz^2}\right)_{(1)} + Q\vec{Z} & \text{(Analog to A.25)} \end{cases}$$

F_{b2} and F_{s2} denoting the complex forces, static analysis yields:

$$\begin{cases} -F_{s2} - F_{b2} + A\rho C_M \Omega^2 \int_0^L \left[r'_{(z)} + e'_{(z)}\right] dz = 0 \\ ic EI \left(\frac{d^2 r'}{dz^2}\right)_{(1)} - ik'T_1 \left(\frac{dr'}{dz}\right)_{(0)} - iL F_{s2} + iA\rho C_M \Omega^2 \int_0^L (r' + e')\, z\, dz = 0 \end{cases}$$

Let

$$I_1 = \int_0^L \left[r'_{(z)} + e'_{(z)}\right] dz$$

$$I_2 = \int_0^L \left[r'_{(z)} + e'_{(z)}\right] \frac{z}{L}\, dz$$

I_1 and I_2 can be calculated by the trapezes method. Replacing

r' = L r

e' = L e

z(j) = jL/N, one obtains:

$$\begin{cases} F_{s2} = -k T_1 \frac{N(1-a_g)}{2} r_1 + c \frac{EI}{L^2} N^2 (1+a_g) r_{N-1} + A\rho C_M \Omega^2 I_2 \\ F_{b2} = A \rho C_M \Omega^2 I_1 - F_{s2} \end{cases}$$

In order to simplify the inputs, the program allows only four different values for e', as shown in Figure B.7. Consequently, the number of points is of the type 4m, and the number of segments is N = 4m - 1.

B.3 Total Forces at Bit and Stabilizer.

One simply has

$$\begin{cases} F_{bit} = F_{b1} + F_{b2} \cdot e^{i\Omega t} \\ F_{sta} = F_{s1} + F_{s2} \cdot e^{i\Omega t} \end{cases}$$